NASA CONTRACTOR REPORT

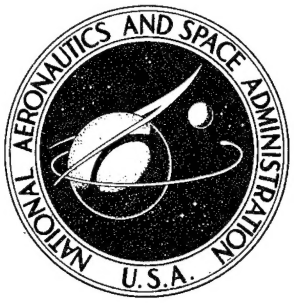

NASA CR-1279

NASA CR-1279

STABLE CRACK PROPAGATION IN A VISCOELASTIC STRIP

by Hans-Karl Mueller

Prepared by
CALIFORNIA INSTITUTE OF TECHNOLOGY
Pasadena, Calif.
for

NATIONAL AERONAUTICS AND SPACE ADMINISTRATION • WASHINGTON, D. C. • MARCH 1969

NASA CR-1279

STABLE CRACK PROPAGATION IN A VISCOELASTIC STRIP*

By Hans-Karl Mueller

*In Partial Fulfillment of the Requirements for the Degree of Doctor of Philosophy

Prepared under Grant No. NsG-172-60 by
CALIFORNIA INSTITUTE OF TECHNOLOGY
Pasadena, Calif.

for

NATIONAL AERONAUTICS AND SPACE ADMINISTRATION

For sale by the Clearinghouse for Federal Scientific and Technical Information
Springfield, Virginia 22151 – CFSTI price $3.00

ACKNOWLEDGEMENTS

Having arrived at this point of my formal education I would like to express my appreciation and gratitude to all of my teachers whose effort is directly or indirectly reflected in this thesis. I am especially indebted to Prof. W. G. Knauss for suggesting this interesting problem area to me and for his many valuable comments and his constant encouragement. Courses taught by Professors Y.C. Fung and C. D. Babcock greatly enhanced my understanding of solid mechanics.

My thanks are also due to Prof. N. W. Tschoegl and Dr. R. F. Landel for helpful discussions on some of the chemical aspects of the thesis problem.

The support and advice given by Mr. M. Jessey and his staff during the experimental phase of this work is gratefully acknowledged. I am greatly indebted to Mrs. E. Fox for the excellent work in typing the manuscript. I would also like to thank Mmes. B. Wood and J. Colbert for their help in the preparation of the figures and in the thesis reproduction.

Financial support of this research was provided by the National Aeronautics and Space Administration Research Grant NsG-172-60.

I dedicate this thesis to my parents.

ABSTRACT

A crack of length 2a which propagates with small, constant speed through a viscoelastic strip of width 2b is considered. The strip is strained by displacing its shearfree edges. Linear theory is applied. The stress on the line of crack advancement and the shape of the crack surface are calculated for a state of plane stress. over

The stress intensity factor which is independent of material properties is given as a function of a/b. It exhibits a maximum at $a/b \cong 0.75$. For $a/b > 1.5$ the stress intensity factor becomes essentially independent of crack length. The crack surface deflection is obtained in the form of a superposition integral and is a function of material properties and crack speed.

The energy which is released when the crack extends a small distance is calculated. This crack energy depends on the crack speed and involves the creep function of the material. A characteristic length enters in the course of its derivation. This length does not appear in the case of an elastic material and is considered as an additional material property necessary to describe viscoelastic crack propagation.

The energy conservation equation is established by considering a small control volume surrounding the crack tip. A relationship emerges from this equation which implicitly gives a stable crack speed as a function of applied strain, temperature, and material properties. The creep function is the controlling factor in this equation.

The relevant material properties are discussed and presented for a Polyurethane rubber (Solithane 113 - 50/50). The lower bound of the surface energy is determined from fracture tests on the swollen material. The results of the material characterization are used to calculate the crack speed as a function of applied strain and temperature. Good agreement is found to exist between theory and experiment.

TABLE OF CONTENTS

TABLE OF CONTENTS (Cont'd)

TABLE OF CONTENTS (Cont'd)

LIST OF FIGURES

LIST OF FIGURES (Cont'd)

LIST OF FIGURES (Cont'd)

LIST OF FIGURES (Cont'd)

LIST OF TABLES

LIST OF SYMBOLS

a	Half crack length
a_T	Time-temperature shift factor
b	Half strip width
C_1	Temperature dependent material constant
C_2	Temperature dependent material constant
D	Dissipated energy
D_{cr}	Creep function
D_i	Inner diameter of ring specimen
D_s	Energy dissipated by creation of new surface
D_{st}	Dissipated energy in a standard viscoelastic solid
D_v	Energy going into viscous dissipation
E	Young's modulus
E_g	Short time or glassy modulus
E_{rel}	Relaxation modulus
g	Volume fraction of gel rubber
G	Shear modulus
G_1	Relaxation function in shear
G_2	Relaxation function in isotropic compression
i	$\sqrt{-1}$
I_1	First strain invariant
I_2	Second strain invariant
K	Kinetic energy
K_n	Nondimensional stress intensity factor
L	Circular boundary of control volume
$L(\tau)$	Retardation function

LIST OF SYMBOLS (Cont'd)

M	Kernel of Fredholm integral equation
p	Arbitrary pressure distribution
P_c	Fourier transformation of p
R	Cylindrical control volume
R	Universal gas constant
s	Laplace transform variable
S	Energy required to create a unit of new surface
t	Time
T	Absolute temperature
T_g	Glass transition temperature
T_s	Reference temperature = $T_g + 50^{\circ}C$
U	Strain energy
u_i	Cartesian components of displacement
v	Speed of crack propagation
V	Molar volume of swelling agent
V_o	Volume of dry specimen
v_2	Polymer volume fraction in the swollen sample
W	External work
W_i	Strain energy function
x	Cartesian coordinate
y	Cartesian coordinate
$Z(r)$	Solution of Fredholm integral equation
δ	Solubility parameter
Δa	Crack extension, characteristic length
ΔE_c	Crack energy = energy release as the crack advances by Δa

LIST OF SYMBOLS (Cont'd)

Δl	Change in distance between pins by which ring specimen is stretched
ϵ_o	Gross strain on strip
ϵ_{ij}	Cartesian components of strain
ϵ'_{ij}	Strain deviator
η	Normalized cartesian coordinate = y/a
η	Viscous coefficient of the dashpot element of standard viscoelastic solid
λ	Extension ratio = $1 + \epsilon$
μ	Polymer-solvent interaction parameter
ν	Poisson's ratio
ν'_e	Number of elastically effective network chains per unit volume of unswollen polymer
ξ	Normalized cartesian coordinate = x/a
σ_{ij}	Cartesian components of stress tensor
σ'_{ij}	Stress deviator
σ_o	Stress on strip edges = $E_r \epsilon_o$
$\sigma_{o\,crit}$	Critical stress at which an initial crack becomes theoretically unstable
τ_m	Relaxation time of a standard viscoelastic solid
Φ	Airy stress function
ω	Fourier transform variable

I. INTRODUCTION

Historical Background

Hand in hand with the increasing application of polymers in structural design over the last decade or two went a growing interest in the fracture process in viscoelastic materials (1, 2, 3, 4, 5). Until then fracture mechanics was mostly concerned with brittle materials. Probably the most important concept put forth was Griffith's hypothesis (6) of brittle fracture which was published in 1921. Based on the principle of conservation of energy it yields a criterion for crack instability. Mott (7), Berry (8) and others investigated the crack kinetics by including a kinetic energy term in the energy balance as established by Griffith. Several values for the maximum speed of crack propagation have been obtained depending on the method of approach. Craggs (9) derived a value of 0.72 x shear wave speed for this limiting velocity. The absolute maximum speed of propagation for a crack which moves through a non-dissipative material and which does not bifurcate is equal to the Rayleigh wave speed (10, 11). Experimentally determined maximum crack speeds however are often considerably smaller than the theoretically predicted values (12). A simplification of the energy method as initiated by Griffith has been given by Irwin (13) and later Sanders (14) who showed that it is sufficient to consider only the energy exchange in the immediate vicinity of the crack tip.

The extension of the Griffith fracture hypothesis to the rupture of rubber by Rivlin and Thomas (15) can be considered the first major step into the field of viscoelastic fracture. They found that

a criterion apparently identical to the one by Griffith holds in this case, too. However the tearing energy which enters in place of the surface energy is not only a measure for the energy necessary to create a unit of new surface but may also include the energy which is dissipated by other processes like viscous dissipation and microscopic tearing in a region surrounding the advancing crack tip. Greensmith and Thomas (16) later found the tearing energy to depend markedly on the rate of tearing.

Theoretical investigations of the crack propagation process in viscoelastic materials have mostly been based on a global energy conservation principle in which a term characterizing viscous energy dissipation is included. Williams and Schapery (17) derived an expression for the viscous dissipation on the assumption that the material behavior is represented by a Voigt model. A small, unstable crack in the center of a large plate is predicted to grow exponentially with time on the basis of this calculation. A limiting crack velocity does not emerge from this theory. Williams (18) later investigated a spherical cavity in an infinite viscoelastic medium subject to uniform tension at infinity. He demonstrates that for a step loading the creep function enters the corresponding Griffith formula instead of Young's modulus. The creep function is evaluated for the time which elapsed between load application and the beginning of fracture.

A theory of defect growth on the basis of the theory of rate processes was developed by Knauss (19). The typical rate dependence of the ultimate properties in uniaxial tension tests is deduced from

this theory. Similar results are obtained by Bueche and Halpin (20) by considering a thin filament at the front of the crack which is assumed to be in a state of uniaxial tension and to behave in the same manner as the bulk material does in this stress state.

More recently Willis (21) solved the dynamic problem of a crack travelling through an infinite standard viscoelastic solid in anti-plane strain. A relationship between applied force and crack velocity is derived by application of a Barenblatt type fracture criterion. This investigation shows that the crack motion is stabilized by the presence of dissipation. The speed above which the stabilization occurs is very high, however. Crack propagation speeds which were measured in hard polymeric materials are about an order of magnitude smaller than predicted by this theory. The crack speeds in highly viscoelastic materials which have longer relaxation times and exhibit a greater degree of relaxation will be even smaller than in hard plastics.

To the author's knowledge all of the theoretical considerations of the viscoelastic crack propagation process put forth so far deal with infinitely large bodies for which the limiting crack velocities are either unbounded or very high. The experimental investigation (22) of a crack propagating longitudinally through a strip of viscoelastic material however shows that there are very small, stable crack speeds which cannot be predicted by existing theories. The speed of crack propagation depends on the strain applied to the strip and on the temperature. A theoretical investigation of the fracture process in a viscoelastic strip seemed to be appropriate

and is attempted in this thesis. The results will also be helpful in the understanding and interpretation of viscoelastic fracture in other practical geometries which give rise to small, stable crack speeds.

Thesis Outline

Instead of employing a global energy conservation equation of the system Irwin's point of view is taken and a local energy balance around the advancing crack tip established. In doing so one equates the crack energy which is the energy released when the crack extends a small distance and the energy going into the creation of new surface. The knowledge of the stresses just ahead of the crack tip and of the crack opening close to the tip is necessary for the calculation of the crack energy. The effect of viscous dissipation in the material will be reflected in the velocity dependence of the stresses or of the crack opening.

The stresses and displacements on the strip centerline and close to the tip of a crack propagating with constant speed through a viscoelastic strip are calculated in part II of this thesis. Instead of a strip which is strained by displacing its edges we consider the for-our-purpose equivalent problem of a pressurized crack in an otherwise unstretched strip. The edges of the infinitely long strip are taken to be shear free for the sake of mathematical simplicity. Clamped edges would be more realistic but the essential features of the problem remain unchanged by this simplification.

The problem of a suddenly pressurized crack of constant length is considered first. The correspondence principle can be applied in this case and the solution to the associated elastic

problem is found by way of the Fourier transform method suggested by Sneddon (23). The resulting Fredholm integral equation is solved numerically. The stress intensity factor which is independent of material properties in this geometry is given as a function of crack length over strip width ratio a/b. This factor grows with increasing crack length and reaches a maximum at $a/b \cong 0.75$. Beyond this point it decreases slightly and becomes essentially independent for $a/b > 1.5$. The shape of the crack surface as a function of time due to a step load is readily obtained by introducing the creep function and inversion of the Laplace transformation of the solution.

The crack opening of a propagating crack is then determined by superposition of solutions to step load problems with increasing but individually constant crack lengths. The result of this operation is a superposition integral. The same answer could have been obtained by way of the so-called extended superposition principle which was very recently suggested by Graham (24). For a constant velocity crack with $a/b > 1.5$ the deflection close to the crack tip becomes independent of crack size and hence independent of time. An expression for the crack opening in this region is then obtained which is similar to the corresponding expression for an elastic material except that the crack speed enters as a parameter. The crack energy is thus readily calculated as in the elastic case because the linear relationship between load and crack opening holds for the viscoelastic material, too. A length which is designated as characteristic length Δa enters the crack energy. In the case of an elastic material this length disappears when the rate of change of the crack energy

is calculated. In the viscoelastic case however it enters along with the crack speed into the argument of the creep function. This characteristic length is viewed as an additional material property which is necessary to describe viscoelastic crack propagation.

The expression for the crack energy is then substituted into the energy conservation equation. A simple relationship between crack speed, applied strain or load, temperature, and material properties emerges from this equation. The creep function is the dominating factor in this relationship. It is not necessary to resort to a mechanical model for material behavior. The creep function can be of any experimentally determined form.

The material properties which enter the theoretical relationships are presented in part III for a Polyurethane rubber. The trade name of this material is Solithane 113 and the particular composition used here is Solithane 50/50 (cf. p. 49). The typical features of viscoelastic materials are exhibited and are shortly discussed together with the experimental methods employed for the determination of these material properties.

The measurement of the surface energy is difficult in strongly viscoelastic materials. Crack propagation tests with materials of this kind seemed to indicate that there is no lower bound for the surface energy. In order to remove some of the uncertainties in defining the lower bound of this energy use was made of the fact that the internal viscosity of crosslinked polymers is largely reduced in the swollen state. A short description of the swelling properties of Solithane 50/50 is given together with some

polymer network characteristics which can be calculated from swelling measurements. The swollen material is demonstrated to behave in a neo-Hookean manner. Crack propagation tests with Solithane 50/50, swollen in Toluene were carried out. A lower bound for the surface energy is seen to exist and is calculated from the data obtained in these tests. A more detailed mechanical characterization of the material can be found in (25).

Having determined all relevant material properties the crack propagation speed is calculated as a function of applied strain and temperature by application of the theoretical relationships derived in part II. There is good agreement between the theoretical results and the experimental data obtained by Knauss (22). The characteristic length yielding the best agreement was found to be 10^{-8} inches. The comparison between theory and experiment is the subject of part IV of this thesis.

II. THEORETICAL INVESTIGATION OF A CRACK MOVING IN A VISCOELASTIC STRIP

The relationships between crack propagation speed, applied strain, or load, temperature, and viscoelastic material properties will be derived for a particular geometry. The geometry chosen is an infinitely long, thin strip with a central crack of length 2a. The strip width is 2b (cf. Fig. 1). The strip is strained by displacing its edges, and depending on the magnitude of this strain, ϵ_o, the initial crack will remain stationary or begin to extend. The speed with which the crack propagates is constant when the crack length exceeds a certain value beyond which the stress field surrounding the crack tip becomes independent of crack size.

The approach outlined on the following pages is not restricted to a strip geometry. Plates with a small central crack are covered in the present derivation because this geometry is approached as the ratio of crack length to strip width becomes very small. The results obtained from the investigation of the simple strip geometry are believed to be descriptive of viscoelastic crack propagation in general within the limits set by simplifications made in order to facilitate the mathematical solution of the problem. In the course of this development it will become apparent that very similar answers can be expected for other geometries and loading conditions if stresses and displacements close to the crack front are known.

The material properties needed in the following context are the short-time or glassy modulus, E_g, the long-time or rubbery modulus, E_r, the creep function, D_{cr}, and the time-temperature

shift factor, a_T. Viscous dissipation is assumed to be the only irreversible process in the material apart from the creation of new surface during fracture. For a thorough mathematical and experimental description of viscoelastic material properties see for instance references (26,27,28,29). Additional relevant material properties for a particular viscoelastic material are also presented in part III of this thesis.

In order to find the quantities which are of interest in this problem we shall first derive the energy conservation equation for a moving crack.

2.1. The Energy Conservation Equation

The explanation of fracture on the basis of the energy balance of a cracked body was initiated by Griffith (6). Irwin arrived at the same fracture criterion as Griffith via the calculation of the work done locally at the crack tip during a small increase in crack length (13). Later it was also pointed out by Sanders (14) that the energy balance does not have to be established globally as in (6) and that it is sufficient to examine a control volume surrounding the crack tip.

We shall now consider a cylindrical control volume, R, the center of which is located at the crack tip. Its circular boundary is denoted by L, see Fig. 2. Let us investigate the effects of a small, virtual change Δa of the crack tip position. The contour L will undergo a small distortion and the forces acting on it will do work as a consequence of the increase in crack length. This work is called external work and is denoted by W. A certain amount of

this work is dissipated within the volume R. This portion of the energy will be called D and consists of the work D_s necessary to create new surface, of the work D_v required to overcome viscous forces within the material, and of work going into plastic deformation and other possible irreversible mechanisms. The motion of material involves kinetic energy which will be designated by K. The remaining energy is stored as internal energy U. The whole process is assumed to take place isothermally. Taking the rates of change of these quantities the first law of thermodynamics can be cast into the following form

$$\dot{W} = \dot{U} + \dot{K} + \dot{D} . \qquad (2.1\text{-}1)$$

The dot denotes differentiation with respect to time.

Our attention is focused on viscoelastic materials and all dissipative processes other than creation of new surface and viscous dissipation will be neglected. We shall furthermore restrict ourselves to crack propagation speeds which are small compared to the shear wave speed based on the rubbery modulus. The kinetic energy term may then be neglected. An investigation of high speed viscoelastic crack propagation can be found in reference (30).

The energy conservation equation is thus reduced to

$$\dot{W} = \dot{U} + \dot{D}_s + \dot{D}_v . \qquad (2.1\text{-}2)$$

We shall now adopt Irwin's point of view (13) and calculate the work which is released at the crack tip when the crack extends a small, virtual distance Δa. This work will be called crack energy

and will be denoted by E_c. A schematic picture of the stresses and displacements close to the crack tip is given in Fig. 3. Because of the symmetry of the geometry there are only normal stresses acting in the plane of crack advancement.

Let us imagine that for a small distance Δa ahead of the present crack tip the material is already physically separated but still held in its original position by surface tractions. Figure 3 which shows the lower half of the crack tip illustrates this situation. The unbroken line represents the original crack position. The surface tractions acting along the imaginary cut from a to $a+\Delta a$ are also indicated. These forces are just large enough to hold the material together along the center line. If the material along Δa is now allowed to separate, then the work done by the surface tractions in the course of this crack opening is given by (10, 13)

$$\Delta E_c = 2 \int_{\xi=a}^{a+\Delta a} \tfrac{1}{2} \sigma_{yy}(\xi)\, u_y\, (\xi - \Delta a)\, d\xi \qquad (2.1\text{-}3)$$

A state of plane stress and a linear relationship between crack opening u_y and tractions σ_{yy} is assumed to exist. The latter is true for an elastic material but holds also in the viscoelastic case to be considered here because the crack speed is going to enter as a parameter only as we shall see later.

There is no energy required to create new surface because we imagined the material to be separated already. The energy conservation equation for the same control volume R and material considered previously reads now

$$\dot{W} + \dot{E}_c = \dot{U} + \dot{D}_v \quad . \tag{2.1-4}$$

A comparison with equation (2.1-2) yields immediately

$$-\dot{E}_c = \dot{D}_s \quad . \tag{2.1-5}$$

This is a greatly simplified statement of the conservation of energy compared to the original form as given by (2.1-2).

The energy dissipation caused by the creation of new surface can be easily calculated with the help of the so-called surface energy S which is the energy required to form a unit of new surface. It is assumed to be independent of the rate of formation and is considered a material constant. For a crack moving with constant velocity v through a sheet of unit thickness one obtains then

$$\dot{D}_s = 2 S v \quad . \tag{2.1-6}$$

The factor 2 enters here because an upper and lower surface is created as the crack extends.

Only the normal stresses and the crack displacements in the immediate vicinity of the crack tip have to be known for the calculation of the crack energy E_c. Their evaluation will be the subject of the next few chapters.

2.2. Formulation of the Boundary Value Problem

Basic Assumptions

The geometry under consideration is shown in figure 1. The half crack length a(t) is a monotonically increasing function of time t.

A state of plane stress is assumed to exist in the strip at all times. The crack surface is stress free and mathematically sharp in the unstrained strip. Prescribed displacements in the y-direction and zero shear stress are taken as boundary conditions on the strip edges $y = \pm b$. The mathematics are considerably simplified by this assumption without changing the essential features of the problem as compared to the strip with clamped edges which should actually be examined with regard to the real experiment. The kernel of the integral equation to be derived is less complicated in our case and in particular does not involve any material properties as would be the case for clamped edges. The stress fields surrounding the crack tip differ little for the two different boundary conditions as can be seen from a study of (19) and (31).

No attention will be paid to transients. The crack is assumed to propagate at constant speed into a viscoelastic material which is in a state of long-time equilibrium far ahead of the crack. The uniaxial stress in the uncracked strip is then given by the rubbery modulus E_r and by the strain ϵ_o on the strip, i.e.,

$$\sigma_o = E_r \epsilon_o \quad . \tag{2.2-1}$$

The applicability of linear theory is assumed. The original geometry and boundary conditions can then also be realized by superposition of a uniaxial tension field σ_o and its corresponding displacements with the stresses and displacements obtained by solving the problem of a crack under internal pressure σ_o in an otherwise unloaded strip.

Our interest is focused on the stresses and displacements in the crack plane in the immediate vicinity of the crack tip. These displacements are directly given by the pressurized crack problem because the displacements resulting from the uniaxial tension field are zero at $y = 0$. The stresses close to the crack tip have a well-known singularity (32,33) which is entirely embedded in the solution of the pressurzied crack problem. The contribution of the uniaxial tension field to these stresses is negligibly small in the immediate neighborhood of the crack tip. The two quantities which interest us can therefore be obtained from the investigation of the pressurized crack problem alone.

Energy Dissipation in the Strip

The stresses in a given element of the strip increase during passage of the crack front of a pressurized crack. The stresses in the same element of a stretched strip with a moving unpressurized crack would decrease however in the process. The question then arises whether the amount of energy dissipated by viscous mechanisms in the material is equal in both cases. This kind of energy dissipation is governed by the rate of deformation, but these are the same in both situations because the uniaxial tension field only contributes constant displacements. An arbitrary loading or unloading history can be made up from a sequence of corresponding step histories since the laws of linear viscoelasticity are assumed to hold. Recognizing the equivalence of deformation rates and the validity of the superposition principle it remains to be shown that the energy dissipated by step loading is equal to the one dissipated by sudden

removal of the load. Let us resort to a mechanical model for viscoelastic behavior in order to be able to perform this comparison.

We select a three-element standard viscoelastic solid (33) as a model. If a material of this kind is exposed to a step strain ϵ_o at time t = 0 or suddenly relieved from a strain of equal magnitude at this time the total dissipated energy per unit volume at time $t \geq 0$ is given in either case by

$$D_{st} = \epsilon_o^2 \frac{\eta}{2 E_g E_r \tau_m} \left[1 - \exp\left(-\frac{2E_r t}{E_g \tau_m}\right)\right]$$

where η = viscosity of the dashpot element

τ_m = relaxation time = $\eta/(E_g - E_r)$.

In spite of the shortcomings of mechanical models they give an adequate representation of the dissipation process in the context of this argument. We do not have to restrict ourselves to mechanical models in any of the following computations necessary for the determination of the crack energy.

The Boundary Value Problem

Because of the symmetry of the problem it is sufficient to investigate the half strip with appropriate boundary conditions. The crack is then represented by a section of length 2a(t) on the boundary y = 0 over which the constant pressure σ_o acts. The remaining part of this boundary has to satisfy the condition of zero normal displacement and zero shear stress for all values of x. The other edge at y = b has to satisfy the same boundary conditions, that is zero normal displacement and zero shear stress, as would have been posed for

the strip of width 2b. Figure 4 shows the geometry and boundary conditions of the half strip.

Let u_i, ϵ_{ij}, and σ_{ij} denote the cartesian components of displacement, strain, and stress, respectively. The field equations for the linear quasi-static problem without body forces are then (34) - in common index notation - strain displacement relationship

$$\epsilon_{ij} = \tfrac{1}{2}(u_{i,j} + u_{j,i}) \tag{2.2-2}$$

equilibrium equation

$$\sigma_{ij,j} = 0 \; ; \qquad \sigma_{ij} = \sigma_{ji} \quad . \tag{2.2-3}$$

The constitutive equation for the material behavior is assumed to be given in the form of a relaxation law

$$\sigma'_{ij} = \epsilon'_{ij} * dG_1 \; ; \; \sigma_{kk} = \epsilon_{kk} * dG_2 \quad , \tag{2.2-4}$$

where the following definitions hold:

Stress deviator $\sigma'_{ij} = \sigma_{ij} - \frac{1}{3}\delta_{ij}\sigma_{kk}$

Strain deviator $\epsilon'_{ij} = \epsilon_{ij} - \frac{1}{3}\delta_{ij}\epsilon_{kk}$

Convolution integral $\Theta * d\psi = \int_0^t \Theta(t-\tau)\frac{d\psi}{d\tau}(\tau)d\tau + \Theta(t)\psi(0)$.

δ_{ij} is the Kronecker delta. The material functions G_1 and G_2 as well as stresses, strains, and displacements are functions of time t and of the space variables in case of the latter quantities. The boundary conditions to be satisfied by the solution of the field equations are

$$\text{on } y = 0: \quad \left.\begin{aligned} \sigma_{xy}(x,0,t) &= 0 && \text{for } |x| < \infty \\ \sigma_{yy}(x,0,t) &= -\sigma_o && \text{for } |x| < a(t) \\ u_y(x,0,t) &= 0 && \text{for } |x| \geq a(t) \end{aligned}\right\} \qquad (2.2\text{-}5)$$

$$\text{on } y = b: \quad \left.\begin{aligned} \sigma_{xy}(x,b,t) &= 0 \\ u_y(x,b,t) &= 0 \end{aligned}\right\} \quad \text{for } |x| < \infty \ . \qquad (2.2\text{-}6)$$

The initial condition is that the strip is completely undisturbed at times $t < 0$.

A convenient method for the solution of problems in viscoelasticity is based on the so-called correspondence principle (34,35). An associated elastic problem is obtained by applying the Laplace transform to all equations describing the viscoelastic problem. The time dependence is removed by this procedure and replaced by the transform parameter. In principle, the problem can then be solved by finding the solution to the associated elastic problem and inverting this answer back into the real time space. This method is however not applicable to mixed boundary value problems in which the parts of the boundary over which specifications are made change with time (36). The Laplace transformations of the boundary conditions cannot be found in this case.

In order to circumvent this difficulty we shall first find the time dependent stresses and displacements in the strip as caused by a step loading σ_o on $y = 0$, $|x| < a$ at time $t = 0$, where the length a is a constant. For a growing crack, i.e., a time dependent length a, the stresses and displacement are then determined by superposition of step loadings. This procedure is graphically indicated in

Fig. 12 and is carried out in section 2.5.

The Step Load Problem

The Laplace transform method can be employed to find the solution to this problem. Let us apply the Laplace transform

$$\bar{f}(s) = \int_0^\infty f(t)\, e^{-st}\, dt$$

to equations (2.2-2) through (2.2-6). Scaling the space variables x and y at the same time by the half crack length a, i.e.,

$$\xi = \frac{x}{a} \quad \text{and} \quad \eta = \frac{y}{a} \ , \tag{2.2-7}$$

results in the following formulation of the step load problem in transformed space:

$$\bar{\epsilon}_{ij} = \tfrac{1}{2}(\bar{u}_{i,j} + \bar{u}_{j,i}) \tag{2.2-8}$$

$$\bar{\sigma}_{ij,j} = 0 \ ; \ \bar{\sigma}_{ij} = \bar{\sigma}_{ji} \tag{2.2-9}$$

$$\bar{\sigma}'_{ij} = s\, \bar{G}_1\, \bar{e}'_{ij} \ ; \ \bar{\sigma}_{kk} = s\, \bar{G}_2\, \bar{e}_{kk} \ . \tag{2.2-10}$$

The boundary conditions are

$$\text{on } \eta = 0: \quad \left.\begin{aligned} \bar{\sigma}_{xy}(\xi, 0, s) &= 0 && \text{for } |\xi| < \infty \\ \bar{\sigma}_{yy}(\xi, 0, s) &= -\frac{a\sigma_o}{s} && \text{for } |\xi| < a \\ \bar{u}_y(\xi, 0, s) &= 0 && \text{for } |\xi| \geq a \end{aligned}\right\} \tag{2.2-11}$$

$$\text{on } \eta = \frac{b}{a}: \quad \left.\begin{aligned} \bar{\sigma}_{xy}(\xi, \tfrac{b}{a}, s) &= 0 \\ \bar{u}_y(\xi, \tfrac{b}{a}, s) &= 0 \end{aligned}\right\} \quad \text{for } |\xi| < \infty \ . \tag{2.2-12}$$

These are the same equations as for an elasto-static problem with

material constants

$$\left.\begin{aligned} \overline{G} &= \tfrac{1}{2}\, s\, \overline{G}_1 \\ \overline{E} &= \frac{3\, s\, \overline{G}_1\, \overline{G}_2}{\overline{G}_1 + 2\overline{G}_2} = s\, \overline{G}_1 (1 + \overline{\nu}) \end{aligned}\right\} \quad . \tag{2.2-13}$$

$\overline{G}$, $\overline{E}$, and $\overline{\nu}$ are the shear modulus, Young's modulus, and Poisson's ratio of the material in the associated elastic problem.

Making use of (2.2-13) the compatibility equation can be derived from the definition of strain (2.2-8). It assumes the following form:

$$\left(\frac{\partial^2}{\partial x^2} + \frac{\partial^2}{\partial y^2}\right)(\overline{\sigma}_{xx} + \overline{\sigma}_{yy}) = 0 \quad . \tag{2.2-14}$$

The equilibrium equations (2.2-9) can be identically satisfied by means of the Airy stress function $\Phi(\xi, \eta)$. In terms of this function the stresses are given by

$$\left.\begin{aligned} \overline{\sigma}_{xx} &= \frac{\partial^2 \Phi}{\partial \eta^2} \\ \overline{\sigma}_{yy} &= \frac{\partial^2 \Phi}{\partial \xi^2} \\ \overline{\sigma}_{xy} &= -\frac{\partial^2 \Phi}{\partial \xi \partial \eta} \end{aligned}\right\} \quad . \tag{2.2-15}$$

Substitution of the appropriate expressions into the compatibility equation yields a biharmonic equation for Φ

$$\nabla^4 \Phi = \frac{\partial^4 \Phi}{\partial \xi^4} + 2\frac{\partial^4 \Phi}{\partial \xi^2 \partial \eta^2} + \frac{\partial^4 \Phi}{\partial \eta^4} = 0 \quad . \tag{2.2-16}$$

We shall follow the Fourier transform method outlined by Sneddon in

(23) for the solution of this equation subject to the boundary conditions (2.2-11,12).

2.3 Derivation and Solution of the Integral Equation

The main steps by which the above problem is reduced to an integral equation are now given. The Fourier transform will be required. It will be denoted by an asterisk and is defined as

$$\left.\begin{aligned} f^*(\omega) &= \frac{1}{\sqrt{2\pi}} \int_{-\infty}^{\infty} f(\xi)\, e^{i\omega\xi}\, d\xi \\ \text{and its inverse as} \\ f(\xi) &= \frac{1}{\sqrt{2\pi}} \int_{-\infty}^{\infty} f^*(\omega)\, e^{-i\omega\xi}\, d\omega \end{aligned}\right\} . \qquad (2.3\text{-}1)$$

Under the assumption of suitable properties of the Airy stress function, Φ, that is assuming that Φ and its first three derivatives with respect to ξ go to zero as $|\xi|$ approaches infinity, the Fourier transforms in the variable ξ of equations (2.2-15) and (2.2-16) are easily obtained. The stresses are now given by

$$\left.\begin{aligned} \bar{\sigma}^*_{xx} &= \frac{\partial^2 \Phi^*}{\partial \eta^2} \\ \bar{\sigma}^*_{yy} &= -\omega^2 \Phi^* \\ \bar{\sigma}^*_{xy} &= i\omega \frac{\partial \Phi^*}{\partial \eta} \end{aligned}\right\} . \qquad (2.3\text{-}2)$$

and the biharmonic equation becomes

$$\omega^4 \Phi^* - 2\omega^2 \frac{\partial^2 \Phi^*}{\partial \eta^2} + \frac{\partial^4 \Phi^*}{\partial \eta^4} = 0 \quad . \qquad (2.3\text{-}3)$$

The following expression for the displacement in the y-direction can be derived on account of equations (2.2-8,10,13,15) and their Fourier transformations:

$$\overline{E}\,\overline{u}_y^* = -(2+\overline{\nu})\,\frac{\partial \Phi^*}{\partial \eta} + \frac{1}{\omega^2}\,\frac{\partial^3 \Phi^*}{\partial \eta^3} \quad . \tag{2.3-4}$$

The solution of equation (2.3-3) is

$$\Phi^*(\omega,\eta) = A\,\sinh(\omega\eta) + B\,\cosh(\omega\eta) + C\,\omega\eta\,\sinh(\omega\eta) + D\omega\eta\,\cosh(\omega\eta) \tag{2.3-5}$$

with the factors A,B,C,D being functions of ω, loading, and strip geometry alone. These four factors will now be determined for the following boundary conditions:

$$\left.\begin{array}{lll} \text{On } \eta = 0: & \overline{\sigma}_{xy}^*(\omega,0) = 0 & \\ & \overline{\sigma}_{yy}^*(\omega,0) = -P_c & \\ \text{On } \eta = \frac{b}{a}: & \overline{\sigma}_{xy}^*(\omega,\frac{b}{a}) = 0 & \\ & \overline{u}_y(\omega,\frac{b}{a}) = 0 & \end{array}\right\} \quad \text{for } |\omega| < \infty \tag{2.3-6}$$

P_c stands for the Fourier cosine transformation of an arbitrary pressure distribution $p(\xi)$ which is an even function of ξ however, i.e.

$$P_c(\omega) = \sqrt{\frac{2}{\pi}} \int_0^\infty p(\xi)\,\cos(\omega\xi)\,d\xi \quad . \tag{2.3-7}$$

Knowing the stress function Φ^* under these conditions we can

calculate the expression $\bar{u}_y^*$ on the strip boundary $\eta = 0$. Inversion of this quantity yields the normal displacement on this boundary and in connection with the arbitrary pressure distribution $p(\xi)$ one can derive an integral formulation of the remaining boundary conditions to be satisfied (2.2-11).

Applying equations (2.3-2,4,5) to the boundary conditions (2.3-6) furnishes the following expressions for the factors A, B, C, and D:

$$\left.\begin{aligned} B &= \frac{1}{\omega^2} P_c(\omega) \\ A = -D &= C \frac{\sinh(\omega b/a)}{\cosh(\omega b/a} \\ &= -\frac{P_c(\omega)}{\omega^2} \frac{\sinh^2(\omega b/a)}{\omega b/a + \sinh(\omega b/a)\cosh(\omega b/a)} \end{aligned}\right\} . \qquad (2.3\text{-}8)$$

Substitution of these expressions into equation (2.3-5) and subsequent employment of $\Phi^*(\omega, 0)$ in equation (2.3-4) yields the normal displacement $\bar{u}_y^*(\omega, 0)$ in the transformed plane. After inversion of the Fourier transformation this expression reads

$$\bar{u}_y(\xi, 0) = \frac{2}{\bar{E}} \sqrt{\frac{2}{\pi}} \int_0^\infty \frac{P_c(\omega)\sinh^2(\omega b/a)\cos(\omega\xi)}{\omega[\omega b/a + \sinh(\omega b/a)\cosh(\omega b/a)]} d\omega \ . \qquad (2.3\text{-}9)$$

Now let

$$P_c(\omega) = \omega[1 + m(\omega b/a)]\, H(\omega) \qquad (2.3\text{-}10)$$

with $$m(r) = \frac{r + e^{-r}\sinh(r)}{\sinh^2(r)} \qquad (2.3\text{-}11)$$

and equation (2.3-9) becomes

$$\bar{u}_y(\xi, 0) = \frac{2}{\bar{E}} \sqrt{\frac{2}{\pi}} \int_0^\infty H(\omega) \cos(\omega\xi)\, d\xi \quad . \tag{2.3-12}$$

Inversion of the Fourier transform of the second boundary condition of (2.3-6) yields the traction on the boundary $\eta = 0$ to be

$$\bar{\sigma}_{yy}(\xi, 0) = -\sqrt{\frac{2}{\pi}} \frac{\partial}{\partial \xi} \int_0^\infty [1+m(\omega b/a)]\, H(\omega) \sin(\omega\xi)\, d\xi \tag{2.3-13}$$

on account of (2.3-10).

A comparison of equations (2.3-12) and (2.3-13) with the corresponding boundary conditions of (2.2-11) leads to the following formulation:

$$\left.\begin{aligned} \sqrt{\frac{2}{\pi}} \int_0^\infty H(\omega) \cos(\omega\xi)\, d\omega &= 0 \qquad \text{for } |\xi| \geq 1 \\ \sqrt{\frac{2}{\pi}} \int_0^\infty [1+m(\omega b/a)]\, H(\omega) \sin(\omega\xi) d\omega &= \frac{a\sigma_o}{s} \xi \qquad \text{for } |\xi| < 1 \end{aligned}\right\} . \tag{2.3-14}$$

All boundary conditions will be satisfied if a function $H(\omega)$ is found which obeys this dual integral equation.

The first of equations (2.3-14) is identically satisfied (23) if

$$H(\omega) = \int_0^1 R(r)\, J_o(\omega r)\, dr \tag{2.3-15}$$

with $R(r)$ as a new unknown function. Substitution of this expression into the second of equations (2.3-14) results in

$$\int_0^{\xi} \frac{R(r)dr}{\sqrt{\xi^2 - r^2}} = \sqrt{\frac{\pi}{2}} \frac{a\sigma_o}{s} \xi$$

$$- \int_0^1 R(q) \left[\int_0^{\infty} J_o(\omega q) m(\omega b/a) \sin(\omega \xi) d\omega \right] dq \ .$$

This is an Abel integral equation for R(r) if the right hand side of the equation is considered a known function. The solution of this equation is (37)

$$Z(r) + \int_0^1 Z(q)\ M(r,q)\ dq = \sqrt{\frac{\pi}{2}}\ r \qquad (2.3\text{-}16)$$

where

$$M(r,q) = r\left(\frac{a}{b}\right)^2 \int_0^{\infty} \omega m(\omega)\ J_o(\omega qa/b)\ J_o(\omega ra/b)\ d\omega \qquad (2.3\text{-}17)$$

and where the following relationship holds between the old unknown function R(r) and the new unknown Z(r):

$$Z(r) = \frac{s}{a\sigma_o} R(r) \qquad (2.3\text{-}18)$$

Equation (2.3-16) is a Fredholm integral equation of the second kind for Z(r). It should be noted that none of the material properties enter this equation for the boundary conditions considered in this problem.

The standard form of the Fredholm equation of the second kind is

$$f(r) - \lambda \int_0^1 f(q)\ M(r,q)\ dq = g(r).$$

According to the theory of integral equations, e.g. (37), the solution of this equation will be unique and continuous in the given interval if the eigenvalues of the homogeneous equation are not equal to the parameter λ. In our case the parameter λ is equal to -1. The homogeneous equation cannot have negative eigenvalues if the kernel $M(r,q)$ is positive definite (37). It can be shown that the latter is the case for our kernel as given by (2.3-17). This proof is carried out for a very similar kernel in the appendix of reference (38).

Solution of the Integral Equation

A closed form solution of equation (2.3-16) cannot be obtained because of its complicated kernel $M(r,q)$. However an asymptotic solution can be found for crack length over strip width ratios a/b which are small compared to unity. The big plate geometry with a small central crack is approached in the case of very small a/b ratios. Apart from its usefulness for this geometry the asymptotic solution will serve as a check for the numerical solution of the integral equation.

The function $\omega m(\omega)$ approaches zero rapidly as ω increases. The Bessel functions in the integrand of (2.3-17) which now contain the very small parameter a/b in their arguments can therefore be approximated by their series expansion for small arguments. The following approximate expression is obtained for the product of Bessel functions:

$$J_o(\omega qa/b)\, J_o(\omega ra/b) \cong 1 - \tfrac{1}{4}\left(\frac{a}{b}\right)^2 (r^2 + q^2)\,\omega^2 + \frac{1}{16}\left(\frac{a}{b}\right)^4 \left(\frac{r^2+q^2}{4} + r^2q^2\right)\omega^4 + \ldots \quad . \qquad (2.3\text{-}19)$$

Substitution of this expression into equation (2.3-17) results in individual terms which can be easily integrated in closed form over the interval $0 \leq \omega < \infty$. The kernel is then reduced to

$$M(r,q) = r\left[\left(\frac{a}{b}\right)^2 \frac{\pi^2}{4} - \left(\frac{a}{b}\right)^4 \frac{\pi^4}{96}(r^2 + q^2) + \left(\frac{a}{b}\right)^6 \frac{\pi^6}{2304}(r^2 + q^2)^2 + \ldots\right] . \qquad (2.3\text{-}20)$$

The method of repeated substitutions (39) can now be applied for the solution of the Fredholm equation. The result of this procedure is

$$Z(r) = r\sqrt{\frac{\pi}{2}}\left[1 - \tfrac{1}{2}\left(\frac{\pi}{2}\right)^2\left(\frac{a}{b}\right)^2 + \tfrac{1}{4}\left(\frac{\pi}{2}\right)^4\left(\frac{a}{b}\right)^4 \frac{7+2r^2}{6} - \frac{1}{8}\left(\frac{\pi}{2}\right)^6\left(\frac{a}{b}\right)^6 \frac{83 + 30r^2 + 6r^4}{54}\right] + 0\left[\left(\frac{a}{b}\right)^8\right] . \qquad (2.3\text{-}21)$$

The same answer up to terms of order $\left(\frac{a}{b}\right)^4$ was obtained by Lowengrub (40).

A numerical method is the only way in which a solution of equation (2.3-16) can be found for large a/b. The original integral equation is reduced to a system of algebraic equations by writing the integral in (2.3-16) as a sum (41). The elements of this sum are calculated by dividing the interval $0 \leq r \leq 1$ into N segments of equal length Δr and then applying some integration formula to each segment. The trapezoidal rule was used in this case. Solution of the system of equations by inversion of the coefficient matrix then supplies the values of Z(r) at the points of subdivision.

The direct numerical evaluation of the kernel M(r,q) requires very small steps in the integration scheme because of the rapid

oscillations of the Bessel functions as their arguments get large. Methods with the help of which time and accuracy can be gained in the numerical evaluation of integrals of this kind are discussed in (42). In the present case the integrand was approximated for large arguments ω by the appropriate approximations for the Bessel functions and by neglecting small terms in the function $\omega m(\omega)$. The integration of this approximation can be easily performed exactly over the interval $0 \leq \omega < \infty$. Rapid convergence of the numerical scheme is then achieved by subtracting the approximate expression from the original integrand and adding the integrated approximate expression.

Equation (2.3-17) then assumes the following form:

$$M(r,q) = \int_0^\infty \left[\omega m(\omega)\, J_o(\omega qa/b) J_o(\omega ra/b) - A(r,q,\omega)\right] d\omega + I(r,q) \qquad (2.3\text{-}22)$$

where $A(r,q,\omega)$ denotes the approximate expression for the integrand as ω becomes large and $I(r,q)$ stands for the integral of this expression. It is, in detail

$$A(r,q,\omega) = \frac{1+2\omega}{e^{2\omega}} \frac{4b}{\pi a} \frac{1}{\sqrt{rq}} \cos(\omega ra/b - \tfrac{\pi}{4}) \cos(\omega qa/b - \tfrac{\pi}{4})$$

and

$$I(r,q) = \int_0^\infty A(r,q,\omega)\, d\omega \,.$$

The modified integrand of equation (2.3-22) rapidly approaches zero as the integration variable increases thereby shortening the numerical procedure.

The numerical solution of the integral equation was first carried out by dividing the interval $0 \leq r \leq 1$ into ten equal parts. In order to check the convergence of the results the number of divisions was doubled. For $a/b = 8$ the first four significant digits - and more as the ratio of a/b becomes less than 8 - were found to agree in both cases. This agreement was considered good enough and the interval size was not further decreased.

The results of the numerical solution are graphically represented in Fig. 5. The function $Z(r)$ is smooth and monotonically increasing in the interval $0 \leq r \leq 1$. It becomes a straight line of slope $\sqrt{2/\pi}$ as a/b approaches zero.

As we shall see later, the behavior of stresses and displacements close to the crack tip is dominated by the value of the function $Z(r)$ at $r = 1$. The dependence of $Z(1)$ on the parameter a/b is shown in Fig. 6. $Z(1)$ approaches the value $\sqrt{2/\pi}$ as a/b tends towards zero. For $a/b > 1.5$ the values of $Z(1)$ based on the numerical solution of the integral equation become practically indistinguishable from the values given by

$$Z(1) = \sqrt{\frac{b}{2a}} \quad . \tag{2.3-23}$$

In the interval $0.5 < a/b < 1.5$ there is a small difference between the numerical result for $Z(1)$ and the value as given by (2.3-23). This difference is too small to show up in Fig. 6 but it becomes evident in Table I which contains values for $Z(1)$ in the interval $0 \leq a/b \leq 3.0$ as obtained from the numerical solution, from the asymptotic solution (2.3-21), and from equation (2.3-23).

An interesting feature of the stress intensity factor and fracture criterion in the interval $0.5 < a/b < 1.5$ results from this small difference between the actual value for $Z(1)$ and the value given by (2.3-23).

The ratio a/b was considered constant in the step load problem and entered only as a parameter. In the case of a moving crack, however, the crack length $2a$ changes with time and the dependence of the function Z on the ratio a/b will have to be considered. From now on we shall therefore write $Z(r, a/b)$.

Knowing the function $Z(r, a/b)$ we can proceed to calculate the desired quantities in the cracked strip.

2.4 Stress Intensity Factor and Fracture Criterion for an Elastic Strip

Although of no direct impact on the development of the viscoelastic problem, a few results which are of interest with regard to cracked elastic strips will be derived in this section.

Making use of equations (2.3-15,17,18) and formally substituting the appropriate expressions into the Laplace transforms of the displacements (2.3-12) and stresses (2.3-13) on the boundary $\eta = 0$ leads to the following equations

$$\bar{u}_\eta(\xi, 0, s) = \frac{2a\sigma_o}{s\,\bar{E}(s)} \sqrt{\frac{2}{\pi}} \int_\xi^1 \frac{Z(r, a/b)dr}{\sqrt{r^2 - \xi^2}} , \quad |\xi| < 1 \qquad (2.4\text{-}1)$$

$$\bar{\sigma}_{\eta\eta}(\xi, 0, s) = -\frac{a\sigma_o}{s}\sqrt{\frac{2}{\pi}} \int_0^\infty \omega[1+m(\omega b/a)] \cos(\omega\xi) \int_0^1 Z(r, a/b) J_o(\omega r) dr d\omega,$$

$$|\xi| \geq 1 \quad , \qquad (2.4\text{-}2)$$

where the integration formula

$$\int_0^\infty J_o(\omega r)\cos(\omega\xi)\,d\omega = \frac{1}{\sqrt{r^2-\xi^2}} \qquad \text{for } r > \xi > 0$$

was applied in the derivation of equation (2.4-1).

Young's modulus E for an elastic material is not a function of time and $\overline{E}(s)$ is simply replaced by E, a constant. The inverse Laplace transforms of (2.4-1) and (2.4-2) are then readily written down. They are

$$u_y^e(x,0) = 2a\,\frac{\sigma_o}{E}\sqrt{\frac{2}{\pi}}\int_{\frac{x}{a}}^1 \frac{Z(r,a/b)}{\sqrt{r^2-(x/a)^2}}\,dr\,, \quad |x| < a \qquad (2.4\text{-}3)$$

$$\sigma_{yy}(x,0) = -\sigma_o\sqrt{\frac{2}{\pi}}\int_0^\infty \omega[1+m(b/a)]\cos(\omega x/a)\int_0^1 Z(r,a/b)J_o(\omega r)\,dr\,d\omega,$$

$$|x| \geq a\,. \qquad (2.4\text{-}4)$$

Material properties do not enter the equation for the stresses because of the shear-free strip edges considered in this problem. The stresses given by (2.4-4) are therefore the same as for a viscoelastic strip. The displacements on the other hand involve Young's modulus and time will appear in the corresponding expression for a viscoelastic strip. In order to make a distinction between the elastic case and the viscoelastic one the superscript e was added to the symbol for the displacement.

The results just arrived at are also valid for a crack moving in an elastic strip as long as its speed of propagation is low enough to safely neglect inertia terms.

The normal displacements $u_y^e(x,0)$ of the crack surface in

the neighborhood of the crack tip are shown in Fig. 7. The contours presented there were obtained with the aid of the function $Z(r, a/b)$ and numerical integration of equation (2.4-3). The crack has a blunt front the radius of curvature of which increases with increasing crack length until it reaches a maximum somewhere between $0.5 < a/b < 1.5$. Then the radius of curvature decreases slightly and assumes an essentially constant value for $a/b > 1.5$. The theoretical value for the crack tip radius will be given a few pages later when the expression for the opening displacement close to the crack tip is derived. Figure 8 shows the normal stresses in the crack plane for two different a/b ratios. The stress distributions differ but little in spite of a considerable increase in crack size. For $a/b > 1.5$ the stress distribution becomes again essentially independent of crack length. The familiar stress singularity at the crack tip is also revealed in Fig. 8.

Stress Intensity Factor

Let us now consider the case of small a/b ratios. Under these circumstances we can make use of the asymptotic expansion for $Z(r, a/b)$, (2.3-21). Substitution of this expression into (2.4-4) and integration results in

$$\sigma_{yy}(x,0) = \sigma_o \frac{a}{\sqrt{x^2 - a^2}} \left\{ 1 - \tfrac{1}{2}\left(\frac{\pi}{2}\right)^2 \left(\frac{a}{b}\right)^2 + \frac{3}{8}\left(\frac{\pi}{2}\right)^4 \left(\frac{a}{b}\right)^4 - \frac{119}{432}\left(\frac{\pi}{2}\right)^6 \left(\frac{a}{b}\right)^6 + 0\left[\left(\frac{a}{b}\right)^8\right] \right\} \text{ for } \left(\frac{x}{a} - 1\right) \ll 1 , \quad (2.4\text{-}5)$$

where use was made of the fact that m(u) is a rapidly decreasing function. The product $P(u) = u[1 + m(u)]$ which assumes the value

2 for u = 0 therefore approaches rapidly P(u) = u as u increases. Employment of this asymptotic form makes the integration in closed form possible.

It is customary to characterize the stress singularity by means of a stress intensity factor. We shall use a nondimensional stress intensity factor K_n which is defined as follows:

$$K_n = \lim_{x \to a} \sqrt{\frac{x - a}{b}} \quad \frac{\sigma_{yy}(x, 0)}{\sigma_o} \quad . \tag{2.4-6}$$

If the limiting process is carried out for $\sigma_{yy}(x, 0)$ one obtains

$$K_n(a/b) = \sqrt{\frac{a}{2b}} \left\{ 1 - \tfrac{1}{2}\left(\frac{\pi}{2}\right)^2 \left(\frac{a}{b}\right)^2 + \frac{3}{8}\left(\frac{\pi}{2}\right)^4 \left(\frac{a}{b}\right)^4 - \frac{119}{432}\left(\frac{\pi}{2}\right)^6 \left(\frac{a}{b}\right)^6 + 0\left[\left(\frac{a}{b}\right)^8\right] \right\} \quad . \tag{2.4-7}$$

The first term of this series corresponds to Inglis's solution for the infinitely large plate with crack (32). The first two terms were also obtained by Knauss (31) by a different method.

In order to get the stress intensity factor for ratios of a/b greater than that covered by the asymptotic expansion we have to resort to the numerical solution for the function Z(r,a/b) as depicted in Fig. 5. Let us subdivide the interval $0 \leq r \leq 1$ into N equal parts as indicated in Fig. 9. Depending on the number of divisions the function Z can be arbitrarily well approximated by a straight line over each subdivision, that is

$$Z_n(r, a/b) = A_n(a/b) + B_n(a/b)r \quad \text{for} \quad r_{n-1} \leq r \leq r_n$$

where

$$A_n(a/b) = Z(r_{n-1}, a/b) - B_n(a/b)\, r_{n-1}$$

$$B_n(a/b) = \frac{Z(r_n, a/b) - Z(r_{n-1}, a/b)}{r_n - r_{n-1}}$$

and the subscript n indicates the n^{th} subdivision.

The integral over r appearing in equation (2.4-4) can now be represented by the sum of integrals over each subdivision. The result of this procedure is

$$\int_0^1 Z(r, a/b) J_o(\omega r)\, dr = \sum_{n=1}^{N} \int_{r_{n-1}}^{r_n} (A_n + B_n r) J_o(\omega r)\, dr$$

$$= \frac{1}{\omega} \sum_{n=1}^{N} \left[Z(r_n, a/b) J_1(\omega r_n) - Z(r_{n-1}, a/b) J_1(\omega r_{n-1}) \right.$$

$$\left. + 2A_n \sum_{m=1}^{\infty} 2m \left\{ \frac{J_{2m}(\omega r_n)}{r_n} - \frac{J_{2m}(\omega r_{n-1})}{r_{n-1}} \right\} \right] , \qquad (2.4\text{-}8)$$

where the infinite series enters because of

$$\int J_o(x)\, dx = 2 \sum_{m=1}^{\infty} J_{2m-1}(x) \quad .$$

Substituting (2.4-8) into equation (2.4-4) and performing the ω integration with the help of the same asymptotic behavior of $u[1+m(u)]$ for large u as discussed previously results in

$$\sigma_{yy}(x,0) = \sigma_o \sqrt{\frac{2}{\pi}} \sum_{n=1}^{N} \left[\frac{r_n \, Z(r_n, a/b)}{\sqrt{\left(\frac{x}{a}\right)^2 - r_n^2}\left[\frac{x}{a} + \sqrt{\left(\frac{x}{a}\right)^2 - r_n^2}\right]} - \frac{r_{n-1} \, Z(r_{n-1}, a/b)}{\sqrt{\left(\frac{x}{a}\right)^2 - r_{n-1}^2}\left[\frac{x}{a} + \sqrt{\left(\frac{x}{a}\right)^2 - r_{n-1}^2}\right]} \right.$$

$$\left. -2A_n(a/b) \sum_{m=1}^{\infty} \frac{(-1)^{2m-1}}{2m} \left\{ \left(\frac{r_n}{\frac{x}{a} + \sqrt{\left(\frac{x}{a}\right)^2 - r_n^2}} \right)^{2m} - \left(\frac{r_{n-1}}{\frac{x}{a} + \sqrt{\left(\frac{x}{a}\right)^2 - r_{n-1}^2}} \right)^{2m} \right\} \right] . \tag{2.4-9}$$

The first term of this series tends towards infinity as $x \rightarrow a$ and $n = N$. All other terms remain finite under all conditions because $x/a \geq 1$ and $r_n \leq 1$.

The stress intensity factor is easily obtained from (2.4-9) by application of definition (2.4-6),

$$K_n(a/b) = \sqrt{\frac{a}{b\pi}} \; Z(1, a/b) \quad . \tag{2.4-10}$$

It is seen that the behavior of the stresses in the immediate vicinity of the crack tip is characterized by the value of the function $Z(r, a/b)$ at $r = 1$. If one substitutes the asymptotic expansion for Z (2.3-21) into (2.4-10) there results the stress intensity factor obtained from the asymptotic expansion by different means (2.4-7).

The stress intensity factor for arbitrary values of a/b is plotted in Fig. 10 together with its values as given by the expansion for small a/b ratios and as given by the Inglis solution. It is seen that the asymptotic expansion for $K_n(a/b)$ holds up to $a/b \cong 0.35$ whereas the Inglis solution is only applicable up to $a/b \cong 0.1$.

An interesting feature revealed by Fig. 11 is the maximum of the stress concentration factor at $a/b \cong 0.75$. At this point K_n is about 1.5% higher than the constant value it assumes as $a/b \to \infty$. The consequence of this behavior with regard to crack propagation is discussed later in connection with the fracture criterion. For $a/b > 1.5$ the stress intensity becomes practically constant and assumes the value

$$K_n = \sqrt{\frac{1}{2\pi}} \quad .$$

This result agrees with the value obtained for a semi-infinite crack by means of an energy consideration as described in reference (43).

Failure Criterion

The crack displacements close to the tip are found in a way similar to the one which was taken to determine the normal stresses in this region. In this case, however, it suffices to approximate $Z(r, a/b)$ by a straight line segment close to $r = 1$ because the integration which is to be carried out, see (2.4-3), ranges over the interval $x/a \leq r \leq 1$ where $(1 - x/a) << 1$. The result of this operation is

$$u_y^e(x, 0) = \frac{\sigma_o}{E} \frac{4}{\sqrt{\pi}} \sqrt{\frac{a-x}{a}}\ a\ Z(1, a/b)$$

$$\text{for } \left(1 - \frac{x}{a}\right) << 1 \qquad (2.4\text{-}11)$$

Based on this equation the radius of curvature ρ^e at the crack tip is easily calculated to be

$$\rho^e(a/b) = a\,\frac{8}{\pi}\left(\frac{\sigma_o}{E}\right)^2 Z^2(1,a/b) \quad . \tag{2.4-12}$$

Knowing the stresses and displacements close to the crack tip we can now proceed to determine the crack energy. Substitution of (2.4-11) and of the stresses as found with the aid of (2.4-10) into equation (2.1-3) yields

$$\Delta E_c^e(a/b) = -2\pi\,\frac{\sigma_o^2}{E}\,K_n^2(a/b)\,b\,\Delta a \tag{2.4-13}$$

where Δa denotes a small virtual crack advancement.

A stationary crack becomes unstable when the energy released during a small increase in crack length Δa as given by the crack energy is greater than the energy necessary to create the new surface. This condition is expressed by equation (2.1-5). However dealing with a virtual crack motion we replace the time derivative by the derivative with respect to a. The instability condition thus reads

$$-\frac{\Delta E_c^e}{\Delta a} \geqslant \frac{\Delta D_s}{\Delta a} \quad . \tag{2.4-14}$$

With $\Delta D_s = 2S\Delta a$ and equation (2.4-13) one obtains

$$\frac{\sigma_o^2}{E}\,K_n^2\,b\pi \geqslant S \quad . \tag{2.4-15}$$

The critical load at which the crack becomes theoretically unstable is thus given by

$$\sigma_{o\ crit.} = \sqrt{\frac{S\,E}{\pi b\,K_n^2}} \quad . \tag{2.4-16}$$

This is the equivalent of the Griffith criterion which also gives the critical load for an infinitely large plate with crack under uniaxial tension (6). For that case one substitutes the value for the stress intensity factor as $a/b \to 0$ and

$$\sigma_{o\ crit.} = \sqrt{\frac{2SE}{\pi a}}$$

which is, as expected, the Griffith criterion for an infinitely large plate with pressurized crack of length 2a under plane stress conditions (44).

Figure 11 depicts the critical load as a function of a/b. Note the steep slope of this curve as a/b approaches zero. The consequence of this behavior is a very high acceleration rate for an unstable crack with an initial length such that $a/b < 0.1$.

The small minimum in the critical load at $a/b \cong 0.75$ reflects the maximum in the stress intensity factor at this point. This minimum means that a crack with an initial value of a/b in the neighborhood of $a/b = 0.75$ could extend a short distance and then come to rest again if the critical load $\sigma_{o\ crit.}$ for the particular initial crack length was carefully approached, that is if

$$\sigma_{o\ crit.min.} < \sigma_{o\ crit.} < \sqrt{\frac{2ES}{b}} \quad .$$

The upper bound of this inequality is given by the essentially constant critical load for $a/b > 1.5$. No experimental data are available against which this particular conclusion could be checked.

The other consequence of the minimum in the critical load with respect to a propagating crack with initial length such that

$a/b < 0.75$ is a deceleration of the crack after passage of the minimum. This deceleration period will last until the crack length is large enough, i.e., $a/b > 1.5$, to have the critical load remain constant with increasing crack size. This result agrees well with an experimental crack acceleration history presented in Fig. 11 of reference (19). This curve shows a velocity maximum for a crack length which corresponds to roughly $a/b = 1$. This particular behavior was as yet unexplained.

2.5. Crack Tip Displacements and Crack Energy for a Crack Propagating in a Viscoelastic Strip

The expressions for the stress intensity factor as derived in the last chapter for an elastic strip are directly applicable to a viscoelastic strip subject to the same boundary conditions. The displacements however will become functions of time which enter through the time dependent material properties.

Crack Tip Displacements

The Laplace transform of the normal displacements of the crack surface is given by equation (2.4-1) for a step load σ_o applied at time $t = 0$ and for constant crack length $2a$. The inversion of this expression is easily accomplished by introduction of the creep function $D_{cr}(t)$. The Laplace transforms of the creep function, of the relaxation function $E_{rel}(t)$, and of the time dependent Young's modulus are related as follows:

$$\overline{D}_{cr}(s) = \frac{1}{s^2 \overline{E}_{rel}(s)} = \frac{1}{s \overline{E}(s)} \quad . \tag{2.5-1}$$

The equation for the crack displacements in x,y,t-space then becomes

$$u_y^v(x,0,t) = 2a\,\sigma_o D_{cr}(t)\sqrt{\frac{2}{\pi}}\int_{x/a}^{1}\frac{Z(r,a/b)}{\sqrt{r^2-\frac{x^2}{a}}}\,dr \qquad (2.5\text{-}2)$$

$$\left.\begin{array}{l} \\ \\ \end{array}\right\} |x|<a.$$

$$\text{or} \qquad u_y^v(x,0,t) = D_{cr}(t)\,E\,u_y^e(x,0) \qquad (2.5\text{-}3)$$

The superscript v was introduced to distinguish this result from the corresponding expression for an elastic strip. E is a constant and stands for the Young's modulus of the material for which the elastic displacements u_y^e were calculated. It is seen that the time dependence of the displacements is completely contained in the creep function $D_{cr}(t)$ which is found by inversion of (2.5-1). The determination of this function will be discussed in part III of this thesis.

The response to an extending crack can be made up from a sequence of step loadings. For instance, at time $t = t_o$ a boundary segment of length $2a = 2a_o$ is loaded. A short time later at $t = t_1 > t_o$ the segments $a_o \geq |a| \geq a_1$ are loaded stepwise, etc. This scheme is illustrated in Fig. 12. By virtue of the first of equations (2.5-2) one thus obtains the following series for an extending crack with a = a(t):

$$u_y^{vp}(x,0,t) = 2\sqrt{\frac{2}{\pi}}\,\sigma_o\left[a_o\int_{x/a}^{1}\frac{Z(r,a_o/b)}{\sqrt{r^2-(x/a_o)^2}}\,dr\,D_{cr}(t-t_o)\right.$$

$$+\left\{a_1\int_{x/a_1}^{1}\frac{Z(r,a_1/b)dr}{\sqrt{r^2-(x/a_1)^2}} - a_o\int_{x/a_o}^{1}\frac{Z(r,a_o/b)dr}{\sqrt{r^2-(x/a_o)^2}}\right\}D_{cr}(t-t_1)$$

$$\left.+\ \cdots\cdots\cdots\right] \quad . \qquad (2.5\text{-}4)$$

where the additional superscript p was introduced in order to indicate that we are now dealing with the response to a propagating crack. The sum in this equation is replaced by an integral if the number of steps is imagined to approach infinity whereby the time difference between consecutive loadings tends towards zero, i.e., $t_i - t_{i-1} \to 0$. Assuming the crack to have zero length at time $t = 0$ equation (2.5-4) then reduces to the following convolution integral:

$$u_y^{vp}(x,0,t) = \int_0^t \frac{\partial}{\partial\tau}\left\{2\sqrt{\frac{2}{\pi}}\,\sigma_o\,a(\tau)\int_{x/a(\tau)}^{1}\frac{Z(r,a(\tau)/b)\,dr}{\sqrt{r^2-(x/a(\tau))^2}}\right\}D_{cr}(t-\tau)\,d\tau$$

or (2.5-5)

$$u_y^{vp}(x,0,t) = E\int_0^t \frac{\partial}{\partial\tau}\left\{u_y^e(x,0,a(\tau))\right\}D_{cr}(t-\tau)\,d\tau \quad .$$

The elastic displacement u_y^e becomes a function of time through the crack length $2a(t)$.

Partial differentiation yields the time derivative of the elastic displacement to be

$$\frac{\partial}{\partial t} u_y^e(x,0,a(t)) = \frac{\partial u_y^e}{\partial a} \frac{\partial a(t)}{\partial t} \quad . \qquad (2.5\text{-}6)$$

Differentiating equation (2.4-3) with respect to the half crack length a and using integration by parts leads to the following expression:

$$\frac{\partial u_y^e}{\partial a} = 2\sqrt{\frac{2}{\pi}} \frac{\sigma_o}{E} \left\{ \frac{Z(1,a/b)}{\sqrt{1-(x/a)^2}} - a \int_{x/a}^{1} \frac{\frac{\partial Z}{\partial a}(r,a/b)}{\sqrt{r^2-(x/a)^2}} \, dr \right.$$

$$\left. + \int_{x/a}^{1} \frac{Z(r,a/b) - r\frac{\partial Z}{\partial r}(r,a/b)}{\sqrt{r^2-(x/a)^2}} \, dr \right\} , \; 1 - \left|\frac{x}{a}\right| << 1 \; . \qquad (2.5\text{-}7)$$

The function $Z(r,a/b)$ and its derivatives with respect to r or a are all well behaved and the integrals in equation (2.5-7) give rise to finite terms for all values of $0 \leq x/a \leq 1$ and $0 \leq r \leq 1$. With respect to the determination of the crack energy we are only interested in the displacements in the immediate vicinity of the crack tip where $1 - \left|\frac{x}{a}\right| << 1$. The terms given as integrals in equation (2.5-7) become negligibly small compared to the first term in this case. We thus obtain for $1 - \left|\frac{x}{a}\right| << 1$

$$\frac{\partial u_y^e}{\partial a} = \frac{2}{\sqrt{\pi}} \frac{\sigma_o}{E} \sqrt{\frac{a}{a-x}} \; Z(1,a/b)$$

or by virtue of (2.4-10)

$$\frac{\partial u_y^e}{\partial a} = 2 \frac{\sigma_o}{E} \sqrt{\frac{b}{a-x}} \; K_n(a/b) \quad . \qquad (2.5\text{-}8)$$

Combining this expression with equation (2.5-6) and substituting into the second of equations (2.5-5) results in

$$u_y^{vp}(x,0,t) = 2\sigma_o \int_0^t \sqrt{\frac{b}{a(\tau)-x}}\, K_n\left(\frac{a(\tau)}{b}\right) \frac{\partial a(\tau)}{\partial \tau}\, D_{cr}(t-\tau)\, d\tau$$

$$\text{for } 1 - \left|\frac{x}{a(t)}\right| \ll 1 \quad . \qquad (2.5\text{-}9)$$

Restricting ourselves to cracks with constant speed of propagation v we have

$$a(t) = v\,t \quad .$$

With the constant velocity assumption and the change in variable

$$\zeta = v\,t$$

equation (2.5-9) can be simplified to the following form:

$$u_y^{vp}(x,0,v) = 2\sigma_o \int_x^{a_t} \sqrt{\frac{b}{\zeta - x}}\, K_n(\zeta/b)\, D_{cr}\left(\frac{a_t-\zeta}{v}\right) d\zeta$$

$$\text{for} \quad 1 - \left|\frac{x}{a_t}\right| \ll 1 \qquad (2.5\text{-}10)$$

where $a_t = v\,t$ stands for the crack length at time t. The lower limit x appears because $u_y^{vp} = 0$ for $t < \frac{x}{v}$.

The stress intensity factor K_n changes only little with ζ because $1 - \left|\frac{x}{a_t}\right| \ll 1$ and $x \leq \zeta \leq a_t$. For $a_t/b > 1.5$ it becomes essentially independent of crack length, see Fig. 11. Limiting our consideration to cracks for which $a_t/b > 1.5$ we can thus write

$$K_n\left(\frac{\zeta}{b}\right) = \sqrt{\frac{1}{2\pi}}$$

and equation (2.5-10) reduces to

$$u_y^{vp}(x,0,v) = 2\sigma_o K_n\left(\frac{a_t}{b}\right) \int_x^{a_t} \sqrt{\frac{b}{\zeta - x}}\, D_{cr}\left(\frac{a_t - \zeta}{v}\right) d\zeta$$

$$\text{for } 1 - \left|\frac{x}{a_t}\right| \ll 1 \quad . \qquad (2.5\text{-}11)$$

The displacements in the neighborhood of the crack tip as a function of crack propagation speed are shown in Fig. 13. The creep function employed in this numerical evaluation of equation (2.5-5) is discussed in part III of this thesis. The contours shown in Fig. 13 give the impression that the crack tip becomes sharp when the crack propagation speed is different from zero. The very tip is, however, still blunt. But its radius of curvature is considerably smaller than in the zero velocity case because of the generally large difference in the order of magnitude between the glassy modulus and rubbery modulus. For the material on which Fig. 13 is based the ratio between these two moduli is 1.5×10^2. The change in curvature associated with this change in material properties can be calculated with the help of equation (2.4-12); it amounts to roughly 2×10^4.

Crack Energy

The two quantities which are necessary for the calculation of the crack energy of a crack propagating in a viscoelastic strip are now available. Let us assume that the creep function is given in terms of a retardation spectrum L(t), that is (26)

$$D_{cr}(t) = \frac{1}{E_r} - \int_0^\infty L(\tau) \exp(-t/\tau)\, \frac{d\tau}{\tau} \quad . \qquad (2.5\text{-}12)$$

Substitution into equation (2.5-11) leads to

$$u_y^{vp}(x,0,v) = 2\sigma_o K_n(\frac{a_t}{b}) \int_x^{a_t} \sqrt{\frac{b}{\zeta - x}} \left\{ \frac{1}{E_r} - \int_0^{\infty} L(\tau) \exp(-\frac{a_t - \zeta}{v\tau}) d\tau \right\} d\zeta \ .$$

(2.5-13)

The order of integration may be interchanged, the inner integral can then be evaluated resulting in

$$u_y^{vp}(x,0,v) = 2\sigma_o K(\frac{a_t}{b}) \sqrt{a_t - x} \left\{ \frac{1}{E_r} - \int_0^{\infty} \frac{L(\tau)}{\tau} \sum_{\nu=0}^{\infty} \frac{\left[-2\frac{a_t - x}{v\tau}\right]^{\nu}}{(1;2;\nu+1)} \ d\tau \right\}$$

(2.5-14)

where $(1;2;\nu+1) = 1 \times 3 \times 5 \ldots\ldots (2\nu-1) \times (2\nu+1)$.

Substituting equation (2.5-14) and the stresses close to the crack tip as characterized by the stress intensity factor (2.4-10) into equation (2.1-3) yields

$$\Delta E_c^{vp} = 4K_n^2 \sigma_o^2 b \int_0^{\Delta a} \left\{ \frac{1}{E_r} \sqrt{\frac{\Delta a - \zeta}{\zeta}} - \int_0^{\infty} \frac{L(\tau)}{\tau} \sum_{\nu=0}^{\infty} \frac{(\frac{-2}{v\tau})^{\nu}}{(1;2;\nu+1)} \frac{(\Delta a - \zeta)^{\nu+\frac{1}{2}}}{\sqrt{\zeta}} d\tau \right\} d\zeta \ .$$

(2.5-15)

The order of integration can again be interchanged and the inner integral be evaluated. One thus arrives at

$$\Delta E_c^{vp} = -2\pi K_n^2 \sigma_o^2 b \left\{ \frac{\Delta a}{E_r} - \int_0^{\infty} \frac{L(\tau)}{\tau} \sum_{\nu=0}^{\infty} (\frac{-1}{v\tau})^{\nu} \frac{(\Delta a)^{\nu+1}}{(\nu+1)!} d\tau \right\} \ .$$

(2.5-16)

As far as the energy balance of a moving crack is concerned we are only interested in the rate of change of the crack energy. With the approximation

$$\Delta E_c^{vp} \cong \frac{\partial \Delta E_c^{vp}}{\partial \Delta a} \ \Delta a$$

and for constant crack speed v one obtains

$$\dot{E}_c^{vp} = -2\pi K_n^2 \sigma_o^2 b v \left\{ \frac{1}{E_r} - \int_0^\infty \frac{L(\tau)}{\tau} \exp\left(-\frac{\Delta a}{v\tau}\right) d\tau \right\} \qquad (2.5\text{-}17)$$

where the infinite series in (2.5-16) has been summed out after differentiation. The bracketed term in (2.5-17) is the value of the creep function at time $t = \frac{\Delta a}{v}$. The rate of change of the crack energy can thus be written as

$$\dot{E}_c^{vp} = -2\pi K_n^2 \sigma_o^2 b v \frac{273}{T} D_{cr}\left(\frac{\Delta a}{v a_T}\right) \quad . \qquad (2.5\text{-}18)$$

The temperature dependence of the creep function was additionally introduced in this equation. D_{cr} is now the creep function at absolute temperature $T = 273^{o}K$ and a_T is the time-temperature shift factor with respect to this temperature (45). The factor $\frac{273}{T}$ enters on the assumption that the temperature dependence of the modulus as predicted by the classical theory of rubber elasticity is also applicable for the creep function.

Equation (2.5-18) gives the crack energy as a function of material properties expressed by the creep function, as a function of crack propagation speed, temperature, and applied load. The length Δa is some kind of characteristic length a possible physical interpretation of which will be discussed in part IV of this thesis. It will be viewed as an additional material property necessary to characterize crack propagation in a viscoelastic material.

2.6. Relationships between Crack Propagation Speed, Load, Temperature, and Material Properties

The energy conservation equation (2.1-5) has to be satisfied for a propagating crack. The rate of change of energy dissipated by the creation of new surface is given by equation (2.1-6). Substituting this expression and the one for the crack energy as given by (2.5-18) into equation (2.1-5) results in

$$\pi K_n^2(a/b)\,\sigma_o^2\, b\, v\, \frac{273}{T}\, D_{cr}\left(\frac{\Delta a}{v a_T}\right) = S\, v \quad . \tag{2.6-1}$$

This equation has two solutions:

1. The trivial solution $v = 0$.
2. A velocity which is given implicitly by the condition

$$D_{cr}\left(\frac{\Delta a}{v a_T}\right) = \frac{1}{\pi}\,\frac{1}{b\sigma_o^2}\,\frac{S}{K_n^2(a/b)}\,\frac{T}{273} \quad . \tag{2.6-2}$$

The fracture criterion based on the rubbery modulus $E_r = 1/D_r$ of the material is given by

$$\sigma_{o\,crit.} = \sqrt{\frac{S\,E_r\,T}{\pi\, b\, K_n^2(a/b)273}} \quad . \tag{2.6-3}$$

In order to allow the crack to propagate the applied load σ_o has to be greater than $\sigma_{o\,crit.}$. The case $\sigma_o = \sigma_{o\,crit.}$ corresponds to an unstable equilibrium state. Let us write

$$\sigma_o = n\,\sigma_{o\,crit.} \tag{2.6-4}$$

where $n > 1$.

The factor n will be called load factor. Equation (2.6-2) reduces to the following form by virtue of this factor

$$n = \sqrt{\frac{D_r}{D_{cr}(\frac{\Delta a}{v\, a_T})}} \quad . \tag{2.6-5}$$

The load σ_o which has to be applied in order to enable the crack to propagate with constant speed v is given by this equation provided all the material properties entering it and equation (2.6-3) are known.

Let us now consider two different loads σ_{01} and σ_{02} which are applied at equal temperatures. The relation between these loads, respectively strains, and the corresponding propagation speeds is easily derived from (2.6-5), it reads

$$\frac{\epsilon_{02}}{\epsilon_{01}} = \frac{\sigma_{02}}{\sigma_{01}} = \sqrt{\frac{D_{cr}(\frac{\Delta a}{v_1 a_T})}{D_{cr}(\frac{\Delta a}{v_2 a_T})}} \quad . \tag{2.6-6}$$

A similar relationship between strains and temperatures can be derived for a fixed crack propagation speed. The following equation holds in this case:

$$\frac{\epsilon_{02}}{\epsilon_{01}} = \frac{\sigma_{02}}{\sigma_{01}} \frac{T_1}{T_2} = \sqrt{\frac{T_1\, D_{cr}(\frac{\Delta a}{v\, a_{T1}})}{T_2\, D_{cr}(\frac{\Delta a}{v\, a_{T2}})}} \quad , \tag{2.6-7}$$

where the elastic modulus is assumed to be directly proportional to

the absolute temperature (46).

The validity of these surprisingly simple relationships will be tested in part IV of this report. Experimental data will be compared to the predictions made on the basis of these equations and of the material properties for a particular polymer which will be presented in part III.

III. MECHANICAL CHARACTERIZATION OF SOLITHANE 50/50

The experimental determination of the material properties entering the relationships derived in part II will be described subsequently for a Polyurethane elastomer of the type used as a solid propellant binder. This material is commercially produced by the Thiokol Chemical Corporation and carries the trade name Solithane 113. A so-called Urethane Resin and Catalyst (manufacturer's designation) are the two components from which Solithane 113 can be relatively easily produced in the laboratory. Chemically the "Resin" is a trifunctional isocyanate which is the product of a reaction between Castor Oil and Tolylenediisocyanate (TDI). The "Resin" is liquid and chemically stable at room temperature. Urethane crosslinks are then introduced between the "Resin" chains by adding the "Catalyst" and curing the mixture at an elevated temperature. The "Catalyst" is a triol and consists essentially of Castor Oil. The "Resin-Catalyst" mixture flows easily and can be cast into molds without great difficulty. The "Catalyst" used for the production of Solithane 113 is Thiokol Urethane Resin Catalyst C113-300 and the "Resin" is Thiokol Solithane 113 Urethane Resin. The curing temperature is 165°C.

For the purpose of this investigation the material was cast into 12" x 12" sheets of 1/10" or 1/32" thickness. Ferroplates, which are normally used for the production of glossy photographic prints, served as mold surfaces and assured a high surface quality. The sheets were stored in a dry box after completion of the curing process of $1\frac{1}{2}$ hours at 165°C. Specimens with the desired

dimensions are easily cut from the sheets with the aid of a razor blade or similar tool. More information on the chemical aspects and the synthesis of Polyurethanes can be found in reference (47). A detailed description of the manufacturing facility in the GALCIT laboratory is given in (48).

Solithane is one of the contenders in a program conducted for the purpose of selecting a suitable standard viscoelastic material which would facilitate the compilation of experimental data and would provide a common test material for theoretical results in the field (49, 50). One of the advantages of Solithane is that the material properties can be changed over a wide range by varying the "Resin" to "Catalyst" ratio (25). The composition used for the present work is equivoluminal, that is equal volumes of "Resin" and "Catalyst" go into the final product, and will be designated as Solithane 50/50. Great care was taken in the production of the material in order to minimize the variation of material properties from batch to batch. A certain amount of scatter is, however, unavoidable and a quick mechanical characterization of each batch was carried out. The real and imaginary part of the shear modulus were calculated for this purpose from the time record of free torsional oscillations as measured with the help of a torsion pendulum (49). A deviation of $\pm 5\%$ from the mean was considered permissible and all other batches were discarded.

All the experiments to be described on the following pages were performed in a standard Instron testing mechine. This machine has constant extension rates ranging from 0.02 to 20.0

in/min and an automatic load and extension recorder built in. Tests at different temperatures were run with the aid of a temperature chamber which enclosed the test section of the Instron tester.

3.1. Uniaxial Stress-Strain Behavior

Some of the typical features of viscoelastic materials are exhibited in simple uniaxial tension tests. The classical theory of rubber elasticity predicts the following relation between stress and extension ratio (46)

$$\sigma = 2 C_1 (\lambda - \lambda^{-2}) \qquad (3.1\text{-}1)$$

where C_1 = temperature dependent material constant

λ = extension ratio = $1 + \epsilon$.

Equation (3.1-1) is based on the statistical theory of polymer networks and the following main assumptions are made in the course of its derivation:

a. The chain length distribution is Gaussian,

b. the chains are completely flexible, there are no chain entanglements, loose ends, etc.,

c. the internal energy does not change during the deformation, that is the network elasticity is entirely an entropy effect,

d. the deformation is affine.

The above stress-strain relationship for uniaxial tension corresponds to a stored energy function which involves only the first strain invariant, i.e.,

$$W_1 = C_1 (I_1 - 3) \qquad (3.1\text{-}2)$$

where

$$I_1 = \lambda_1^2 + \lambda_2^2 + \lambda_3^2$$

A material with this strain energy function is called a neo-Hookean material.

The response of most elastomers is not adequately described by equation (3.1-1) however. Mooney (51) and Rivlin (52) improved the agreement with experimental data by including the second strain invariant in the simplest possible way. The strain energy function reads in this case

$$W_2 = C_1 (I_1 - 3) + C_2 (I_2 - 3) \qquad (3.1\text{-}3)$$

where

$$I_2 = \lambda_1^2 \lambda_2^2 + \lambda_2^2 \lambda_3^2 + \lambda_1^2 \lambda_3^2 \quad .$$

This equation characterizes a so-called Mooney-Rivlin material. The stress-strain law for uniaxial tension of a material of this kind becomes

$$\sigma = 2 (C_1 + C_2/\lambda) (\lambda - \lambda^{-2}) \quad . \qquad (3.1\text{-}4)$$

The two constants C_1 and C_2 can be easily determined by representing experimental data in the form of a Mooney-Rivlin plot. The quantity $\sigma/(\lambda-\lambda^{-2})$ is plotted versus $1/\lambda$ in this case and a straight line results if the material obeys equation (3.1-4). The constants

are then readily calculated from the values at which the straight line intersects the normals on $1/\lambda = 0$ and $1/\lambda = 1$.

The Mooney-Rivlin plot is a convenient method of representing stress-strain data for elastomers because deviations from any of the two simple constitutive equations just discussed become immediately apparent.

The uniaxial tension tests with Solithane 50/50 were performed on ring specimens with an inner diameter of ca. 0.65", an outer diameter of ca. 0.75", and with a thickness of 0.1". These specimens were cut from 0.1" thick sheets with the aid of a special rotating cutting tool. The surfaces cut with this tool were not of the same high quality as the surfaces of the cast sheet but visual inspection of each specimen guaranteed a good degree of uniformity and helped to single out faulty specimens before the test was run. The dimensions of each ring were also measured with an optical comparator and the ring cross-section was calculated from the results of these measurements.

During a test a ring was stretched by two pins of 0.4" diameter which were separated at a constant rate. These pins were greased with Vaseline in order to lower the friction between the specimen and the pin during extension. It was found by Smith (53) that there is good agreement with stress-strain curves obtained from experiments with conventional dog-bone shaped specimens if the strain in the ring specimen is based on the inner diameter of the unstretched ring. That is

$$\epsilon = \frac{2\Delta l}{\pi D_i} \qquad (3.1\text{-}5)$$

where Δl = distance the pin traveled

D_i = inner diameter of the ring specimen.

The stress is calculated by dividing the force exerted on the pins by twice the cross-sectional area of the undeformed ring.

The results of these measurements for Solithane 50/50 are presented in Figs. 14, 15 and 16 for three different temperatures and ten different strain rates ranging over 3 decades. It is seen that for a temperature of 40°C (cf. Fig. 14) the material behaves very much like a neo-Hookean material. There do not seem to be any strong rate effects present because the data for all tested strain rates fall very close to a horizontal straight line. Only for small strains is there a considerable deviation which is partly blamed on some initial slack in the recording mechanism, however.

As the temperature decreases we find a marked increase in the stresses prior to failure, cf. Fig. 15 for a temperature of 20°C. This upswing is most pronounced for the highest strain rates. Rate effects obviously come into play at this temperature. Up to strains of about 100% the material response is still close to being neo-Hookean for all strain rates tested.

Figure 16 shows the Mooney-Rivlin plot for a temperature of -5°C. The strain rate with which the test is run is an important factor at this temperature and shape and position of the individual curve depend on it. Only the lowest strain rates yield a response

which resembles neo-Hookean behavior up to strains of roughly 100%. A threefold to fourfold increase in the stress is observed beyond this point until failure occurs. For strain rates of 0.9 min^{-1} and greater the curves exhibit a constant slope up to about 30% strain and more as the strain rate increases. This section of the stress-strain curve could therefore be represented by a Mooney-Rivlin equation with rate dependent constants. For strains greater than ca. 65% the stresses increase sharply again and reach values at failure which are several times larger than the stresses at strains smaller than 65%.

The graphs which were just briefly discussed show that the material cannot be represented by one of the classical constitutive equations over the whole range of temperatures and strain rates considered here. The increasing importance of rate effects as the temperature decreases is evident by comparison of Figs. 14, 15 and 16.

3.2. Uniaxial Failure Data

The failure data to be discussed in this section were obtained from uniaxial tension tests on ring specimens as they were described in the previous section. Stresses and strains at failure were calculated in the same manner as employed there. Because of the statistical nature of the failure process several tests were run for each temperature and strain rate and the data points shown in the graphs of this section represent the average value of four or more individual tests.

Figures 17 and 18 give, respectively, the failure strain and failure stress at temperatures ranging from -12.5°C to +40.0°C as a function of strain rate. Both strain and stress at failure increase considerably as the temperature decreases. The effect of the strain rate on the failure strain is strongest for temperatures above 0°C. On the other hand, the failure stress is more affected by the strain rate if the temperatures are less than 20°C.

The master curve for the failure strain as shown in Fig. 19 results from shifting the curves of Fig. 17 along the abscissa until a single continuous curve is obtained. The amount by which each curve has to be shifted with respect to the curve for the reference temperature determines the shift factor a_T which will be discussed in more detail in section 3.4.

It is seen from Fig. 19 that the failure strain conforms well with the time-temperature shift principle. Other investigators noted already that the stress at failure cannot be shifted as well into a single master curve (54). The same observation is made for Solithane 50/50. Figure 20 shows the stress at failure shifted by the same amounts as were necessary to produce a best fit master curve for the failure strain. It can be seen that there is good agreement at low strain rates but a considerable difference exists between the shifted curves for various temperatures at high strain rates.

The so-called failure envelope, that is a plot of stress at failure versus strain at failure, is shown in Fig. 21. Smith suggested that this envelope is a unique property of a viscoelastic material on the basis that it is independent of the deformation

history (5). Although it has been demonstrated that the failure envelope is not entirely independent of the loading history (55) a plot of this kind minimizes the influence of strain history. The failure envelope for Solithane 50/50 has the typical form for elastomers. The strain rate of a constant temperature test increases in counterclockwise direction. The failure strain goes through a maximum of 225% as the test temperature decreases.

3.3. Relaxation Data and Creep Function

The creep function $D_{cr}(t)$ plays an important role in viscoelastic crack propagation as the relationships derived in part II show. Equation (2.5-1) relates the Laplace transforms of the relaxation modulus $E_{rel}(t)$ and of the creep function. The basis of this relationship is a stress-strain law for uniaxial tension of the following type

$$\sigma(t) = \int_0^t E_{rel}(\tau) \frac{\partial \epsilon(\tau)}{\partial \tau} \, d\tau \qquad (3.3\text{-}1)$$

or

$$\epsilon(t) = \int_0^t D_{cr}(\tau) \frac{\partial \sigma(\tau)}{\partial \tau} \, d\tau \quad . \qquad (3.3\text{-}2)$$

If a step strain of magnitude ϵ_o is applied at time t = 0, equation (3.3-1) reduces to

$$\sigma(t) = \epsilon_o \, E_{rel}(t) \quad . \qquad (3.3\text{-}3)$$

Assuming the relaxation modulus to be known an integral equation for the creep function is readily obtained by inversion of the Laplace

transform of equation (2.5-1). This integral equation reads

$$\int_0^t D_{cr}(\tau)\, E_{rel}(t-\tau)\, d\tau = t \quad . \tag{3.3-4}$$

On the basis of equation (3.3-3) the relaxation modulus can be relatively easily determined experimentally although a true step strain history cannot be realized in an actual experiment. In our case ring specimens were stretched to roughly 5% strain at a constant rate of strain instead. The rise time necessary to reach this strain level was on the order of half a second. A period of 5 times the rise time was allowed to pass by before data were taken. The strain in the ring was calculated from an accurate measurement of the pin displacement by means of a cathetometer. The load which acted on the pins stretching the ring was recorded as a function of time. The stress is based on the cross-section of the unstretched ring. Knowing the time dependent uniaxial stress in the specimen the relaxation modulus is immediately given by (3.3-3).

Relaxation curves for several temperatures are presented in Fig. 22 as a function of time. The time scale spans roughly 3 decades which is about all that can be covered without making the experiment too time consuming. The full relaxation curve can be obtained from the individual curves of Fig. 22 by application of the time-temperature shift principle (56). Rather than employ the shift factor a_T as determined by the superposition of failure data we shall shift the individual relaxation curves such as to produce a best fit master relaxation curve and later compare the shift factors obtained by the reduction of these two different sets of data.

The master curve for the relaxation modulus is given in Fig. 23 for a reference temperature of $0^{\circ}C$. The data superpose well into a single curve. The large difference in the order of magnitude between the glassy and rubbery modulus should be noted. At a temperature of $0^{\circ}C$ the material reaches its long time equilibrium state essentially within a tenth of a minute. An increase in temperature reduces the relaxation time drastically as a look at the time-temperature shift factor, a_T, tells (cf. section 3.4 below).

Having determined the relaxation modulus experimentally we can find the creep function by numerically solving the integral equation (3.3-4). The method employed in this case is due to Hopkins and Hamming (57). The result of this calculation is shown in Fig. 24. For a comparison the function $1/E_{rel}(t)$ is included in this graph. The two curves have practically the same shape. They agree completely at long and short times and differ by at most half a time decade at intermediate times.

3.4. The Time-Temperature Shift Factor

It was observed by several investigators that the curves representing a certain time dependent response of a viscoelastic material as measured at various temperatures could be superposed into a single master curve by introducing a reduced time scale, see references (58,59,60) among others. As we saw from the presentation of failure data and relaxation data this so-called time-temperature superposition principle is also well observed in the

case of Solithane 50/50. The shift factor is denoted by a_T and a reduced time t_{red} is defined by it in the following manner

$$t_{red} = \frac{t}{a_T} \tag{3.4-1}$$

where t stands for the real time. The shift factor is always given with respect to a reference temperature at which it assumes the value 0. In the present investigation the reference temperature is chosen to be $T_{ref} = 273^{\circ}K$. The shift factor is positive for temperatures smaller than $T_{ref.}$ and vice versa.

The shift factor for Solithane 50/50 is shown in Fig. 25. Very good agreement between the values obtained by shifting different sets of experimental data exists. The shift factors for swollen Solithane 50/50 are of no interest in the context of this section and will be interpreted later.

Williams, Landel, and Ferry found that the shift factor for a great number of polymers is given by the following semi-empirical equation (45)

$$LOG_{10}\, a_T = \frac{-8.86\ (T - T_s)}{101.8 + T - T_s} \tag{3.4-2}$$

where the temperature T is expressed in degrees centigrade and where T_s is a temperature arbitrarily fixed to be $50^{\circ}C$ above the glass transition temperature T_g.

It is seen from Fig. 25 that in the temperature range from $-15^{\circ}C$ to $+25^{\circ}C$ the experimental data for Solithane 50/50 are well described by the WLF-equation with $T_s = 32^{\circ}C$. The latter corresponds to a glass transition temperature of $T_g = -18^{\circ}C$ which is in

very good agreement with the dilatometrically determined value of -18.5°C for Solithane 50/50 (61).

3.5 Swelling Properties

The volume of crosslinked polymers is considerably increased if the material is submerged in a suitable solvent. The structure or mechanical integrity of the material remains unharmed in the process. Only the sol, that is, uncrosslinked polymer chains contained in the material, will be largely dissolved under the influence of the solvent (62). The study of swelling properties of polymers and of their mechanical behavior in this state allows conclusions on their molecular structure and the calculation of network characteristics. The effect on the mechanical behavior is mainly a great reduction or even elimination of the rate dependence of the material response. The reduced internal viscosity is the motivation for our investigation of the properties of swollen Solithane 50/50.

The first step in an experimental program of this kind is the selection of a suitable swelling agent. The equilibrium swelling properties of a substance are characterized by its solubility parameter δ which is the square root of the cohesive energy density (CED). The latter is defined as the energy required to separate all the molecules of a substance from each other and is given by the ratio of the molar heat of vaporization over the molar volume. The solvents listed in Table II were selected as swelling agents for equilibrium swelling experiments with Solithane 50/50. All of

these solvents were poorly hydrogen bonded and together they span a wide range of solubility parameters as can be seen from Table II.

Small rectangular specimens were cut out of a sheet of cast Solithane 50/50. Their dimensions were roughly 3/4"x1/4"x1/32". Each specimen's length and weight were carefully measured with a travelling microscope and laboratory scale, respectively. The samples were then put in Petri dishes containing a particular solvent and the length of each specimen was measured at increasing time intervals. This measurement was again carried out with the help of a travelling microscope and the specimen remained submerged in the process. The experiment was performed at room temperature of about 23°C. Figure 26 gives the results of these measurements where the volume swelling ratio for two different swelling times is plotted versus the solubility parameter of the solvents.

The typical swelling behavior with a maximum of the volume increase for a particular solubility parameter is exhibited in this figure. On the basis of these results it was concluded that the solubility parameter for Solithane 50/50 is $\delta = 9.5\sqrt{cal/cm^3}$. This value is slightly less than the value of $\delta = 10.0$ which is reported in "Polymer Handbook" (63) for a Polyurethane rubber of unknown composition.

Another distinct maximum was found to exist in a preliminary test in which there was no attention paid to the nature of the solvents used as swelling agents. This maximum was located at $\delta = 12.1$ and the solvent was dimethylformamide, a moderately hydrogen bonded solvent. It seemed the maximum was shifted

towards higher values of the solubility parameter for this kind of solvent. Not enough data for the swelling ratio in moderately, or strongly hydrogen bonded solvents were collected, however, to confirm this observation.

The time required to reach equilibrium conditions depends of course on the volume of the dry specimen V_o, on the swelling agent, and on the temperature. For a volume of $V_o = 0.0068$ in^3 the equilibrium swelling time was less than 45 hrs. at 23°C for all solvents employed here. Only one hour was necessary for Toluene which has a low viscosity compared to other solvents. The dynamic viscosity of Toluene is 0.583 cP at 20°C and 0.316 cP at 80°C.

On the basis of this experiment Toluene was chosen for the further mechanical characterization of Solithane 50/50 in the swollen state. Toluene has a solubility parameter of $\delta = 8.9$ which is close enough to the same parameter for Solithane 50/50 to ensure a high degree of swelling without making the swollen material too difficult to handle as is the case at maximum swelling. The relatively low viscosity of Toluene is also a point in its favor particularly with regard to crack propagation tests. Furthermore it has manageable hazardous properties in the temperature range of interest here, that is in the range from -5°C to 50°C. Toluene has a boiling point of 110.8°C, a flash point of 4.5°C, and an autoignition temperature of 552°C (64).

After completion of the swelling measurements the samples were put in a vacuum vessel and dried at 50°C for several days.

This time was considered long enough to be sure that all solvent rests had evaporated from the samples. They were then weighed again and the sum of their weights was compared to the total weight before swelling. This way the sol-fraction in Solithane 50/50 was found to be 3.4 weight percent.

From the equilibrium swelling ratio and sol content together with the number of elastically effective network chains, which will be determined in the next section, we can calculate the polymer-solvent interaction parameter μ. This parameter is a measure of the energy difference between a solvent molecule immersed in the pure polymer and one which is surrounded by other solvent molecules of the same kind (65). We employ the modified Flory-Rehner equation for this calculation, which reads (66)

$$\nu'_e = -\frac{1}{V}\,\frac{\ell n(1 - v_2) + v_2 + \mu v_2^2}{g^{\frac{2}{3}} v_2^{\frac{1}{3}} - \frac{1}{2} v_2} \qquad (3.5\text{-}1)$$

where v_2 = polymer volume fraction in the swollen sample,

V = molar volume of the swelling agent at test temperature,

g = volume fraction of gel rubber $\cong 1.0$,

μ = polymer-solvent interaction parameter,

ν'_e = elastically effective network chains in moles per unit volume of unswollen polymer.

Inserting the known quantities into this equation yields for the polymer-solvent interaction parameter of the Solithane 50/50-Toluene combination the value $\mu = 0.453$.

3.6. Mechanical Characterization of Swollen Solithane 50/50

Solithane 50/50 becomes very brittle when swollen in Toluene and has to be handled with great care. Another experimental difficulty arises from the fact that Toluene evaporates rapidly from the surface of a swollen sample leading to the development of surface cracks within a short time after the sample is removed from the solvent bath. In order to circumvent these problems a tank device (cf. Fig. 27) was designed in which experiments on swollen specimens could be run while the specimen is completely submerged during the test.

The device consists of a tank the bottom of which is bolted onto the cross-head of the Instron testing machine. Front and rear walls of this tank are made of glass in order to be able to make photographical observations. Inside the tank is mounted a spring loaded, stainless steel jaw which holds the lower end of the specimen. The upper end of the specimen is held by a similar jaw which is free to move vertically on ball bearings which are guided by two stainless steel rods which are part of the tank structure. The position of the ball bearings is adjustable and parallelism of the jaws can be easily obtained by proper adjustment. The latter is important for the performance of crack propagation experiments in strip specimens which can be accommodated in the jaws up to a length of 6". The top jaw is connected to the Instron load cell. The arrangement just described allows the built-in load and displacement recording mechanisms and various cross-head speeds of the Instron tester to be used for experiments in the swollen state.

About three gallons of Toluene are required to fill the tank. The temperature of the Toluene can be easily changed within a certain range by installation of copper coils through which a cooled or heated mixture of water and Ethyleneglycol is pumped. This way the temperature can be varied from ca. $-5^{\circ}C$ to $+50^{\circ}C$ and can be kept constant within $\pm 1^{\circ}C$ at any desired level in this range.

Uniaxial Stress-Strain Behavior

We noted already in section 3.1 that the material response of Solithane 50/50 cannot be described adequately by the neo-Hookean or Mooney-Rivlin constitutive equation if the test temperature is about equal to or less than $20^{\circ}C$. The experiments on which Figs. 14, 15 and 16 are based were repeated for swollen Solithane 50/50. Ring specimens are not suitable under these conditions and dogbone shaped specimens were used instead. These specimens were punched out of cast sheets of 1/32" thickness. The cross-sectional area of these specimens was 0.35" x 0.044" in the swollen state and their effective length was experimentally determined and theoretically estimated to be 2.59". Punched out specimens gave the best surface smoothness compared to other techniques like milling or cutting. The surface quality of the surfaces produced by the punch was however not nearly as high as the quality of cast surfaces and every specimen was visually inspected to sort out faulty pieces with obvious surface defects.

The tests were run in the device just described at temperatures of $42^{\circ}C$, $19^{\circ}C$, $4^{\circ}C$, and $-2^{\circ}C$. The strain varied from 0.0077 to 7.7 min^{-1}. Figs. 28-31 contain the results of these tests in

the form of Mooney-Rivlin plots. Considering an experimental accuracy of about ±4%, which can be mainly contributed to friction in the ball bearings guiding the upper jaw, one sees that the uniaxial stress-strain behavior of swollen Solithane 50/50 is in good agreement with classical rubber theory. In other words the swollen material behaves neo-Hookean up to failure for all strain rates and temperatures investigated here. No reasonable explanation can be offered for the tendency of some data points, particularly at high strain rates, to fall considerably below the best fit straight line at small strains, that is for $1/\lambda$ close to unity. However it is believed that this effect is caused partly by some initial slack in the recording mechanism which becomes noticeable at high extension rates.

The remarkable feature of the behavior of swollen Solithane 50/50 under uniaxial tension as compared to the dry material is the fact that it is completely independent of the strain rate although the latter is changed by up to three decades. The data scatter does not exhibit any particular trend except for the already mentioned deviation at small strains. This result allows the conclusion that rate dependent friction forces in the material are largely removed by swelling. It also seems that the large discrepancy between classical theory and real response at temperatures equal to and less than $20^{\circ}C$ is due to the presence of rate dependent mechanisms in the material for which there is no allowance made by this theory. This disagreement is hence not caused by some inherent defect of the classical theory of rubber elasticity.

The coefficient C_1 appearing in equation (3.1-1) is given by classical theory (46,65) to be

$$C_1 = \tfrac{1}{2} R\, T\, \nu'_e\, v_2^{\frac{1}{3}} \qquad (3.6\text{-}1)$$

where T = absolute temperature,

R = universal gas constant,

ν'_e = number of elastically effective network chains in moles per unit volume of unswollen material,

v_2 = volume fraction of polymer in the swollen state.

According to equation (3.6-1) the coefficient C_1 is directly proportional to the absolute temperature. The following values for the quotient C_1/T were calculated from the data presented in Figs. 28-31,

T ^{o}K	C_1/T psi/^{o}K	
271	0.245	± 0.01
278	0.244	
292	0.247	
315	0.254	

The factor C_1 increases slightly more with increasing temperature than is predicted by the classical theory. Compared to the temperature dependence of the response of unswollen Solithane the agreement is very good, however.

Assuming a value of 0.25 psi/^{o}K for C_1/T, which corresponds roughly to a temperature of 23^{o}C and a Young's modulus for

small strains of 444 psi, one can calculate the number of elastically effective network chains from equation (3.6-1). This calculation yields $\nu'_e = 5.78 \times 10^{-4}$ moles per milliliter of unswollen Solithane 50/50.

Failure Data

A collection of average strains at failure of swollen Solithane 50/50 under uniaxial tension is given in Fig. 32. The strain is based on the dimensions of the unswollen, unstretched specimen in this case in order to make the comparison with similar data in the unswollen state easier. Each point in this plot represents the average of three or more tests. The data are rather widely scattered and only a slight trend towards higher failure strains can be detected as the strain rate increases in spite of the change of the latter by a factor of 1000. This behavior is the same for the three temperatures for which failure data were collected and underlines the practically complete absence of rate effects in the swollen state which was already observed in the stress-strain relationship. A comparison of Fig. 32 with Fig. 17 again reveals the striking difference between swollen and dry Solithane 50/50 with respect to the rate dependence.

Figure 33 is a plot of the stress at failure versus $\lambda - \lambda^{-2}$ at failure. The data points are in this case closely and evenly scattered around a straight line with a slope of 137 psi. The slope is equal to $2C_1$ and the reference temperature is $T = 273^{\circ}K$. The quotient C_1/T as calculated from this plot is hence $C_1/T = 0.2507$ psi/$^{\circ}$K which is in good agreement with the value as obtained previously from stress-strain curves. This figure confirms the statement

which was already made at an earlier point that swollen Solithane 50/50 behaves up to failure like a neo-Hookean material.

3.7 Crack Propagation and Surface Energy

The fracture criterion (2.6-3) establishes a relationship between the surface energy S and basic material parameters which can be directly determined by experiment. The important factor in this equation is the critical load $\sigma_{o\,crit}$ or critical strain $\epsilon_{o\,crit}$, respectively. In order to measure either of these two values accurately the load factor n, cf. section 2.6, should be unity. The initial crack becomes theoretically unstable at this point and begins to propagate. For materials without substantial dissipation the point of instability is easily recognized in an experiment because the crack extends rapidly once it becomes unstable. For highly viscoelastic materials on the other hand the speeds of crack propagation can be extremely low and the minimum stress or strain necessary to make the transition from a stable to an unstable crack possible is difficult to define. Figure 37, which shows crack propagation speeds for Solithane 50/50 in a narrow strip as a function of applied gross strain ϵ_o, illustrates this situation. Imagine the solid curves to be erased in this plot. One is then tempted to draw straight lines through the experimental data. From these straight lines one then concludes that even smaller rates of propagation could be obtained if one could muster enough patience upon lowering the strain further. There thus appears to be no obvious lower bound for the critical strain.

In order to take some of the uncertainty out of the experimental determination of the surface energy of a highly viscoelastic

material use was made of the fact that the internal viscosity of the material is largely removed in the swollen state (cf. section 3.6). The material behaves like a brittle material under these conditions and the point of crack instability is better defined. The energy S which is required to break the bonds penetrating a unit area is assumed to be unaffected by the presence of the swelling agent. The only difference is then a reduction in the number of bonds per unit area which is caused by swelling the material.

The geometry which was chosen for the experimental determination of the surface energy under these conditions was a narrow strip of 5 1/2'' length, 1'' width, and 0.045'' thickness in the swollen state. A crack of 1'' length was cut along the center line at one of the narrow edges of the strip. The ratio of crack length to strip width is large enough so that the stress field around the crack tip is equal to that of an infinitely long strip with semi-infinite crack (19). The specimens were prepared completely in the dry state and then put in a Toluene bath for a day or longer before the tests were run in the device described above. The test consisted of displacing the strip edges with a constant rate until the initial crack became unstable. Load and displacement were measured in the process with the help of the built-in Instron recorders.

The point of crack instability manifested itself as a sharp break in the load-displacement curve. There was no ambiguity in the definition of this point on the graph. The displacement of the strip edge was on the order of only 0.02'' and an independent measurement of this quantity was carried out as a check on the Instron

measurement and on the parallelity of the two jaws. The displacements at both ends of the jaws were measured with the aid of two linearly variable transformers. There was consistent agreement between all values for the displacement.

Speed of Crack Propagation

Solithane 113 is a very transparent material and especially in the swollen state it can hardly be distinguished from the Toluene surrounding it. Polarized light was therefore used to make the crack tip visible. Only one fringe formed at this point because of the low overall strain level and because of the small sheet thickness. This was no disadvantage, however, because the fringe was only used to mark the position of the crack tip. The time history of this position was recorded on film by means of a Magnifax high speed motion picture camera with a maximum frame rate of about 3200 frames/sec. The film speed could be accurately determined with the help of timing marks on the film and the crack propagation speed was readily calculated from the knowledge of crack tip position and elapsed time.

After the crack passed through an acceleration stage of varying length it propagated at constant speed until it came into the vicinity of the opposite specimen edge. The length of the acceleration period depended on the test temperature and the strain at which the crack became unstable. Increasing temperatures or strains shortened the acceleration time which was about 400 msec long for a temperature of $4^{o}C$ and a strain of 2.15%. For the highest test temperature of $42^{o}C$ the acceleration period was extremely short and hardly recognizable.

In Fig. 34 the gross strain ϵ_o on the strip is shown in relation to the constant crack propagation speed v at the end of the acceleration period. A comparison of this plot with Fig. 37 which contains corresponding data for unswollen Solithane 50/50 shows that the speed of propagation is orders of magnitude higher in the swollen material and a lower bound of the critical gross strain $\epsilon_{o\ crit.}$ will therefore be easier to define.

The curves drawn through the isothermal data points of Fig. 34 have the same shape and can be superposed by shifting them along the abscissa. The shift factor resulting from this operation is plotted in Fig. 25. It is orders of magnitude smaller than the shift factor for the dry material.*

Surface Energy

For the calculation of the surface energy S via the fracture criterion (2.6-3) we are interested in the lowest strain which has to be put on a strip specimen in order to make an initial crack unstable. We eliminated one of the reasons which complicated the definition of a lower bound of this critical strain by swelling the material. There is however another factor which causes some variation in the magnitude of the experimentally determined strain at the point of instability. This variation is caused by the uncertain microscopical shape

* The fact that the shift factor does not vanish completely in the swollen state indicates that the internal viscosity is not entirely removed by swelling. The great difference in the value for the shift factor in the swollen and dry material, however, verifies the large reduction in internal viscosity which was already concluded from other experimental data (cf. section 3.6).

of the crack tip. The fracture criterion (2.6-3) was derived for a mathematically sharp crack which can be only approximately realized by cutting the material with a tool of finite dimensions. The actual stress intensity factor is therefore smaller than the theoretically calculated value and the critical strain is in turn higher than in the ideal case. Apart from possible defects which were already in the material or which were introduced by cutting the material the critical strain for an ideal crack is thus given by the lower bound of the critical strains measured in a series of experiments.

A collection of gross strains ϵ_o on the strip as measured at the point of instability is given in Fig. 35. The tests were run at different temperatures and strain rates and a slight tendency towards higher ϵ_o with increasing strain rate is apparent in this figure. The temperature on the other hand does not seem to have any effect on ϵ_o.

Discarding the very lowest recorded strains as possibly caused by faulty specimens we place the lower bound at $\epsilon_{o\ crit} = 0.0175$. A large number of points falls right on this mark or only slightly above it. Knowing the stress-strain relationship which is independent of time for the swollen material we can calculate the critical load from this information and obtain the surface energy via the fracture criterion.

The fracture criterion as given by equation (2.6-3) was derived by considering a strip with shearfree edges. However in order to adjust this criterion to the clamped edges of the experimental geometry we only have to insert the proper value for the

stress intensity factor. It can be easily shown (43) that the stress intensity factor for a semi-infinite crack in a strip with clamped edges differs only by a factor of $(1-\nu^2)$ from the intensity factor for a strip with the same dimensions but shearfree edges. For a temperature of 273°K the fracture criterion for our experimental situation then reads

$$\sigma_{o\,crit} = E\epsilon_{o\,crit} = \sqrt{\frac{2SE}{b(1-\nu^2)}} \quad . \tag{3.7-1}$$

The material behavior of a neo-Hookean material under uniaxial stress is adequately described for small strains by a Young's modulus which is equal to $E = 6\,C_1$. In the case of swollen Solithane 50/50 we thus find $E = 402$ psi for 0°C. The strip width is $2b = 1''$ and Poisson's ratio is assumed to be $\nu = 0.5$.*

Substituting all known quantities we can solve equation (3.7-1) for S. The result is $S = 2.31 \times 10^{-2}$ lbs per inch of the swollen

*The assumption of incompressibility in the swollen state is not as poor as it appears to be at first sight. Classical rubber theory (46) shows that a strained body can actually absorb more liquid than the unstrained body at the same temperature. The diffusion process involved in reaching a new swelling equilibrium requires however considerably more time than the 20 sec which were necessary to stretch the strip up to the point of crack instability. In order to check this behavior swollen dogbone shaped specimens were held at a constant strain of ca. 3% and the decrease in the load required to maintain this strain was observed. The time which elapsed until a new equilibrium state was reached and the amount of stress relaxation were essentially independent of temperature. This behavior was attributed to a slow increase in volume due to additional swelling in the strained state. About 30 minutes were necessary to reach the new swelling equilibrium although the volume of the dogbone shaped specimen was only about 25% of the volume of the strip specimen used for crack propagation tests.

material. Taking the linear swelling ratio of 1.39 for the Solithane 50/50-Toluene combination into account we obtain the following value for the surface energy of dry Solithane 50/50

$$S = 3.21 \times 10^{-2} \text{ lbs/in.}$$

This value is about an order of magnitude larger than the value for glass. Griffith (6) reports for the latter an extrapolated value of 0.31×10^{-2} lbs/in at room temperature.

All material properties entering the relationships derived in part II are now determined except for the characteristic length Δa. Since we are not absolutely sure about the physical interpretation of this length (cf. part IV) we have no other choice but to wait until theory and experiment are to be compared and then find the value of Δa which gives the best agreement. This comparison is the subject of part IV.

IV. COMPARISON BETWEEN THEORY AND EXPERIMENT

Experimental Data

Knauss (22, 67) measured equilibrium crack propagation speeds for Solithane 50/50 in strip specimens. The latter had a thickness of 0.1'', a width of 1 3/8'', and a length of about 10''. An initial crack of ca. 1 1/2'' was cut along the strip center line at one of the narrow edges. The stress field around the crack tip was thus ensured to be essentially independent of the crack length and a constant rate of crack extension could be expected as soon as the gross strain ϵ_o applied on the specimen was greater than the critical strain. The strain ϵ_o was reached in an almost stepwise manner within 15 msec and was held constant thereafter. The stable speed of crack propagation for a particular ϵ_o was unaffected by the strain history leading to ϵ_o as the results of similar experiments with a small, constant strain rate for $\epsilon < \epsilon_o$ have shown. The experimental data shown in Fig. 37 are the result of these measurements and were taken from references (22, 67). This graph gives the stable speed of crack propagation v as a function of applied strain ϵ_o and of the test temperature T.

Without any theory available at the time when these tests were performed the experimental results seemed to suggest that there is a power law relationship between velocity and gross strain, that is (22)

$$v \sim \exp\left(-\frac{\hat{E}}{kT}\right)\left(\epsilon_o - \epsilon_{o\,crit}\right)^m$$

where k = Boltzmann's constant

$\hat{E}$ = a characteristic energy

m = a dimensionless number $\cong 0.3$.

Although this empirical relationship yields a good agreement with the experimental data we shall see that it may not be the correct theoretical interpretation of these measurements.

The change of speed of propagation v over several decades depending on the magnitude of the applied strain should be noted. Also, the similar shape of the curves which could be drawn through isothermal data points suggests the applicability of the time-temperature superposition principle. The shift factor a_T as obtained by shifting these curves in the familiar way into a single master curve is plotted in Fig. 25. It is seen that it conforms well with the shift factors determined by superposing other experimental data.

Theoretical Relationship between Velocity, Strain, and Temperature for Solithane 50/50

Equation (2.6-2) which was derived in part II of this thesis gives the speed of crack propagation implicitly as a function of the gross strain $\epsilon_o = \sigma_o/E_r$ and of the material properties. This relation was derived for a strip with shearfree edges but it is assumed to hold in the case of clamped strip edges as well if the appropriate value for the stress intensity factor K_n is inserted. For an infinitely

long, clamped strip containing a semi-infinite crack the stress intensity factor is (24) $K_n = \sqrt{(1 - \nu^2)/2\pi}$. As mentioned previously the experimental crack length over strip width ratio was chosen large enough to make the stress field around the crack tip essentially equal to the one around the tip of a semi-infinite crack, cf. reference (23). Equation (2.6-2) modified for our experimental situation thus reads

$$D_{cr}\left(\frac{a}{v\, a_T}\right) = \frac{T}{273}\,\frac{1}{E_r^2 \epsilon_o^2}\,\frac{2}{(1 - \nu^2)}\,\frac{S}{b} \quad . \tag{4-2}$$

The two equations, (2.6-6) and (2.6-7), are unaffected by the change from shearfree to clamped edges because they do not involve the stress intensity factor.

We recall that equation (4-2) is the energy conservation equation (2.1-5) for our particular geometry. The two sides of this equation, that is the rate of change of the crack energy $\dot{E}_c$ and the rate of change of the surface energy $\dot{D}_s$, are plotted in Fig. 36 for Solithane 50/50 as a function of crack speed v and load factor n. This plot is valid for a temperature of 273°K but similar plots for other temperatures are readily obtained by application of the time-temperature superposition principle.

The material properties of Solithane 50/50 as discussed in part III were used for the calculation of the curves in Fig. 36. The characteristic length Δa was taken to be equal to 10^{-8} inches. This value yields the best agreement between theoretical prediction and experimental result as we shall soon see. The order of magnitude of the characteristic length seems to be too small to be acceptable

for a continuum theory. Instead of trying to give this length some direct physical meaning it might therefore be more correct to interpret it in connection with some wave speed c of the material. A characteristic time $t_{char.} = \Delta a/c$ would then have to be considered as the new material property. Possibly Δa has to be interpreted as the thickness of a filament at the crack tip which is essentially under uniaxial tension and which breaks abruptly once a certain critical condition is reached. On a microscopic scale the crack would then have to be pictured as propagating in a stepwise manner from filament to filament each of which is stretched with a rate which is directly proportional to the macroscopic rate of crack propagation. The idea that there is a region of constant tensile stress at the very crack tip has already been suggested by Williams, Blatz, and Schapery and a theory of crack propagation in a Voigt solid has been worked out on this hypothesis (68). Bueche and Halpin (20) utilized the same idea to develop a molecular theory for the tensile strength of elastomers. They make the statement that this filament is very thin and measures perhaps 1 to 100 Å. The value of Δa = 2.5 Å falls right into the range suggested by them intuitively. In the course of development of the Bueche-Halpin theory the thickness of this filament is absorbed in some other constant which is determined by finding the value which gives the best agreement between theory and experiment.

The rate of change of the surface energy is represented by the solid line of constant slope in Fig. 36. The broken curves depict the rate of change of the crack energy for various load factors n.

The non-trivial solution of the energy conservation equation which yields the stable crack propagation speed for a certain load factor is given by the intersection of the solid line with the appropriate broken curve. This graph illustrates how strongly the speed of propagation depends on the load factor, that is on the applied strain ϵ_o in our case. An increase of the latter by a factor of ten involves a theoretical change in crack speed by a factor of about 10^5. It is also seen that the two curves become tangent as the load factor approaches $n = 1$. They do not intersect for $n < 1$, in other words the crack is stable under these circumstances and does not propagate at all. As the load factor becomes large the two curves become tangent again. For load factors greater than the value corresponding to this situation the crack propagates theoretically in a material with Young's modulus equal to E_g. The creep behavior of the material is of no importance any more in this case and the crack will accelerate up to a velocity at which inertia effects control the crack propagation process.

Instead of the graphical solution just discussed we can solve equation (4-2) directly for the strain ϵ_o if the velocity v is given. Equilibrium crack propagation speeds calculated in this manner are shown in Fig. 37 as a function of applied strain and temperature. The temperatures range from 0^oC to 50^oC and the corresponding experimental data are included in this plot. The agreement between theoretical and experimental results is very good except for the lowest temperature. The value of the creep function at very short times is important in this case which in turn is dependent on the relaxation modulus for very short times. The latter is difficult to

determine accurately by experiment, however, and the greater disagreement between crack propagation theory and experiment might be attributed to this difficulty.

Figure 38 contains the same experimental data in the form of a master curve at temperature T = 273°K. This data reduction is readily accomplished by application of equation (2.6-7). This graph shows very good agreement between experimental evidence and theoretical expectation over the whole range of crack velocities of about 6 decades.

The agreement between theory and experiment is surprisingly good considering the fact that the derivation of the theoretical relationships was based on the linear theory of elasticity and that the problem was idealized to be two-dimensional.

Conclusions

The important points may now be summarized as follows:

1. The relationships given in section 2.6 describe the typical features of slow, stable crack propagation in a strip of viscoelastic material.
2. Except for the so-called characteristic length Δa all material properties entering these relationships are obtained from tests other than crack propagation tests.
3. An additional material property which is called characteristic length Δa is necessary to describe the crack propagation process in a time dependent material. This length may be interpreted as the thickness of a filament which is essentially in a state of uniaxial tension at the tip of the crack.

4. The creep function (i.e., the viscous energy dissipation in the material) controls the crack propagation speed in a viscoelastic material.

5. The applicability of the time-temperature superposition principle to viscoelastic crack propagation data is theoretically and experimentally verified. The shift factor is the same as the shift factor for other time dependent material responses.

6. The shorter the relaxation process is in a material the higher the crack propagation speed has to be in order to be affected by the time dependent material properties. Materials which do not exhibit any measurable rate dependence at normal laboratory loading rates may have an extremely short relaxation time, which is brought out only at high crack speeds with correspondingly high loading rates at the crack tip. Viscous dissipation may then come into play and cause a limiting crack velocity which is smaller than the one which could be expected if inertia forces alone controlled the process.

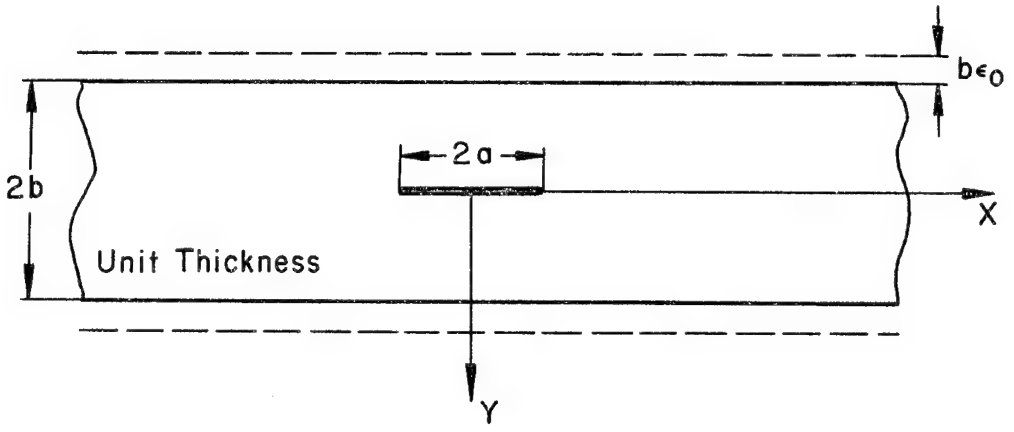

FIG. 1 STRIP GEOMETRY

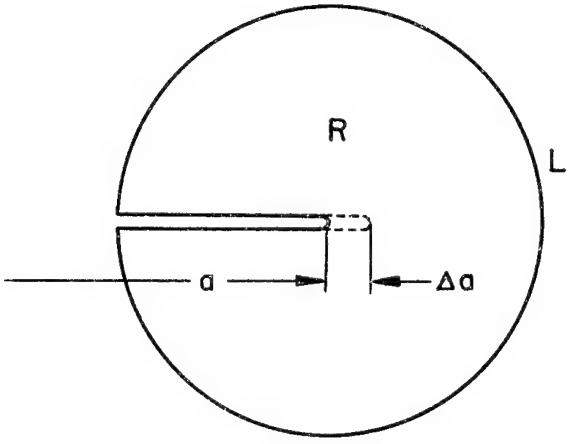

FIG. 2 CONTROL VOLUME

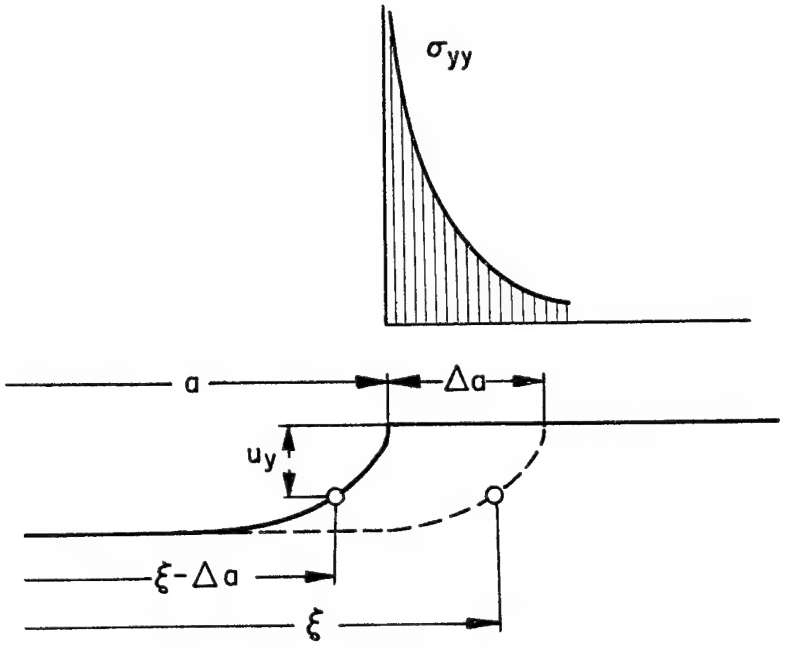

FIG. 3 CRACK OPENING

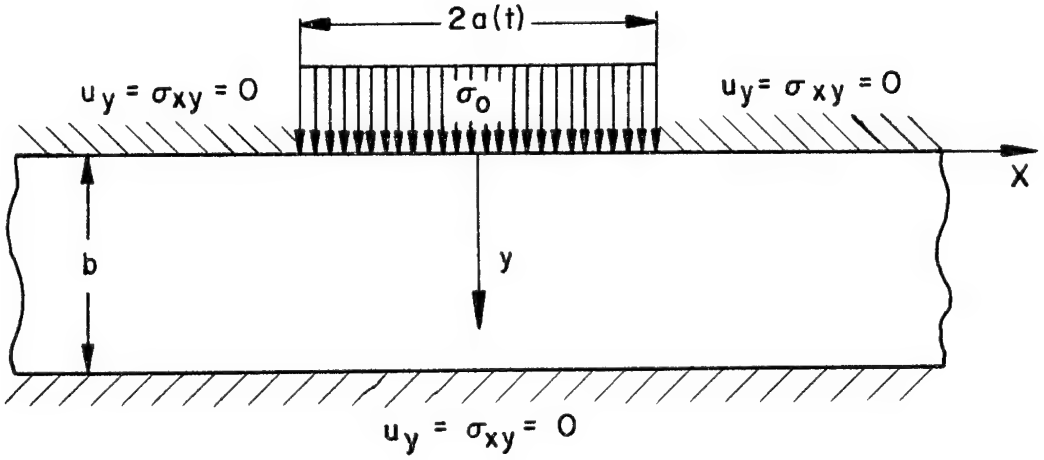

FIG. 4 HALF STRIP GEOMETRY

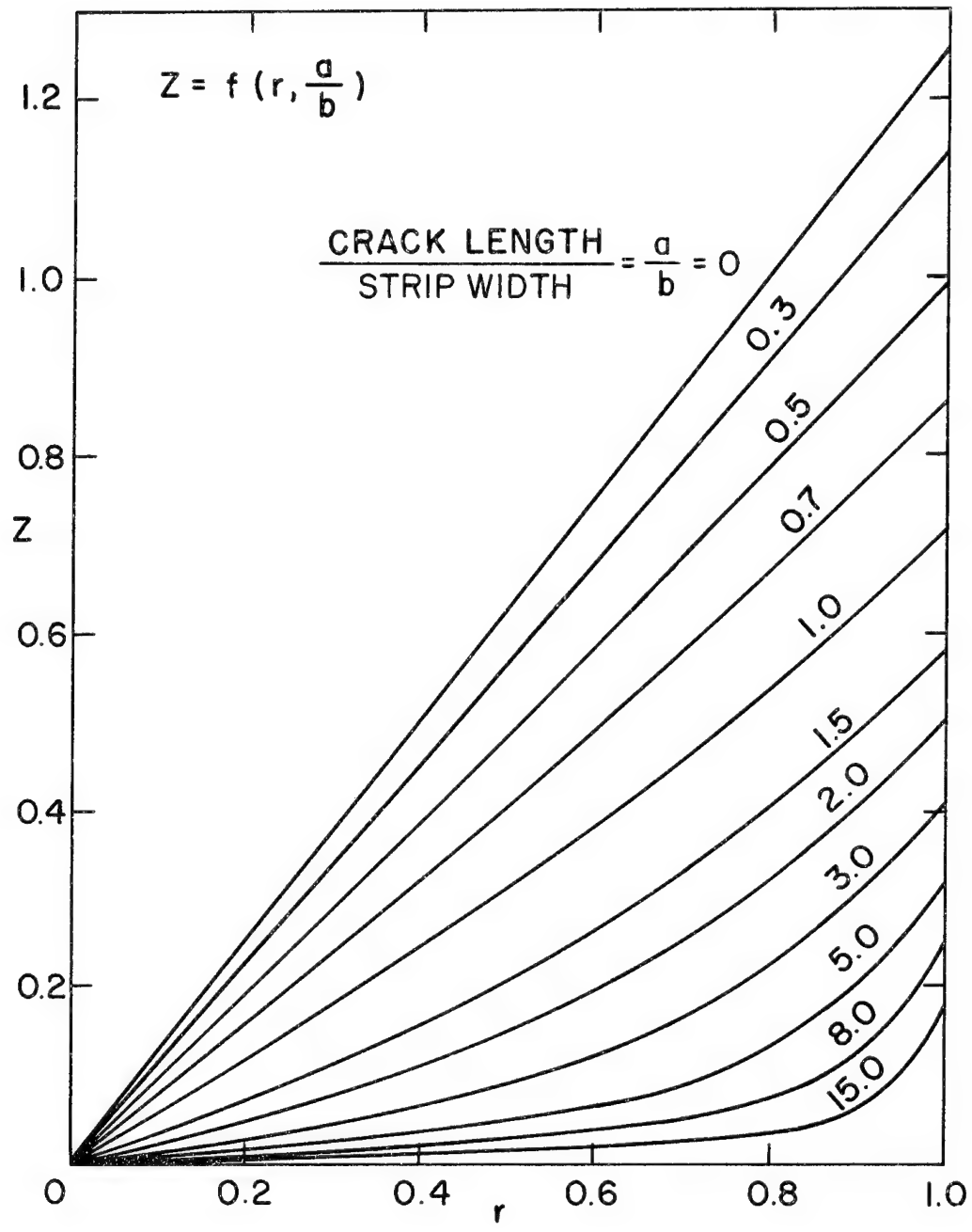

FIG. 5 SOLUTION OF THE FREDHOLM INTEGRAL EQUATION

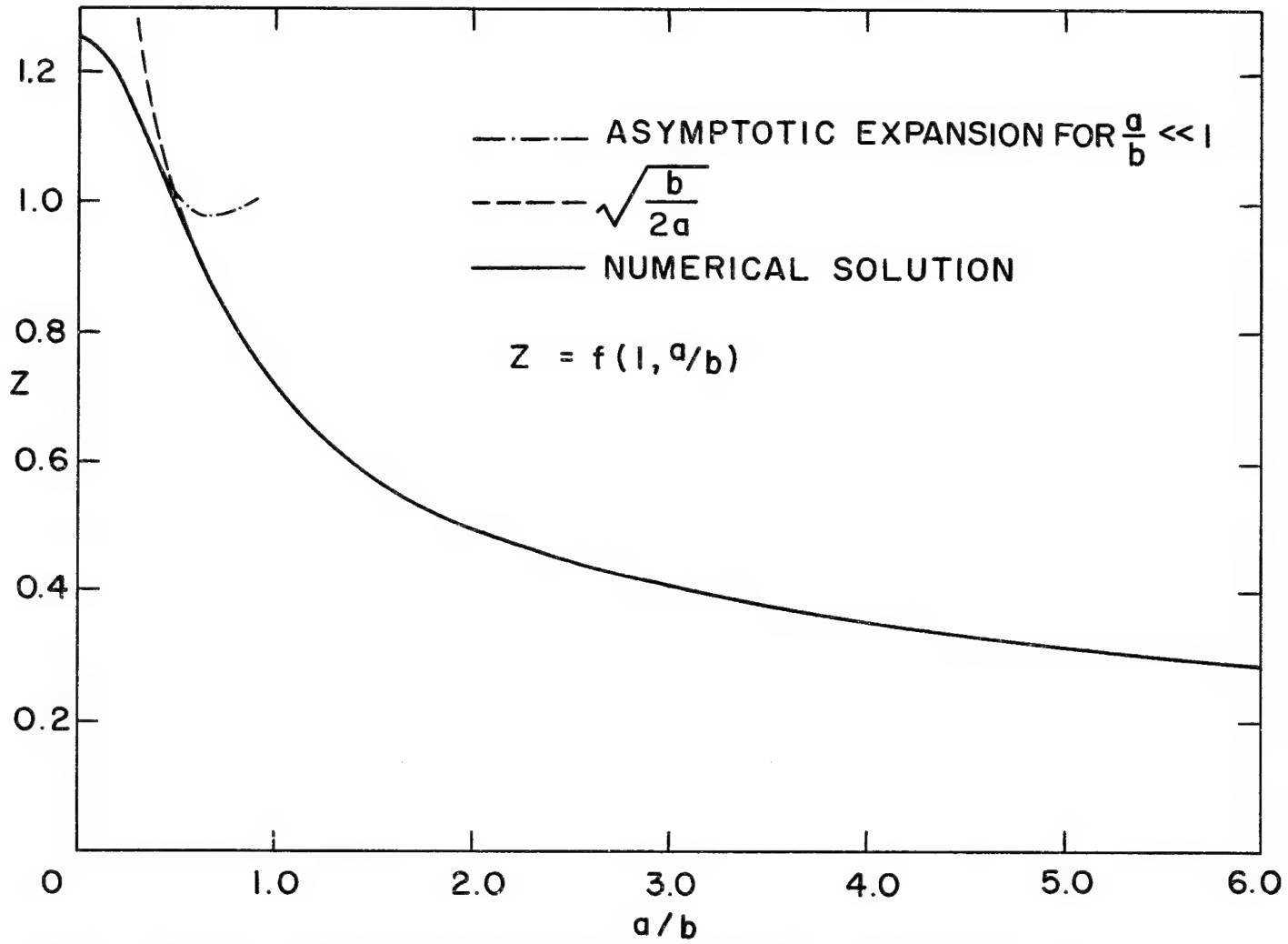

FIG. 6 Z(I) AS A FUNCTION OF CRACK LENGTH OVER STRIP WIDTH RATIO

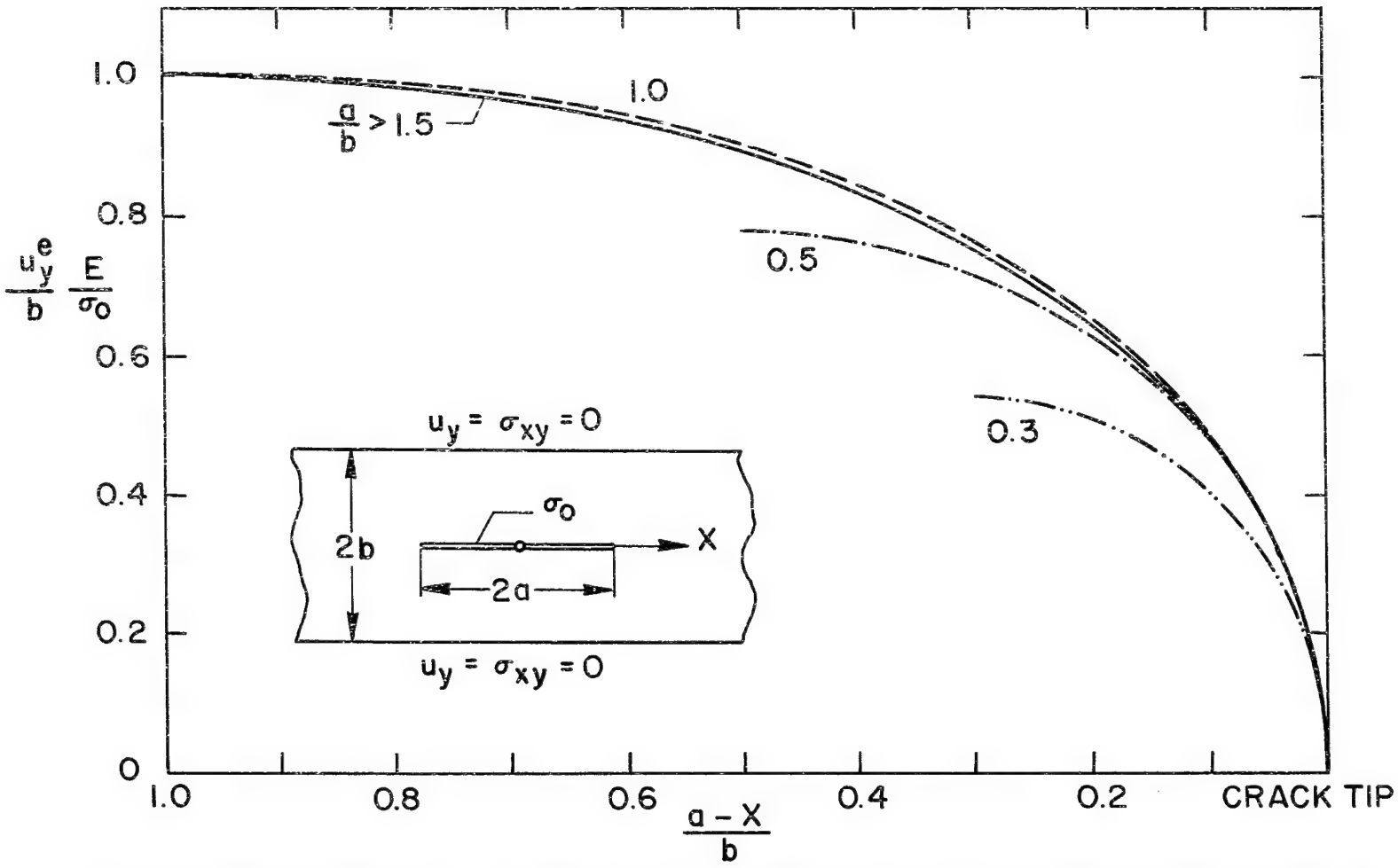

FIG. 7 DISPLACEMENTS CLOSE TO THE CRACK TIP FOR AN ELASTIC STRIP

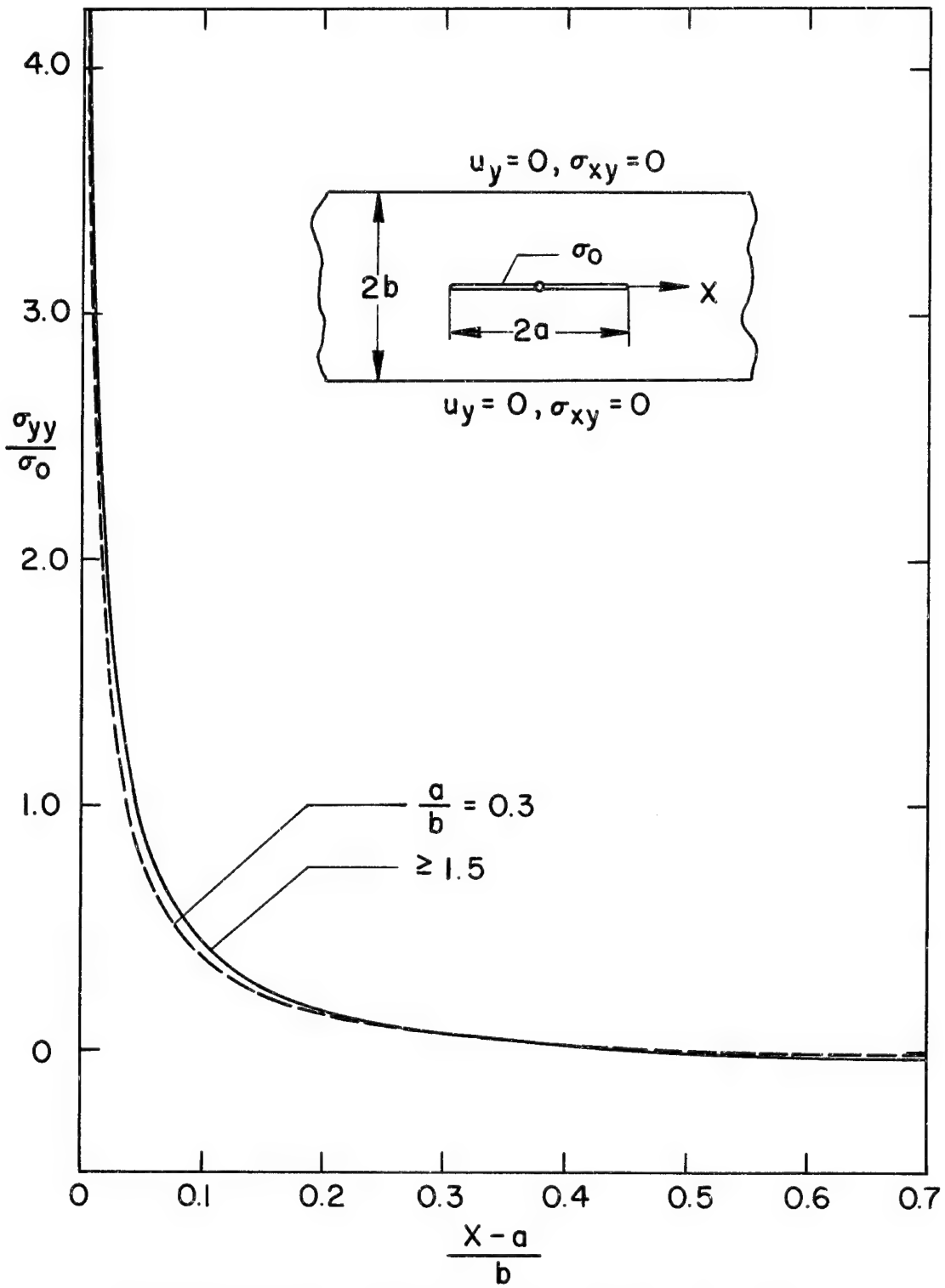

FIG. 8 NORMAL STRESS IN CRACK PLANE

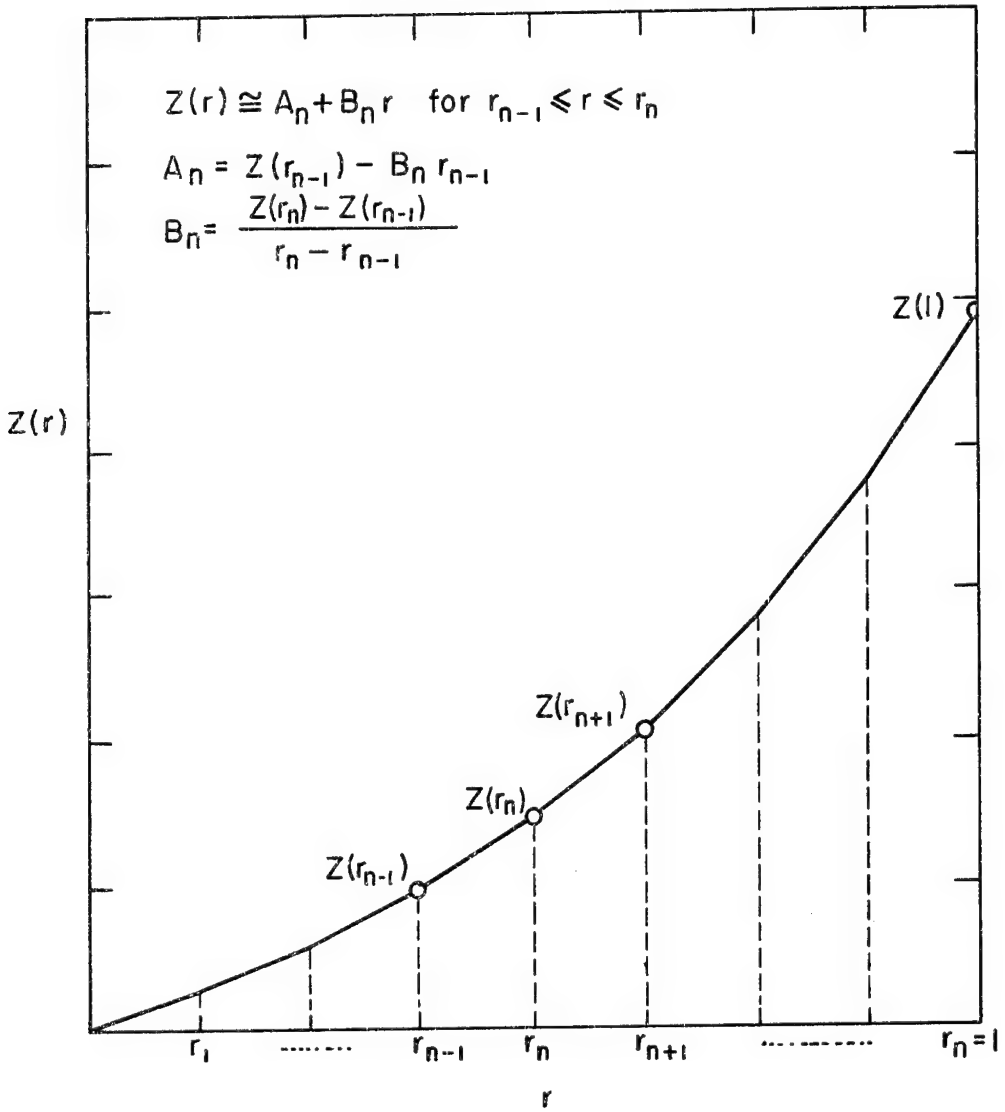

FIG. 9 APPROXIMATION OF Z(r) BY STRAIGHT LINE SEGMENTS

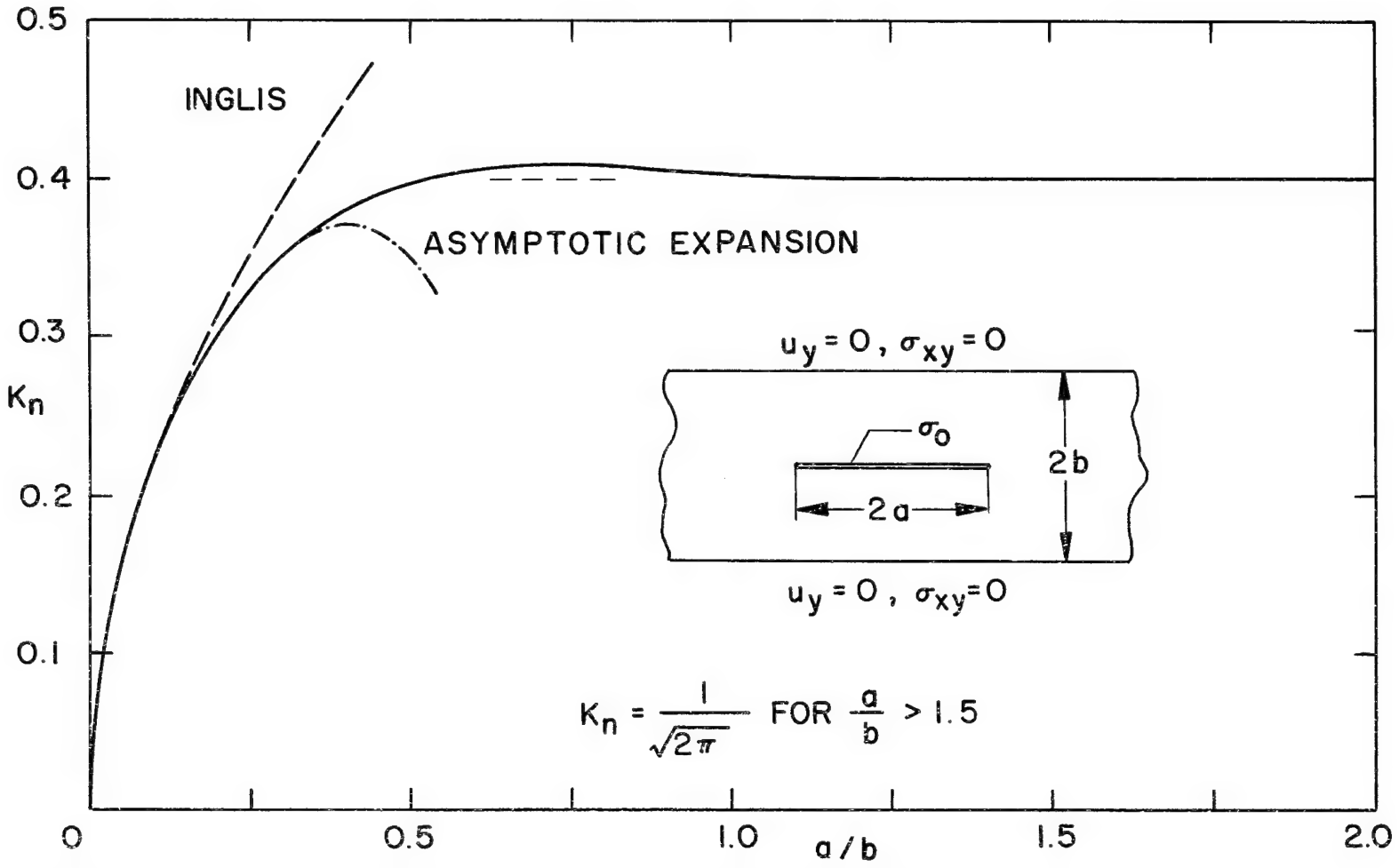

FIG. 10 NON DIMENSIONAL STRESS INTENSITY FACTOR AS A FUNCTION OF CRACK LENGTH

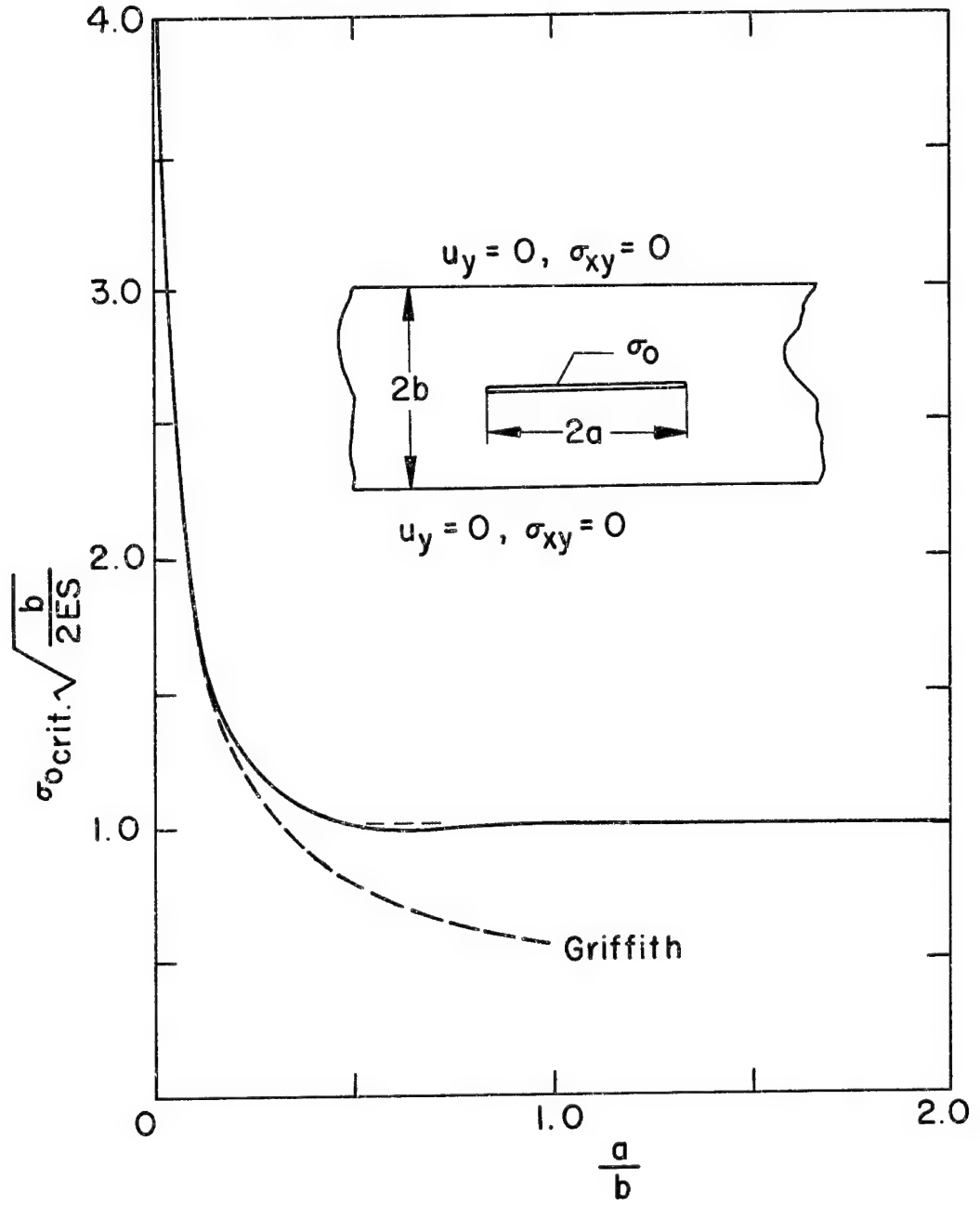

FIG. 11 CRITICAL LOAD AS A FUNCTION OF CRACK-LENGTH FOR AN ELASTIC STRIP

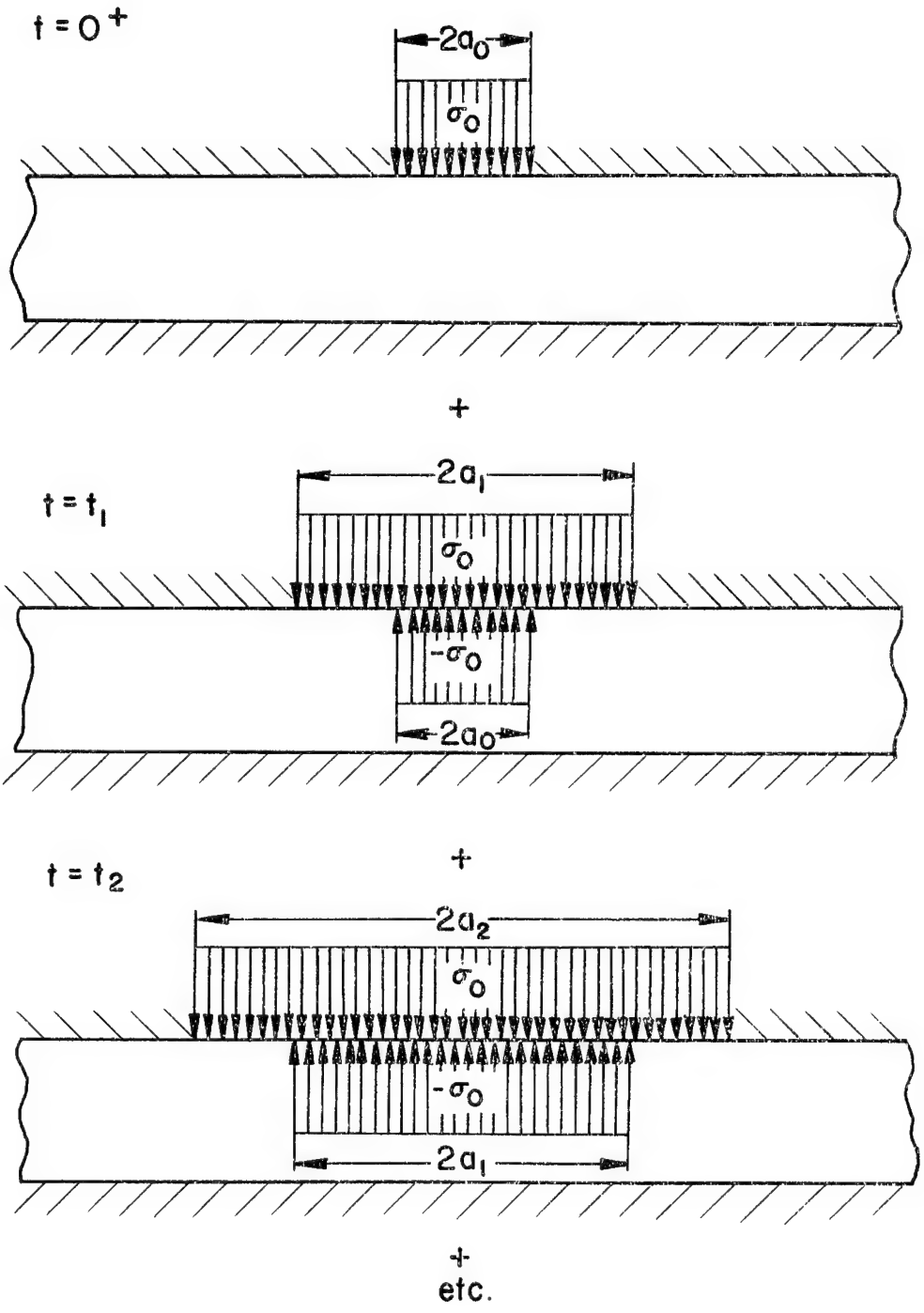

FIG. 12 SUPERPOSITION SCHEME

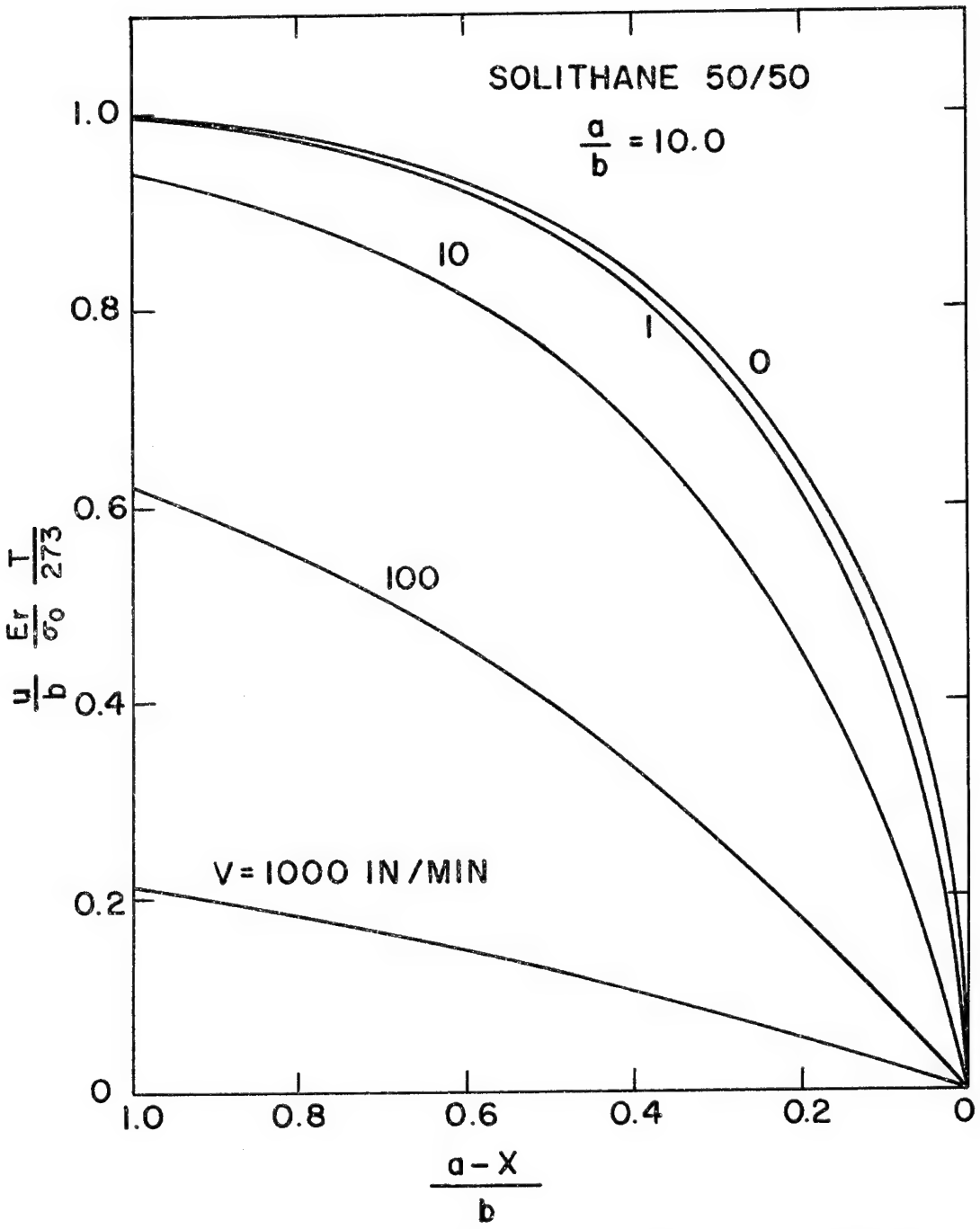

FIG. 13 DISPLACEMENTS NEAR THE CRACK TIP AS A FUNCTION OF CRACK VELOCITY

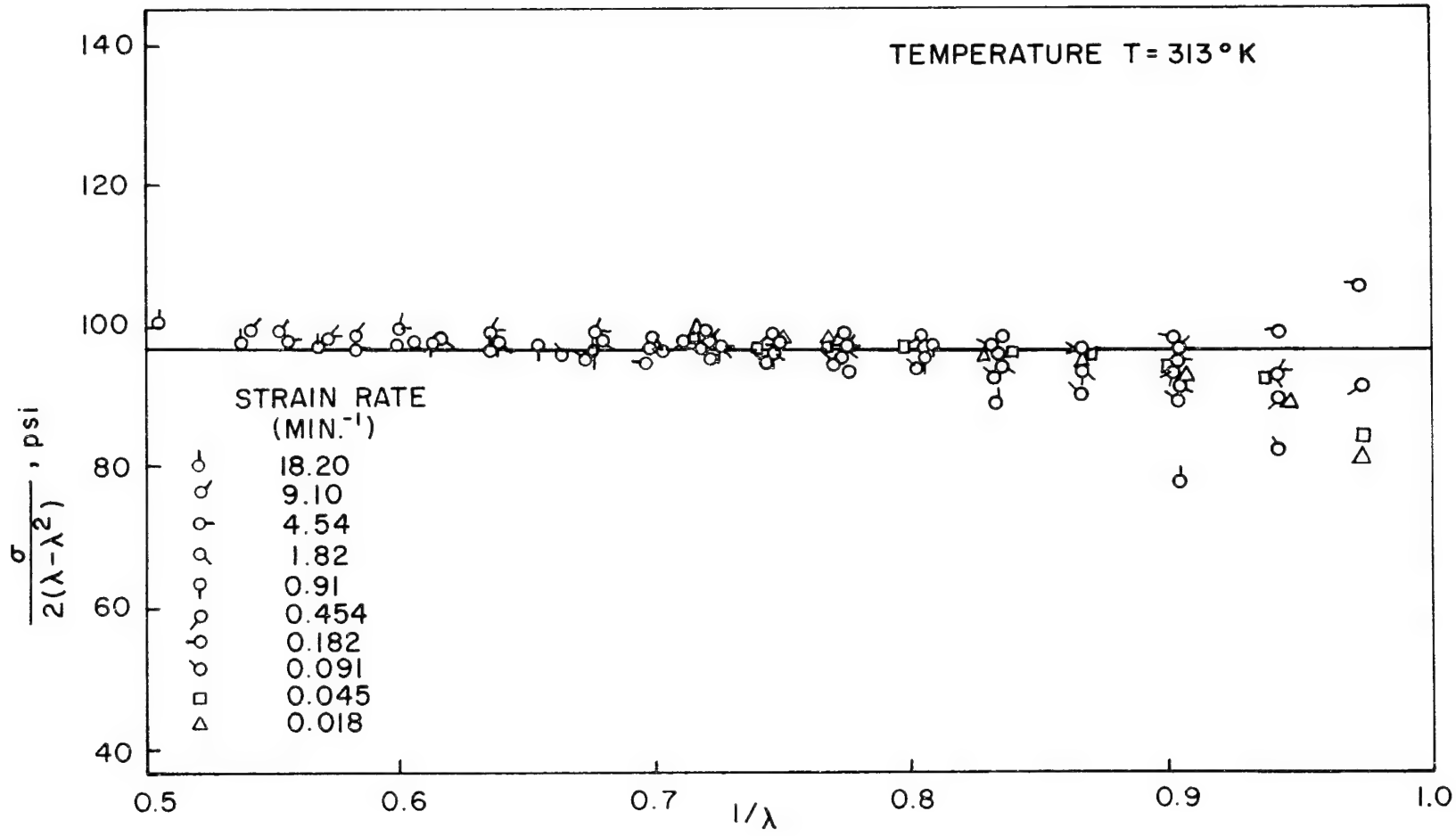

FIG. 14 MOONEY–RIVLIN PLOT FOR UNSWOLLEN SOLITHANE 50/50 AT 40° C

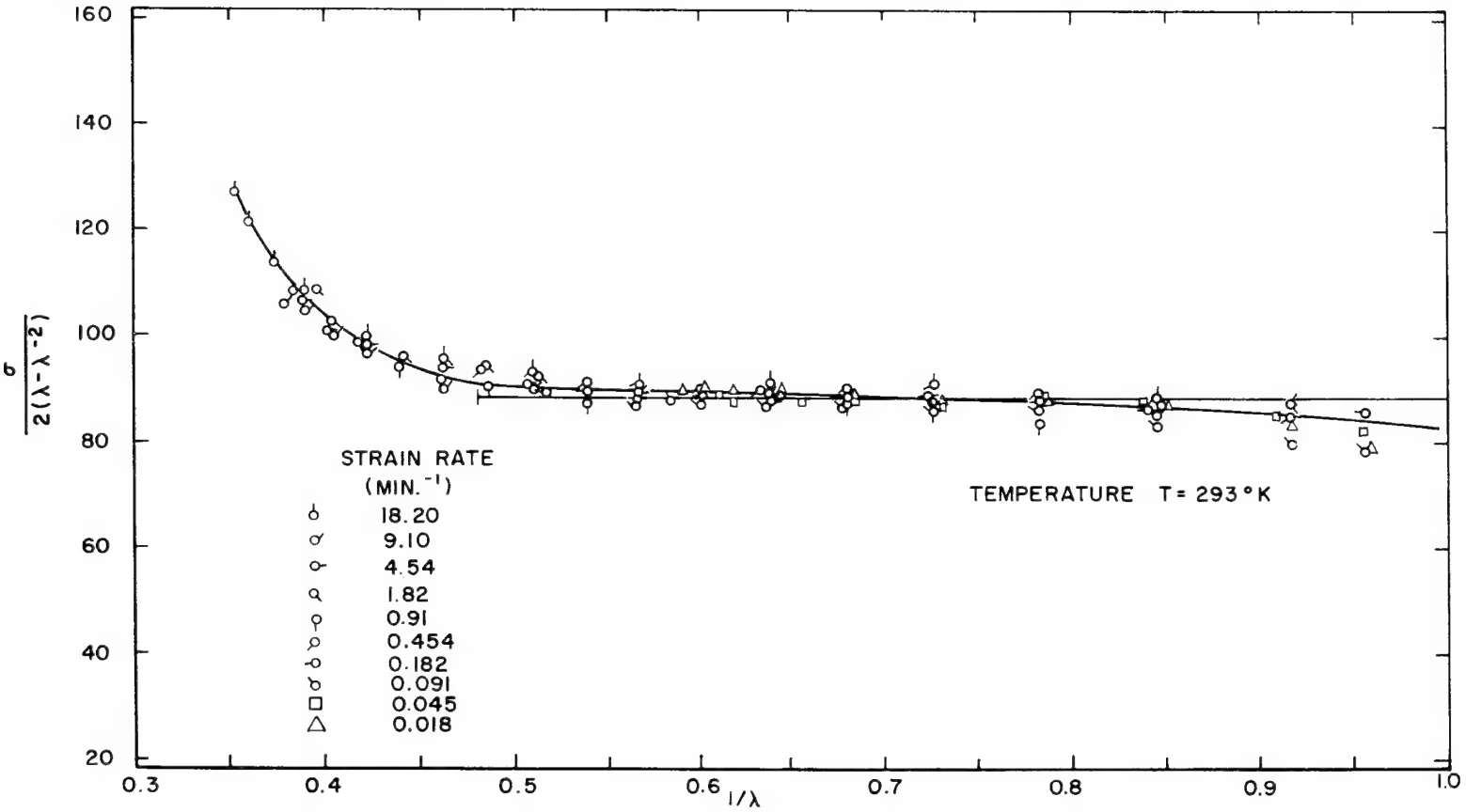

FIG. 15 MOONEY-RIVLIN PLOT FOR UNSWOLLEN SOLITHANE 50/50 AT 20 °

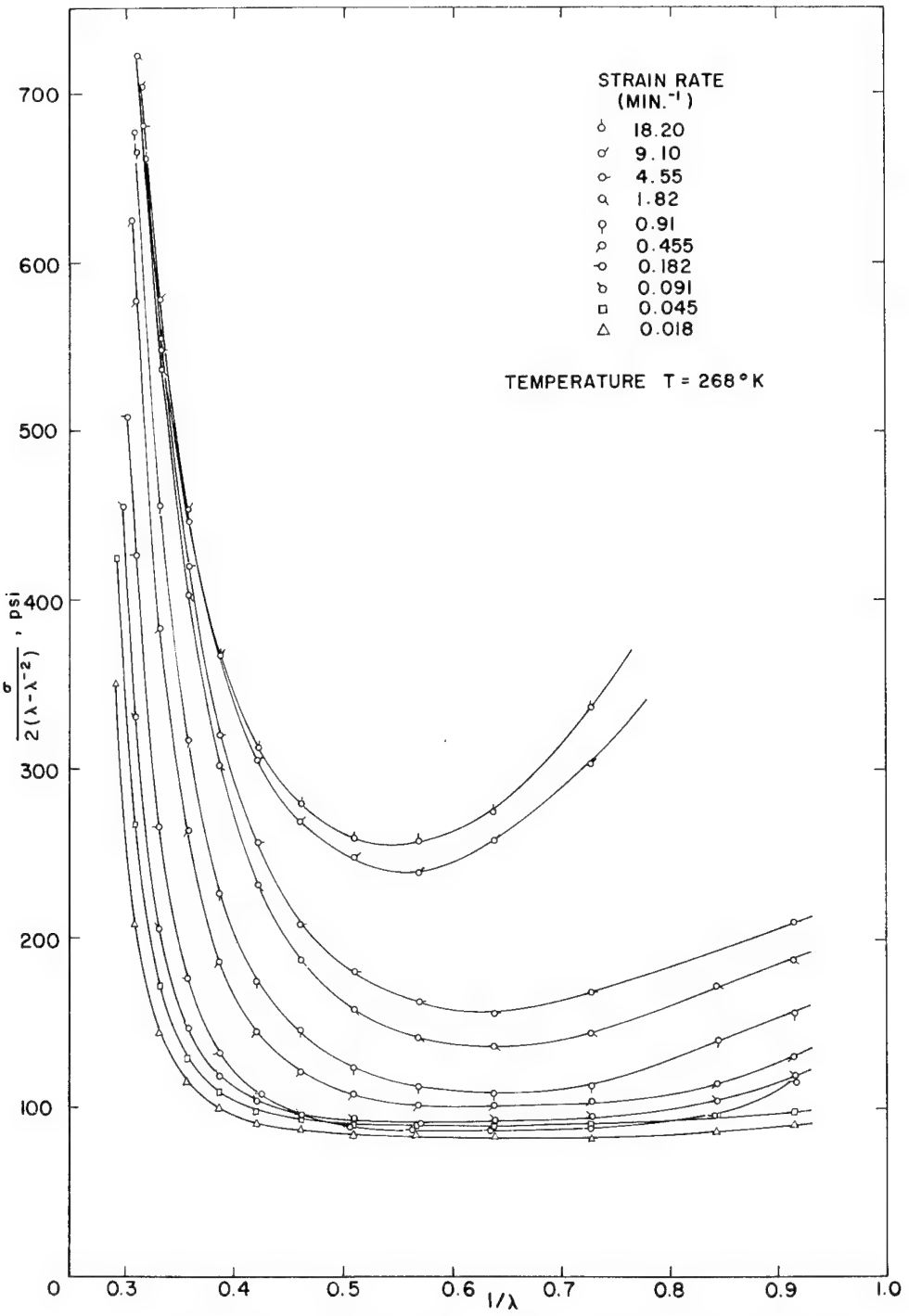

FIG. 16 MOONEY-RIVLIN PLOT FOR UNSWOLLEN SOLITHANE 50/50 AT -5°C

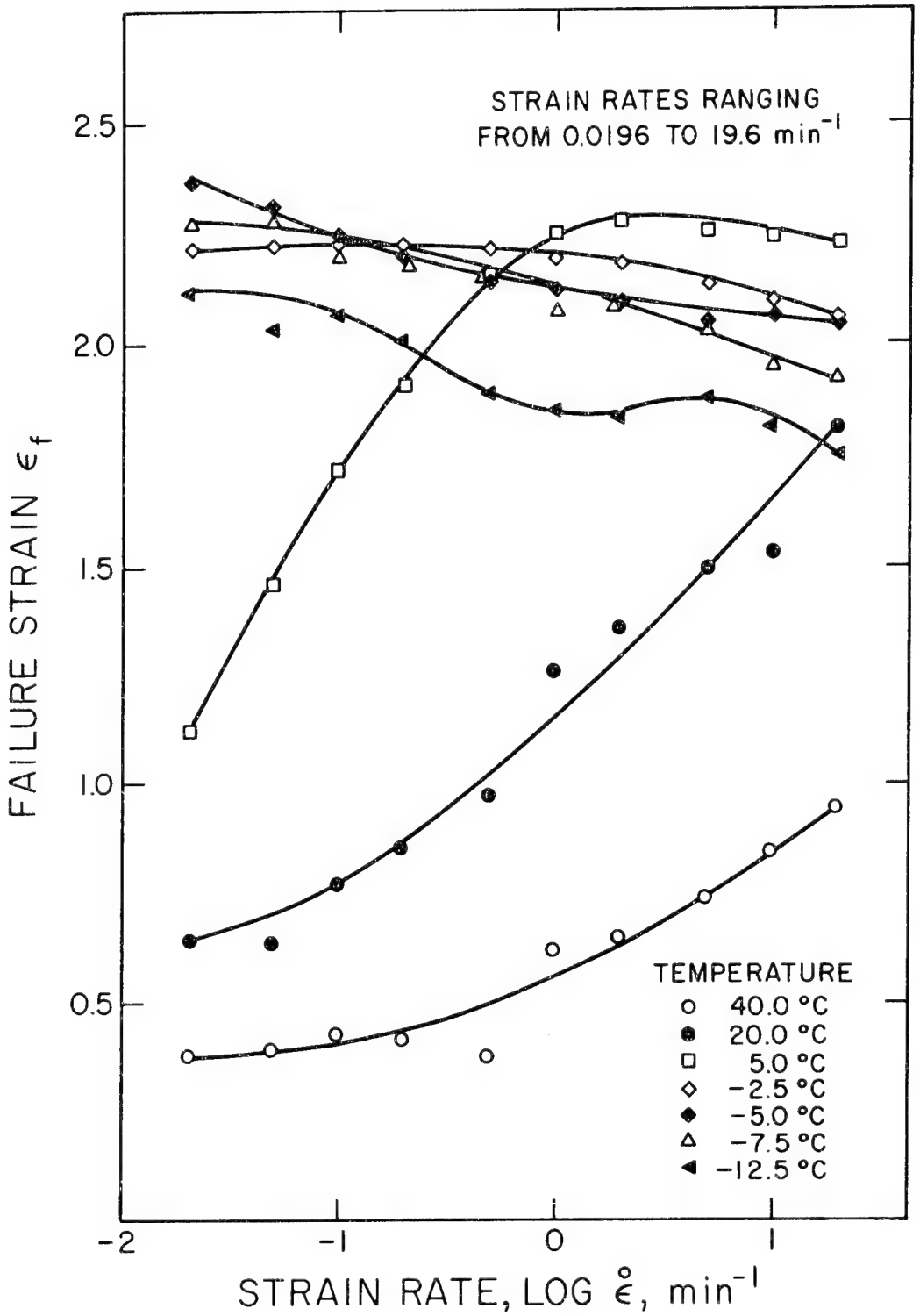

Fig. 17 FAILURE STRAIN VS. LOGARITHM OF STRAIN RATE FOR UNSWOLLEN SOLITHANE 50/50

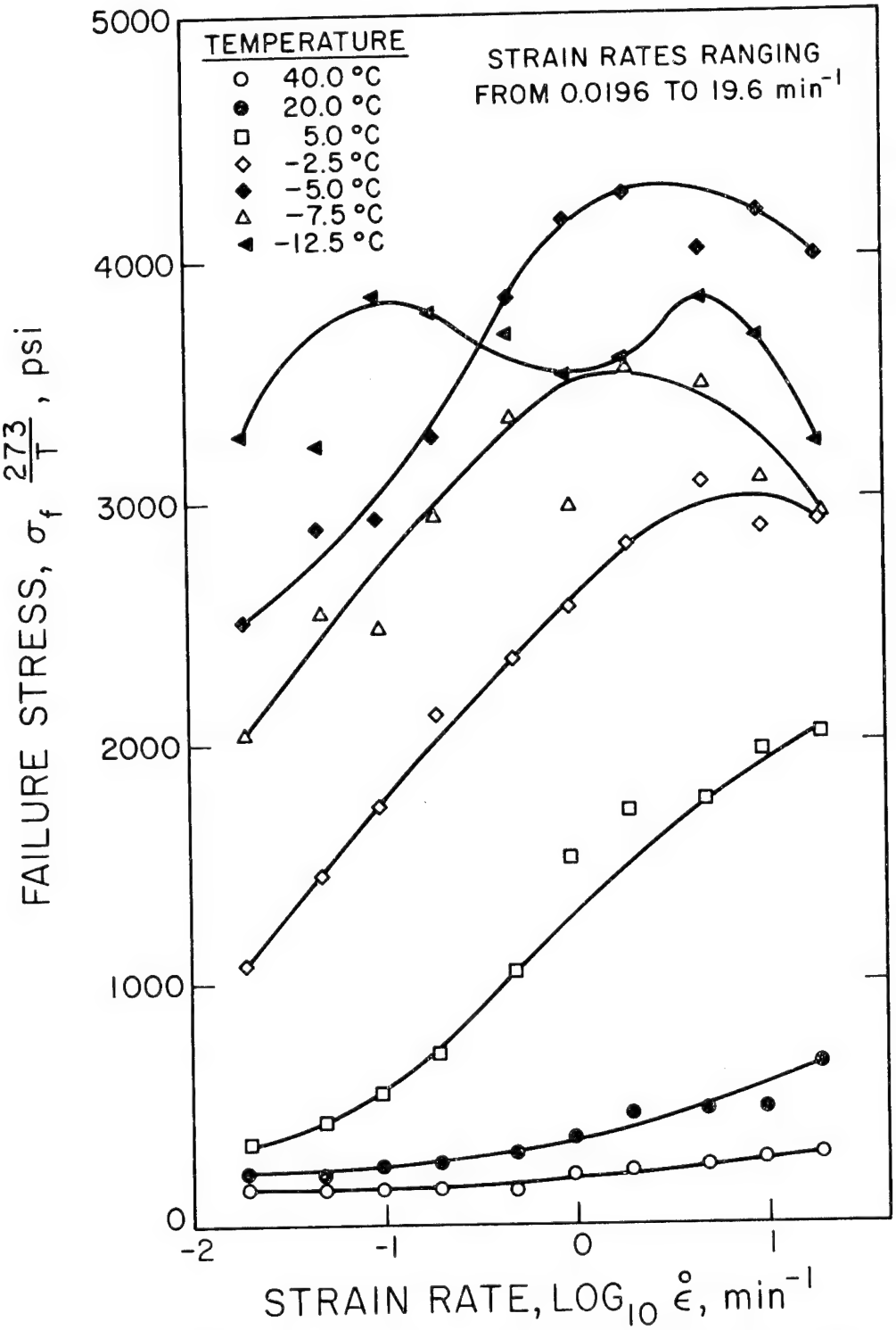

Fig. 18 FAILURE STRESS VS. LOGARITHM OF STRAIN RATE FOR UNSWOLLEN SOLITHANE 50/50

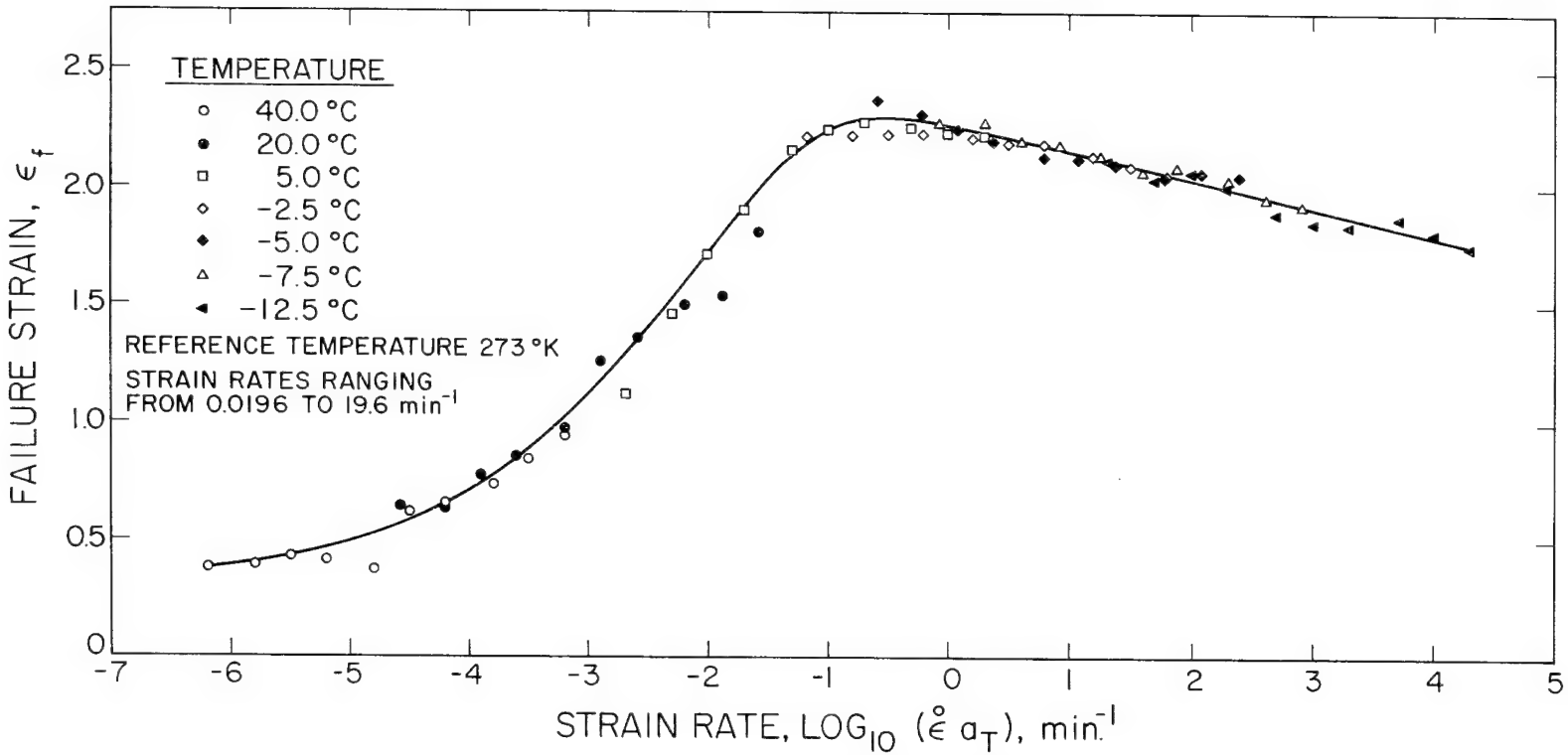

Fig. 19 SHIFTED FAILURE STRAINS FOR UNSWOLLEN SOLITHANE 50/50

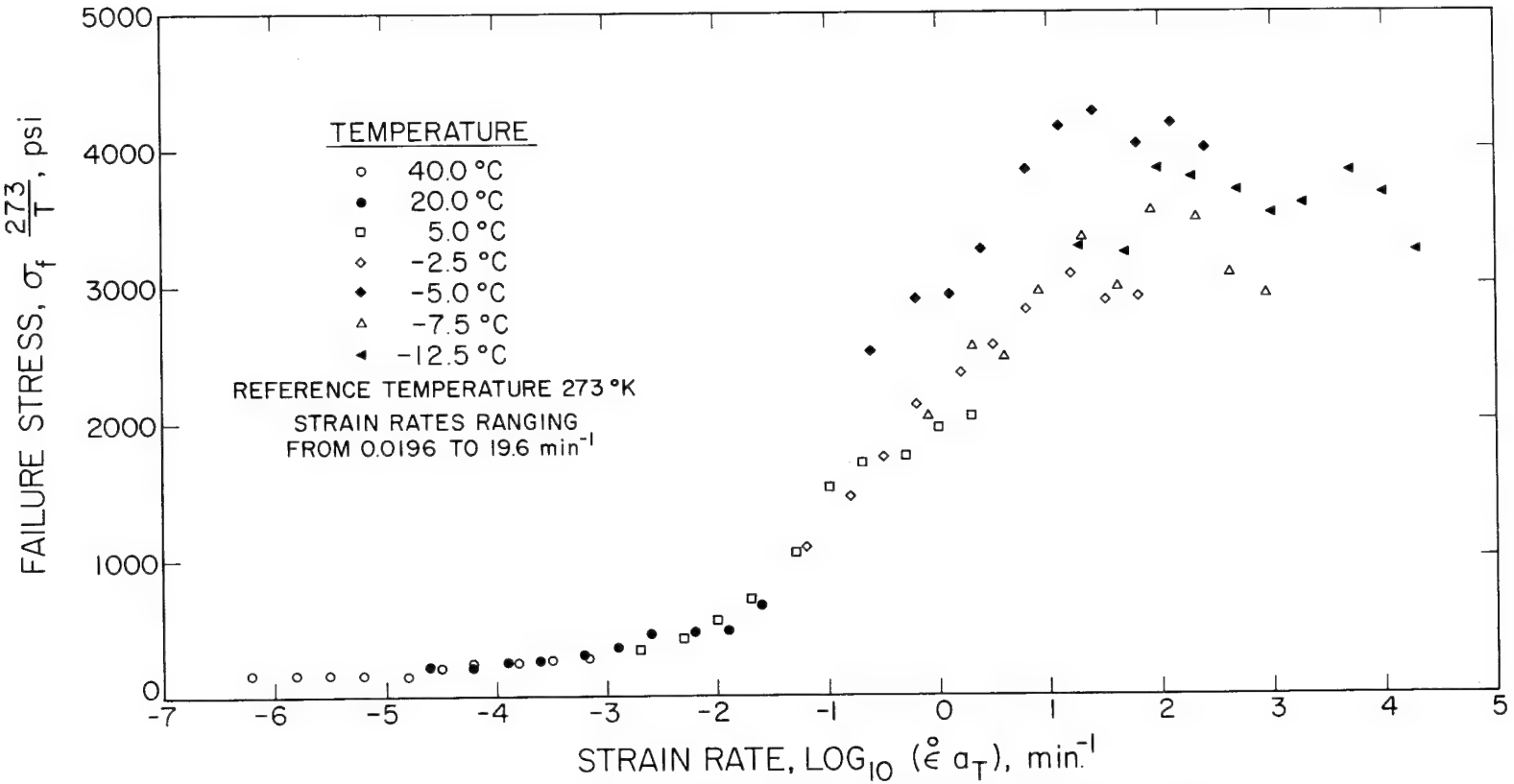

Fig. 20 SHIFTED FAILURE STRESS FOR UNSWOLLEN SOLITHANE 50/50

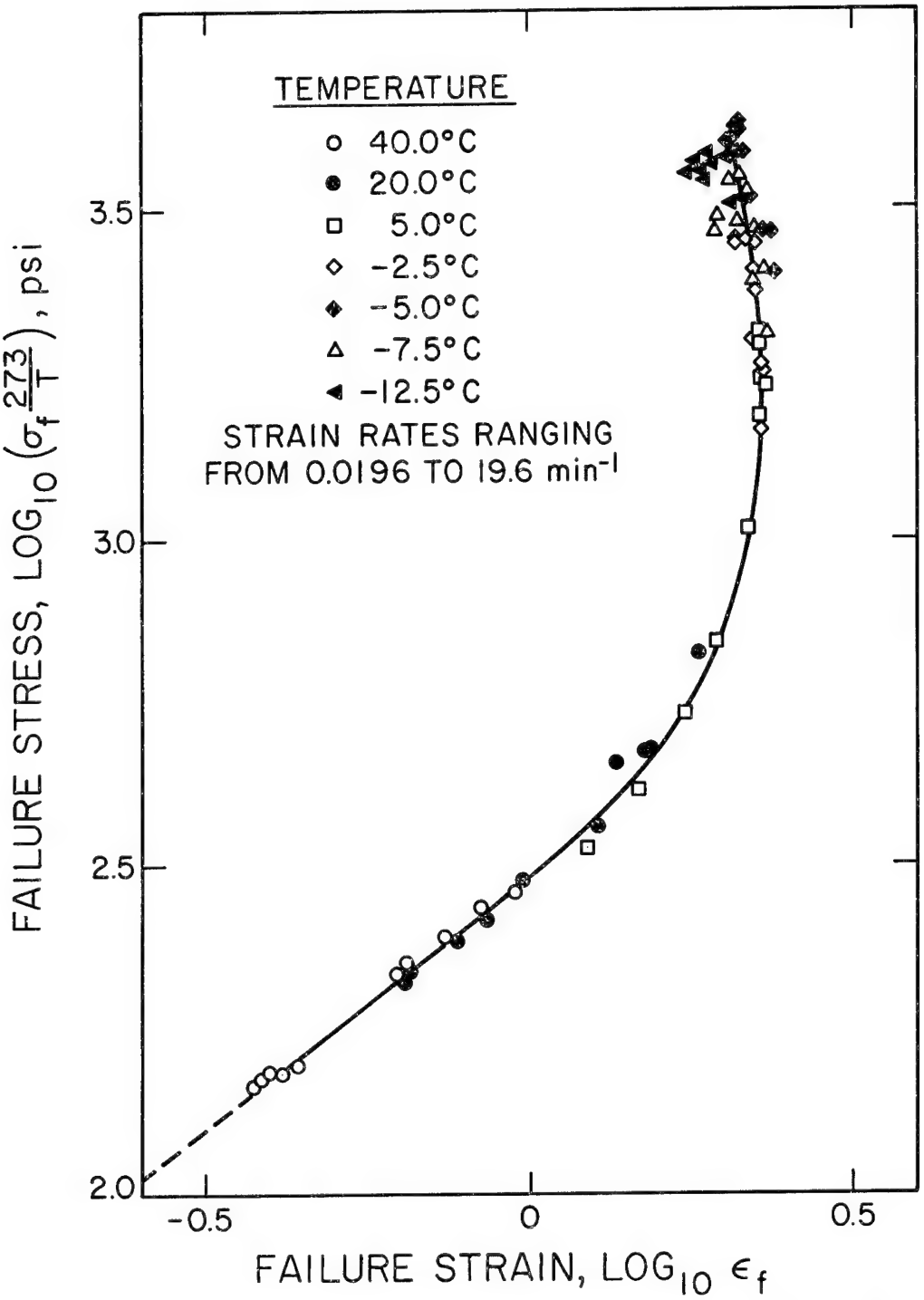

Fig.21 FAILURE ENVELOPE FOR UNSWOLLEN SOLITHANE 50/50

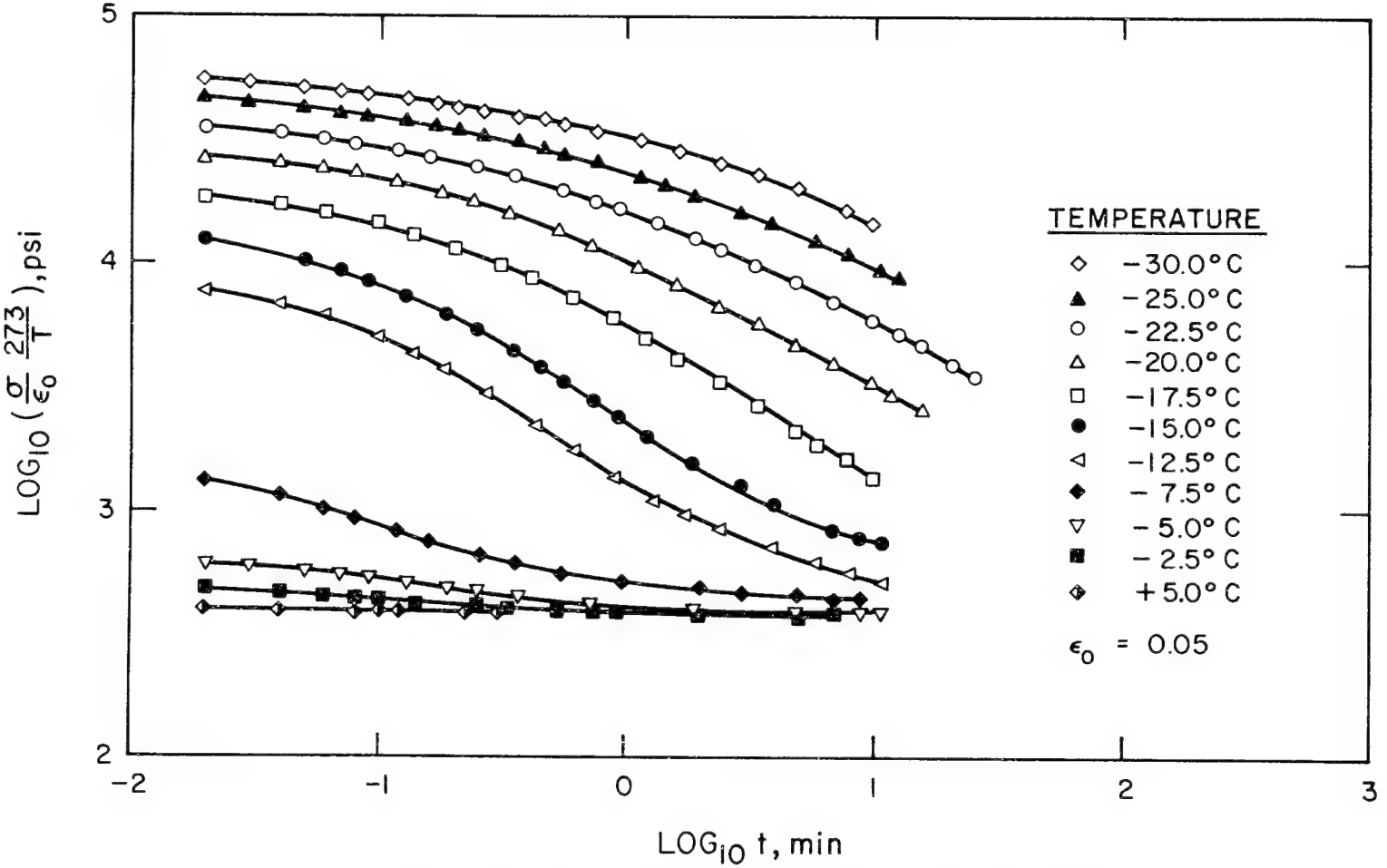

Fig. 22 TEMPERATURE REDUCED RELAXATION MODULUS OF UNSWOLLEN SOLITHANE 50/50

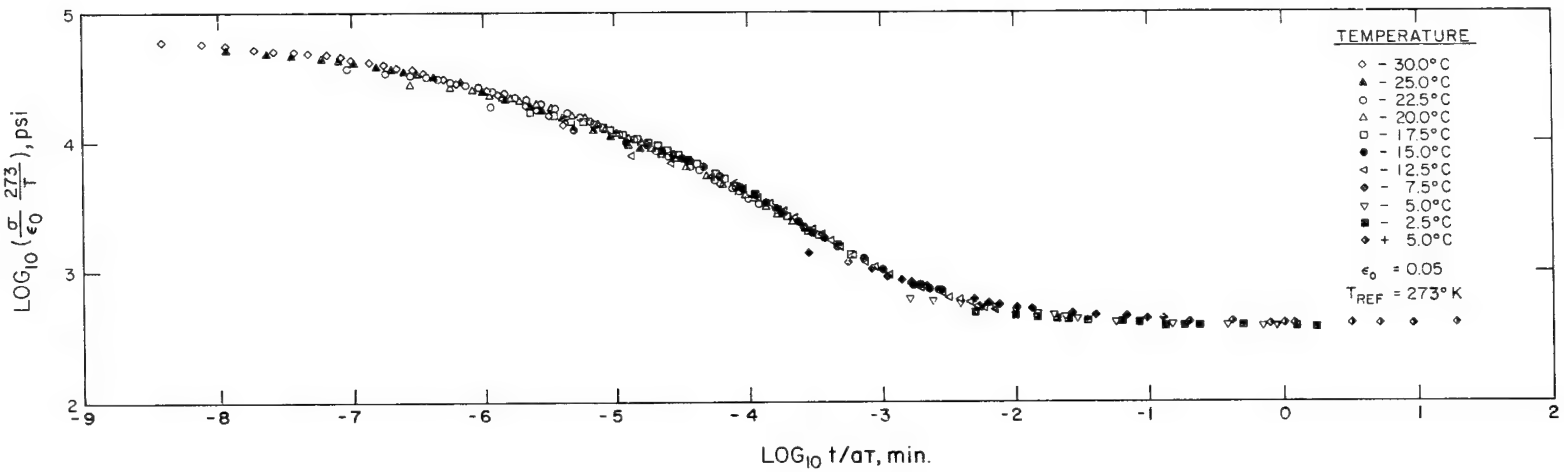

Fig. 23 MASTER CURVE FOR TEMPERATURE REDUCED RELAXATION MODULUS OF UNSWOLLEN SOLITHANE 50/50, REFERENCE TEMPERATURE 0°C

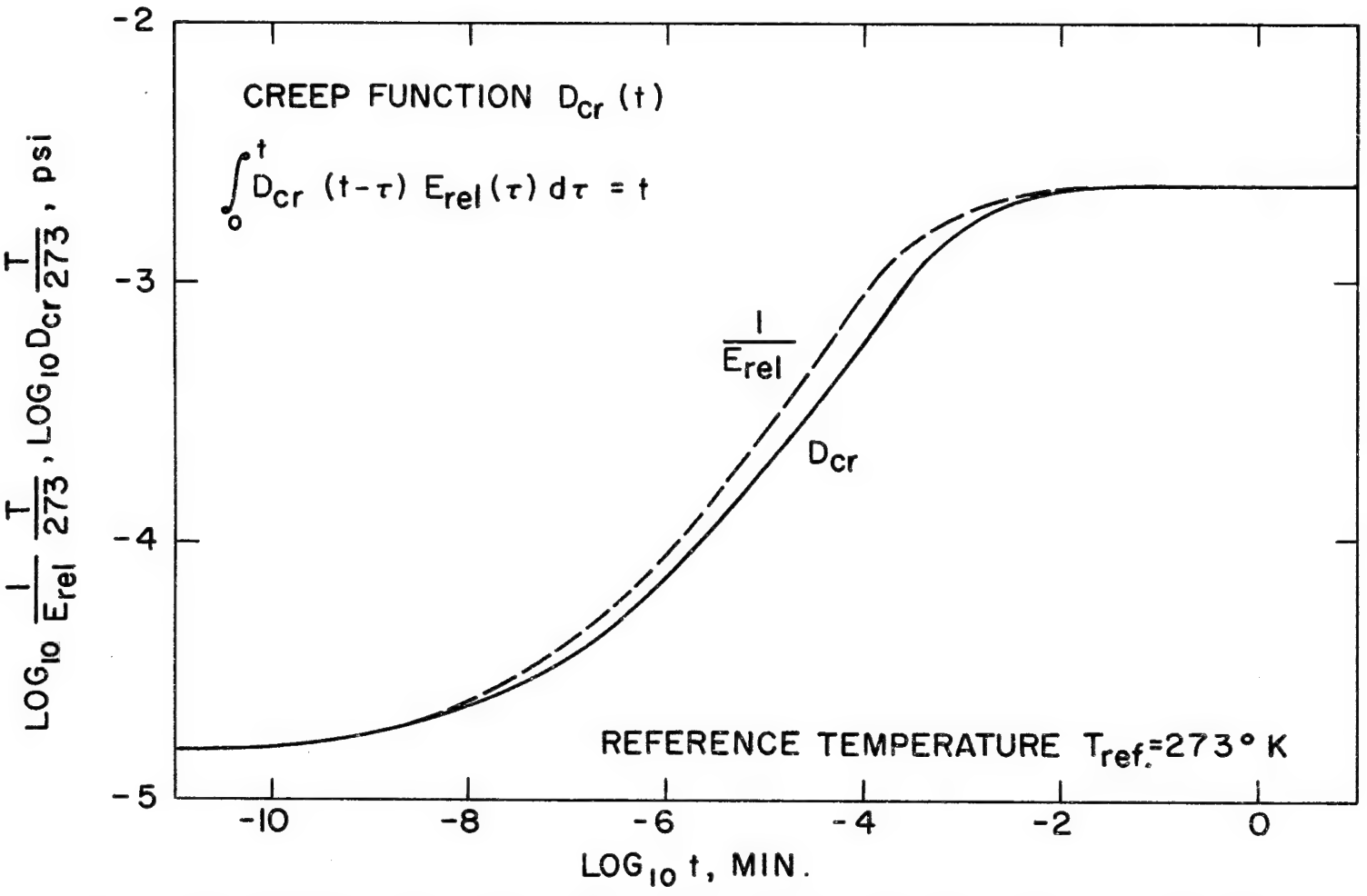

FIG. 24 CREEP AND RELAXATION FUNCTION FOR SOLITHANE 50/50

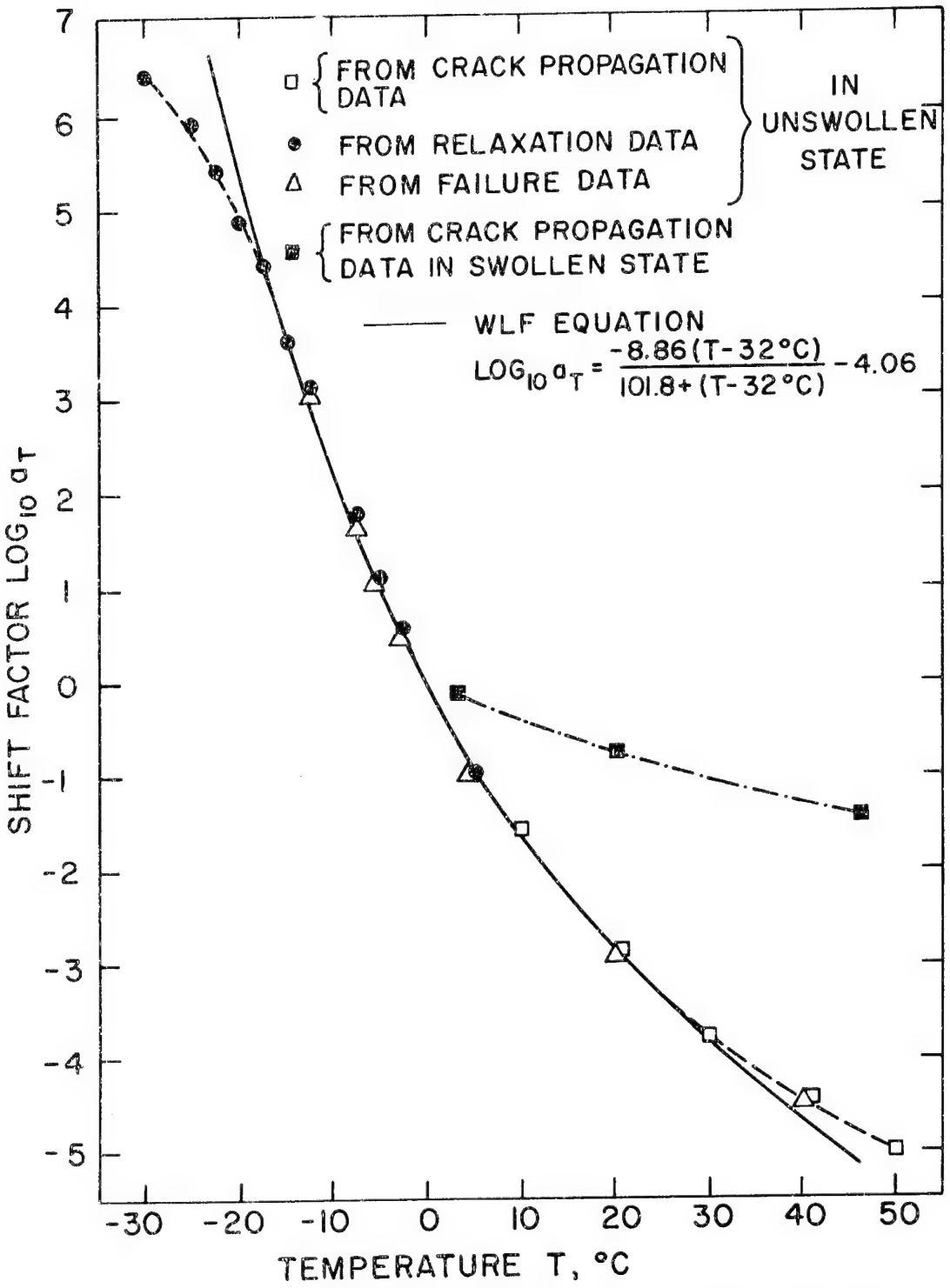

FIG. 25 TIME-TEMPERATURE SHIFT FACTOR FOR SOLITHANE 50/50

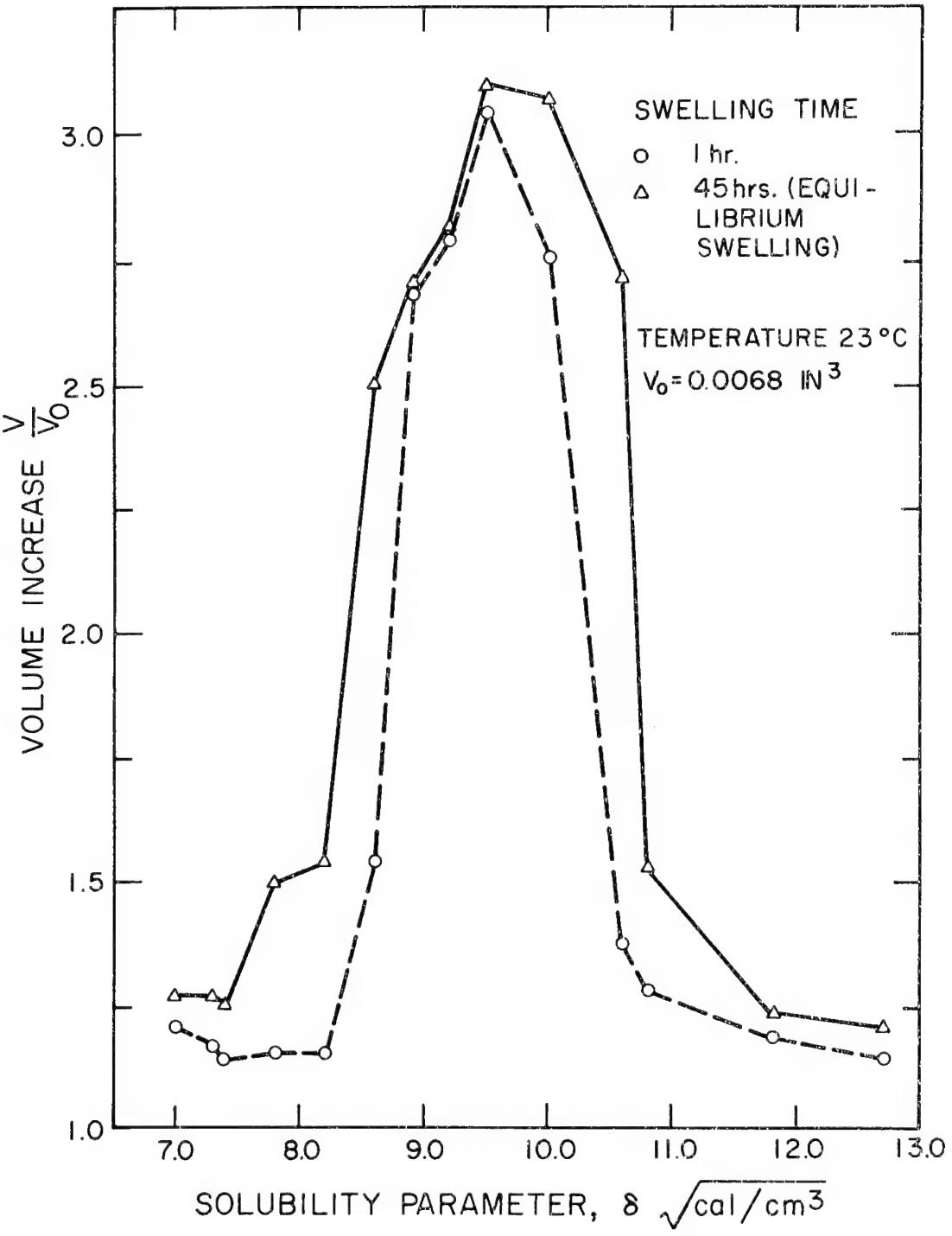

Fig. 26 SWELLING RATIO OF SOLITHANE 50/50 IN POORLY HYDROGEN BONDED SOLVENTS

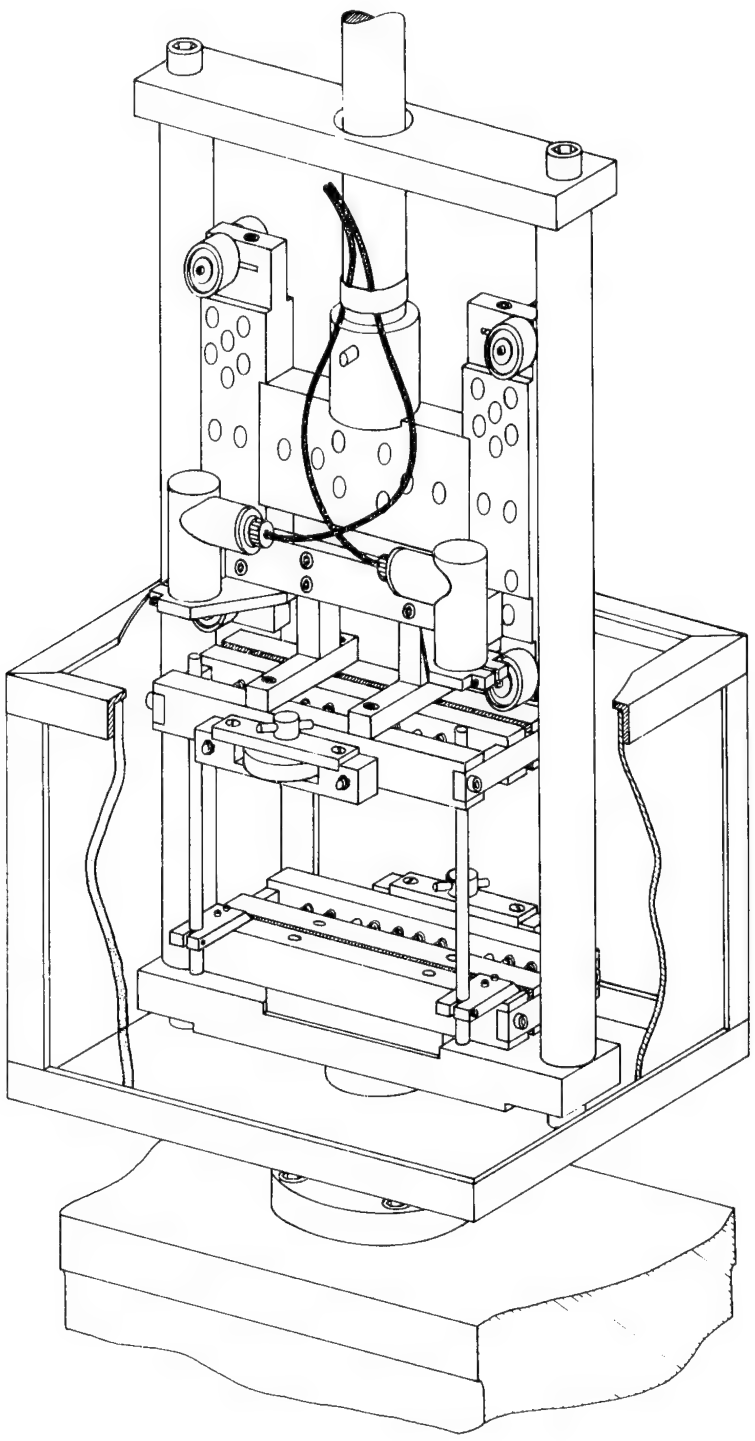

FIG. 27 DEVICE FOR THE MECHANICAL CHARACTERIZATION OF SWOLLEN SOLITHANE

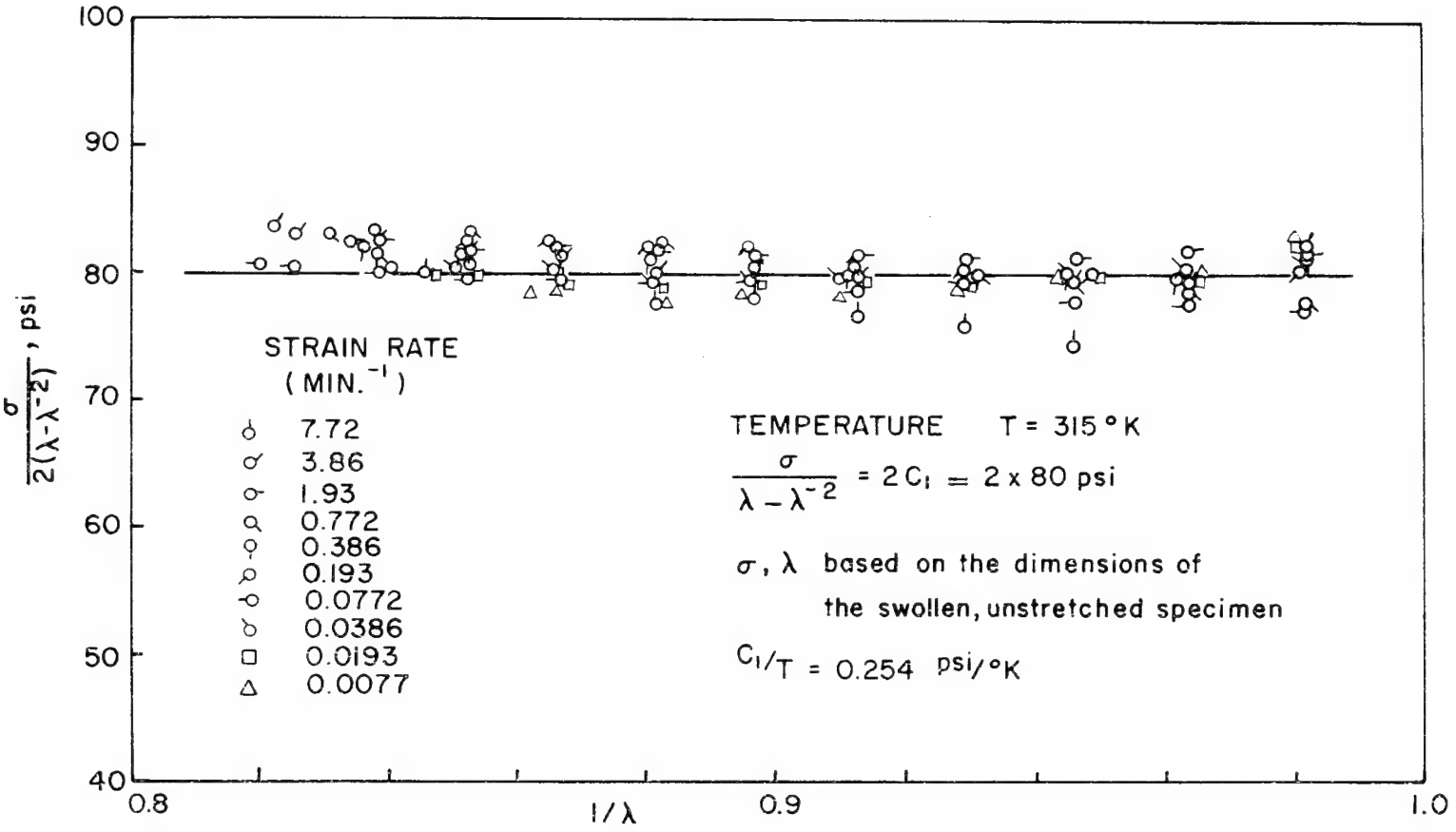

FIG.28 MOONEY-RIVLIN PLOT FOR SOLITHANE 50/50 SWOLLEN IN TOLUENE AT 42°C

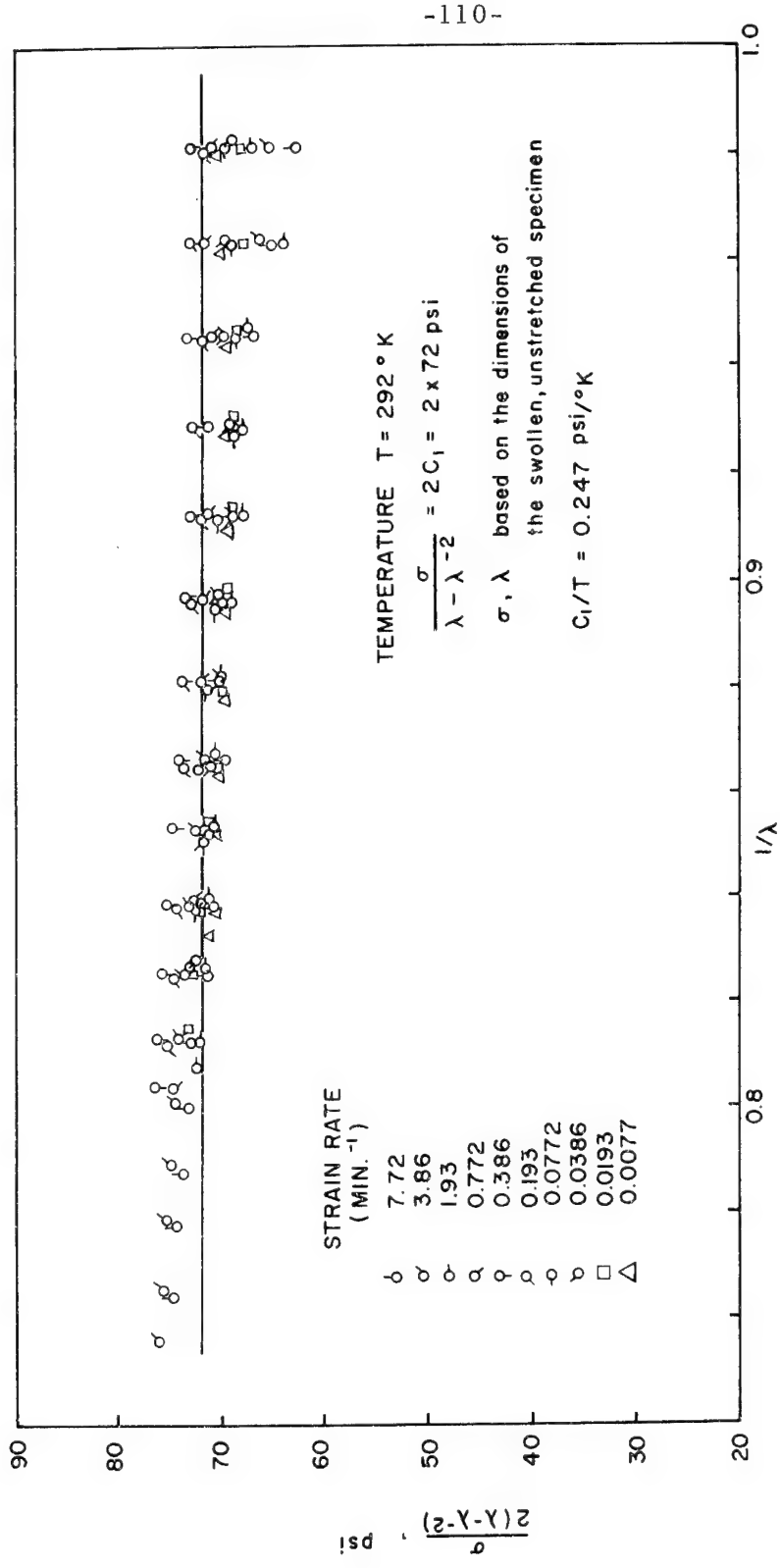

FIG. 29 MOONEY-RIVLIN PLOT FOR SOLITHANE 50/50 SWOLLEN IN TOLUENE AT 19°C

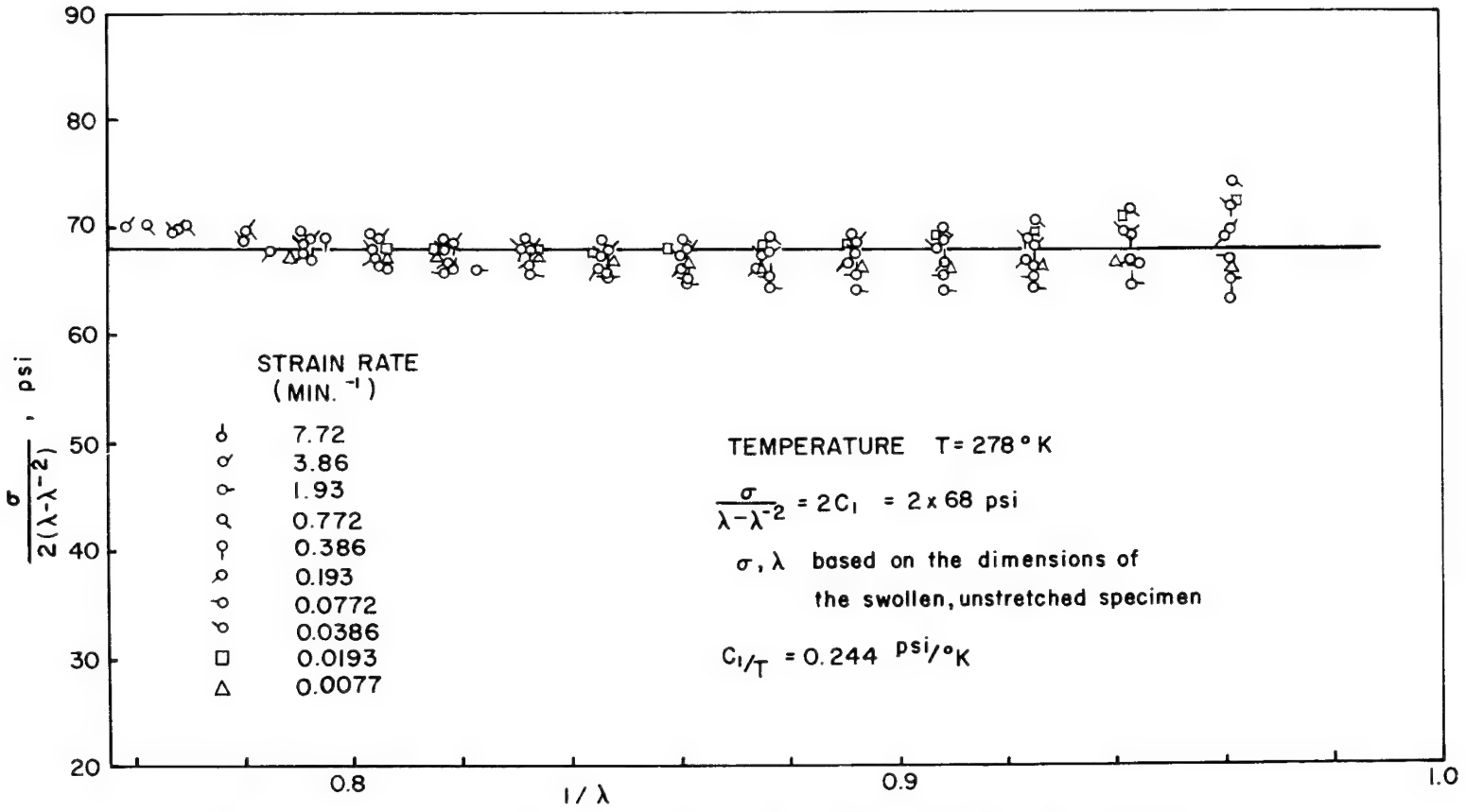

FIG. 30 MOONEY-RIVLIN PLOT FOR SOLITHANE 50/50 SWOLLEN IN TOLUENE AT 5°C

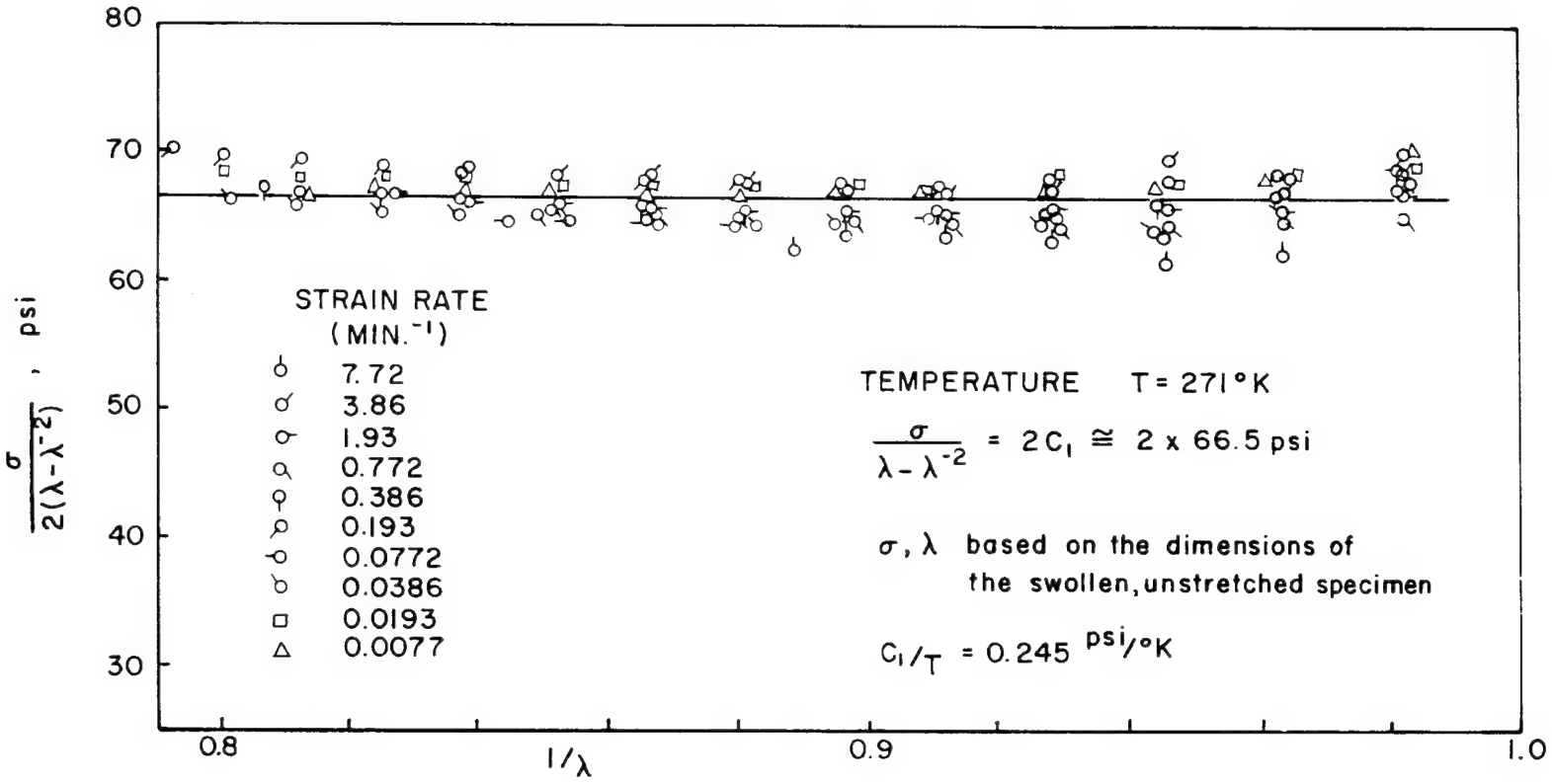

FIG.31 MOONEY-RIVLIN PLOT FOR SOLITHANE 50/50 SWOLLEN IN TOLUENE AT -2°C

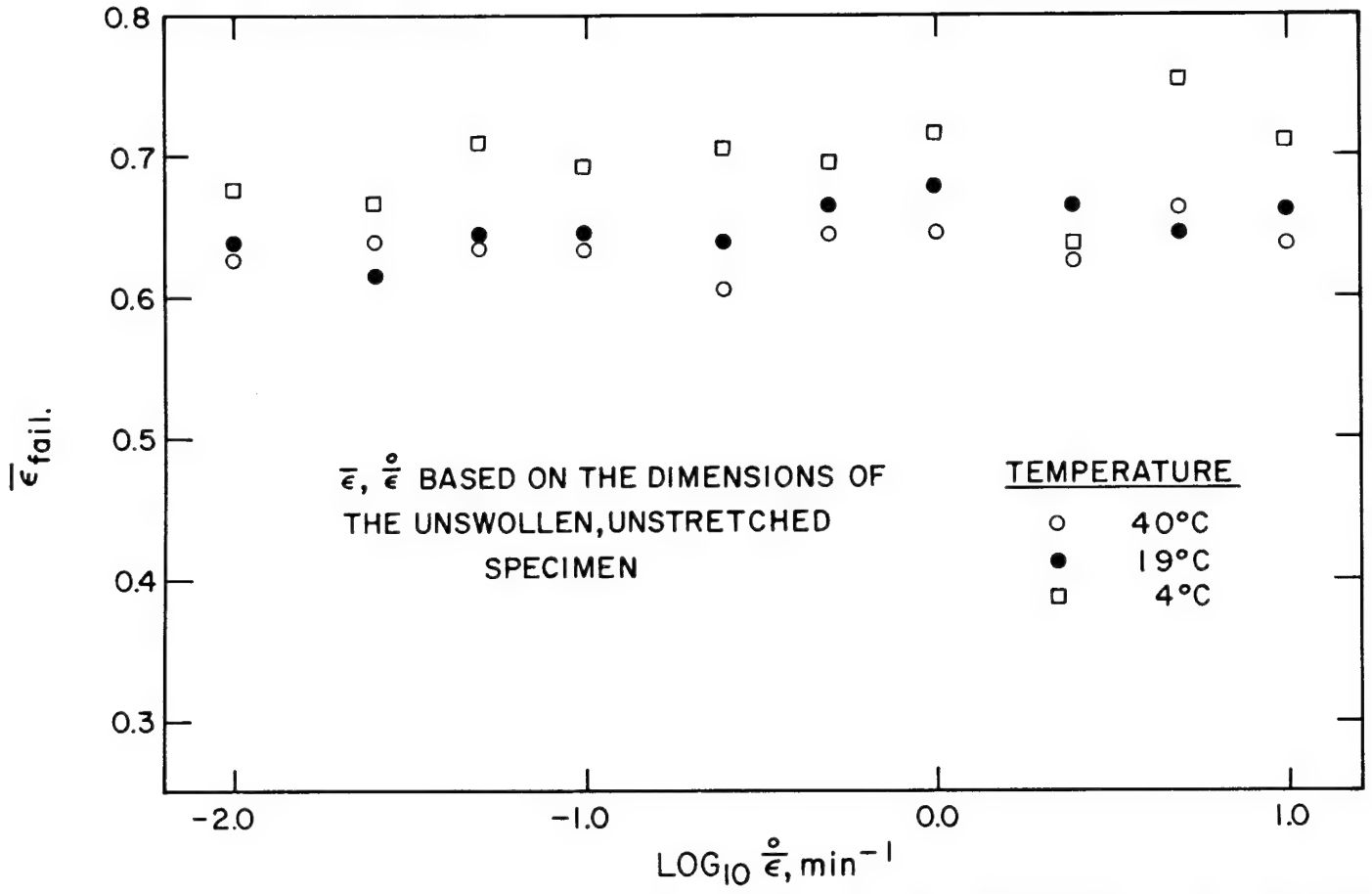

Fig. 32 FAILURE STRAIN VS. STRAIN RATE OF SOLITHANE 50/50 SWOLLEN IN TOLUENE

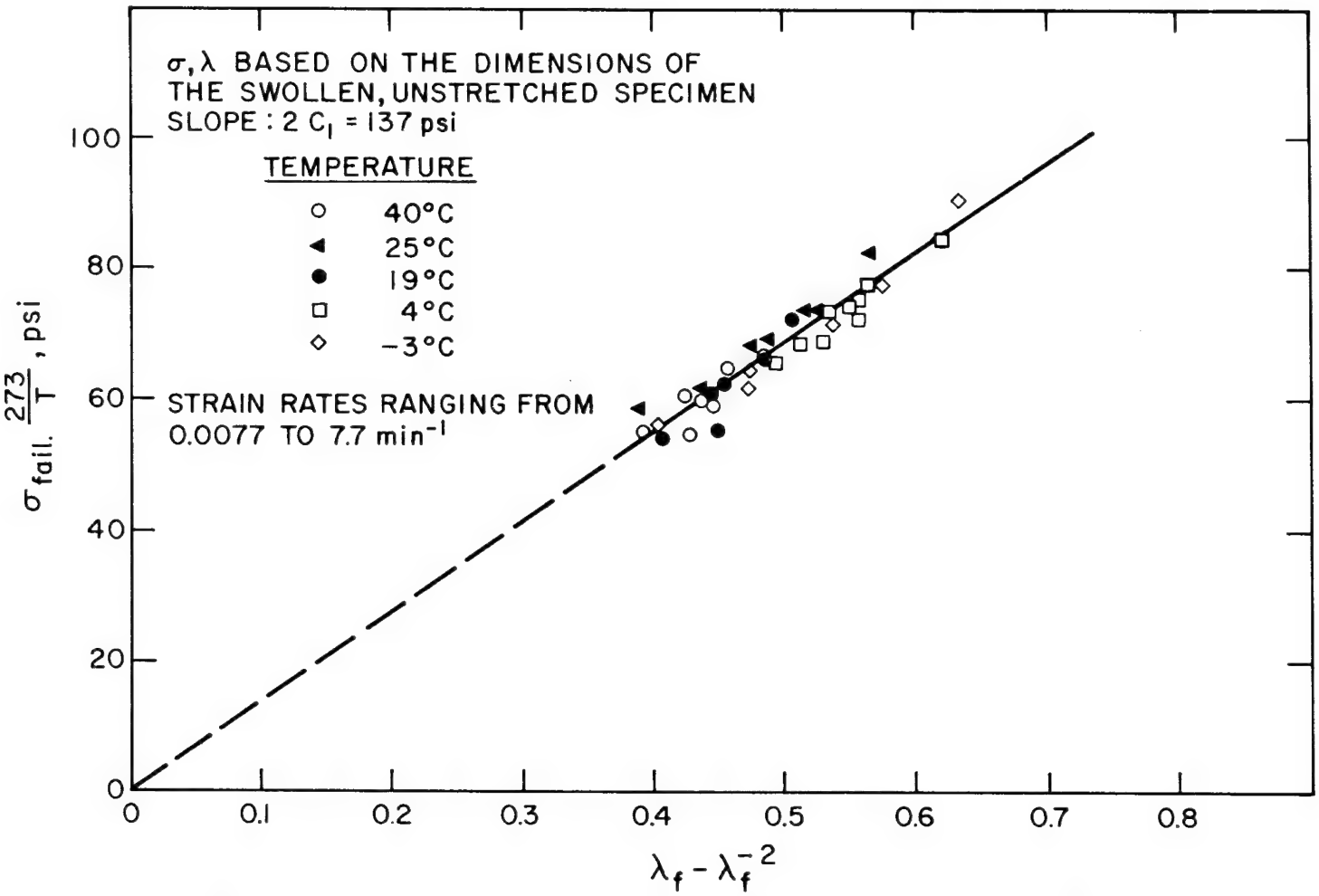

Fig. 33 TEMPERATURE REDUCED FAILURE STRESS VS. $\lambda - \lambda^{-2}$ AT FAILURE FOR SOLITHANE 50/50 SWOLLEN IN TOLUENE

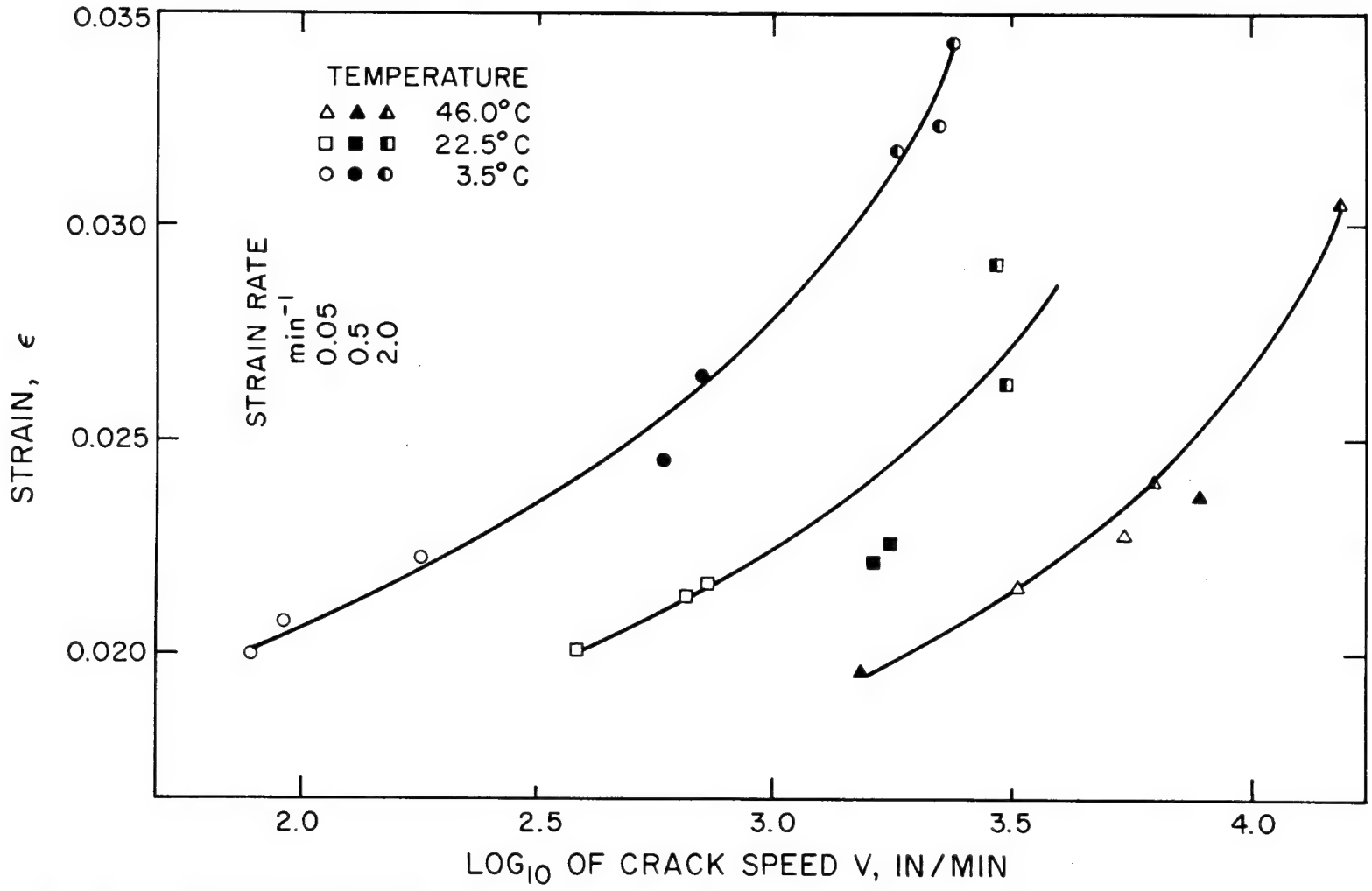

Fig. 34 CRACK PROPAGATION SPEEDS IN SOLITHANE 50/50 SWOLLEN IN TOLUENE

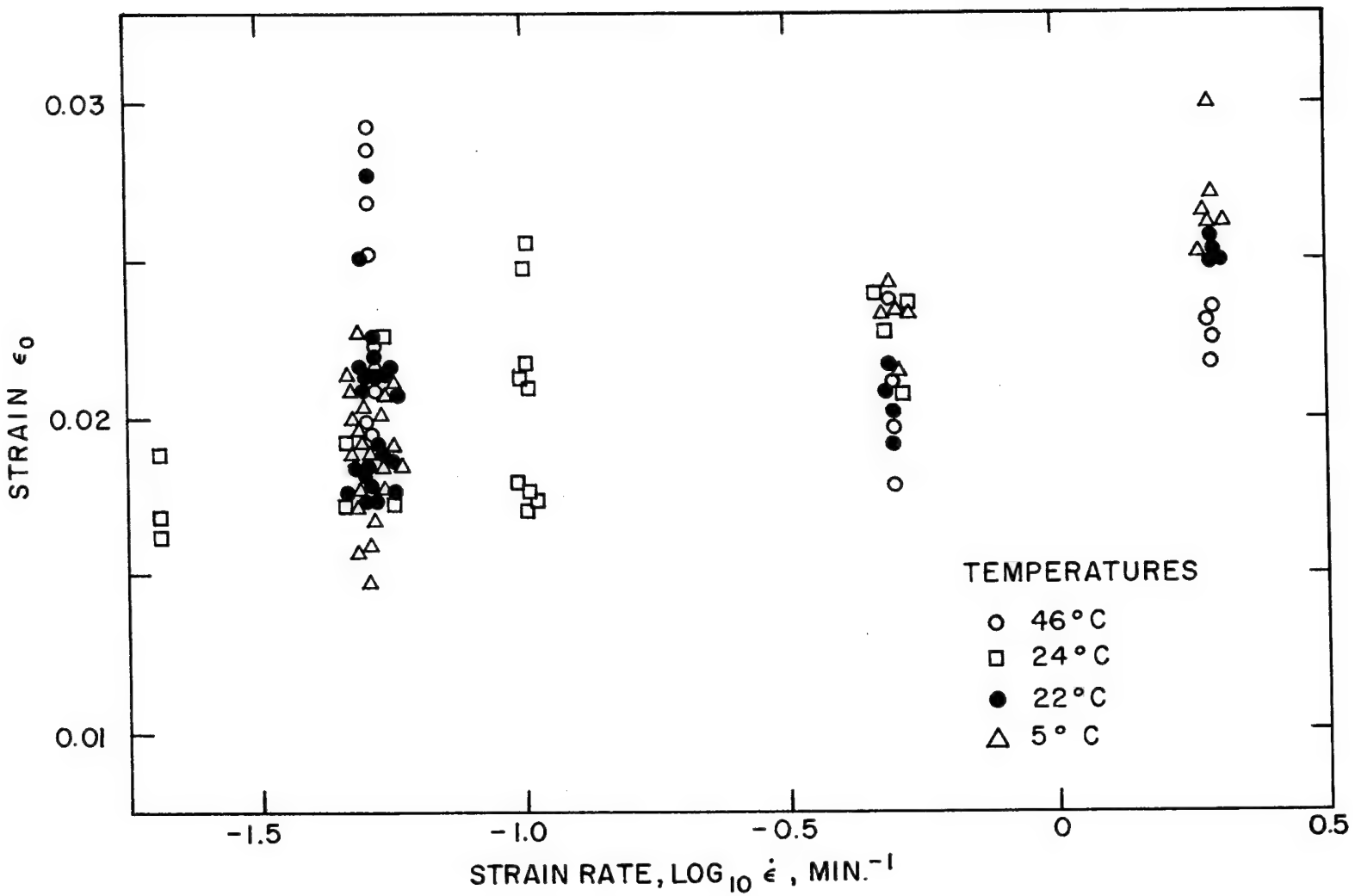

FIG. 35 GROSS STRAIN AT THE BEGINNING OF CRACK PROPAGATION

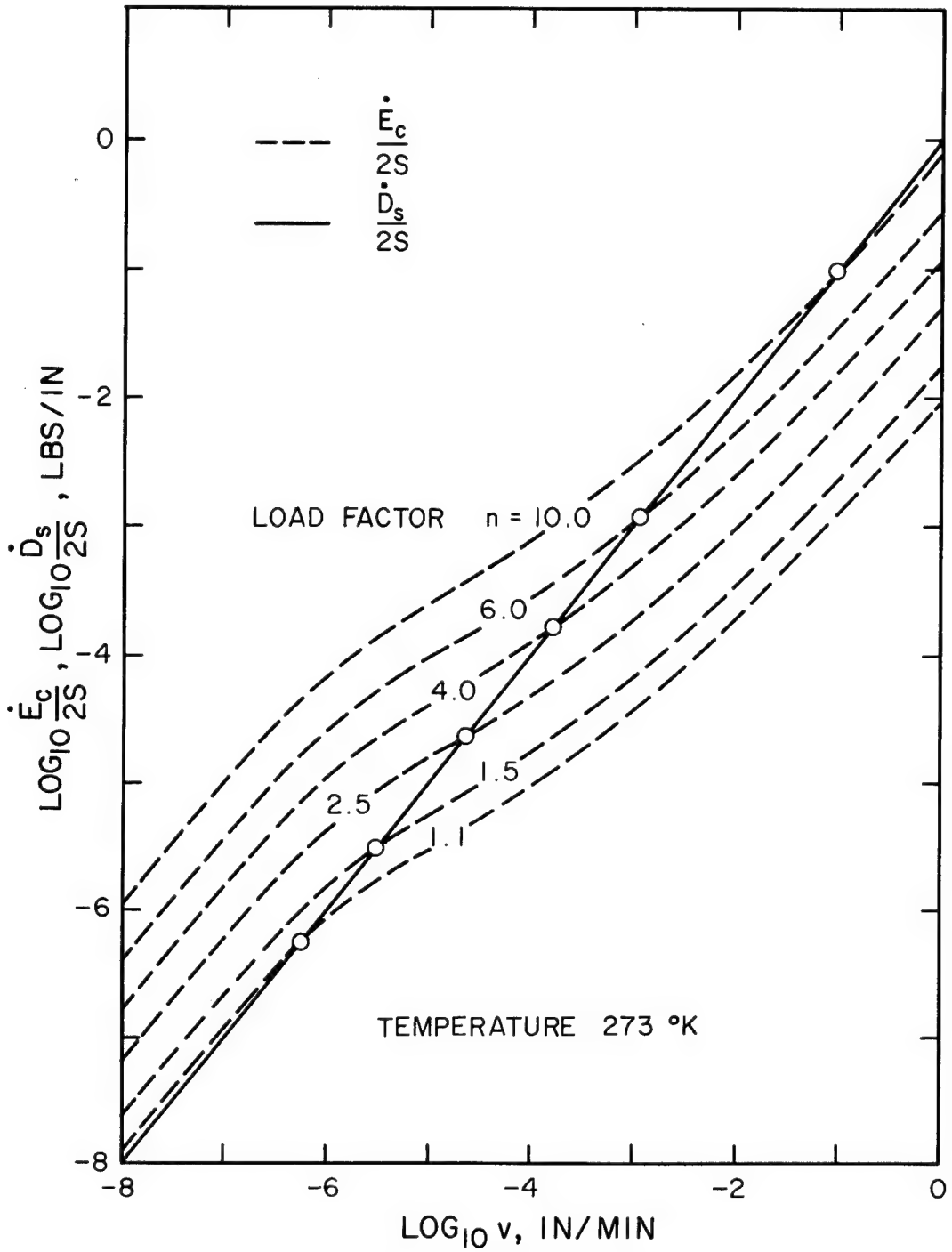

Fig. 36 ENERGY BALANCE FOR A CRACK PROPAGATING IN SOLITHANE 50/50.

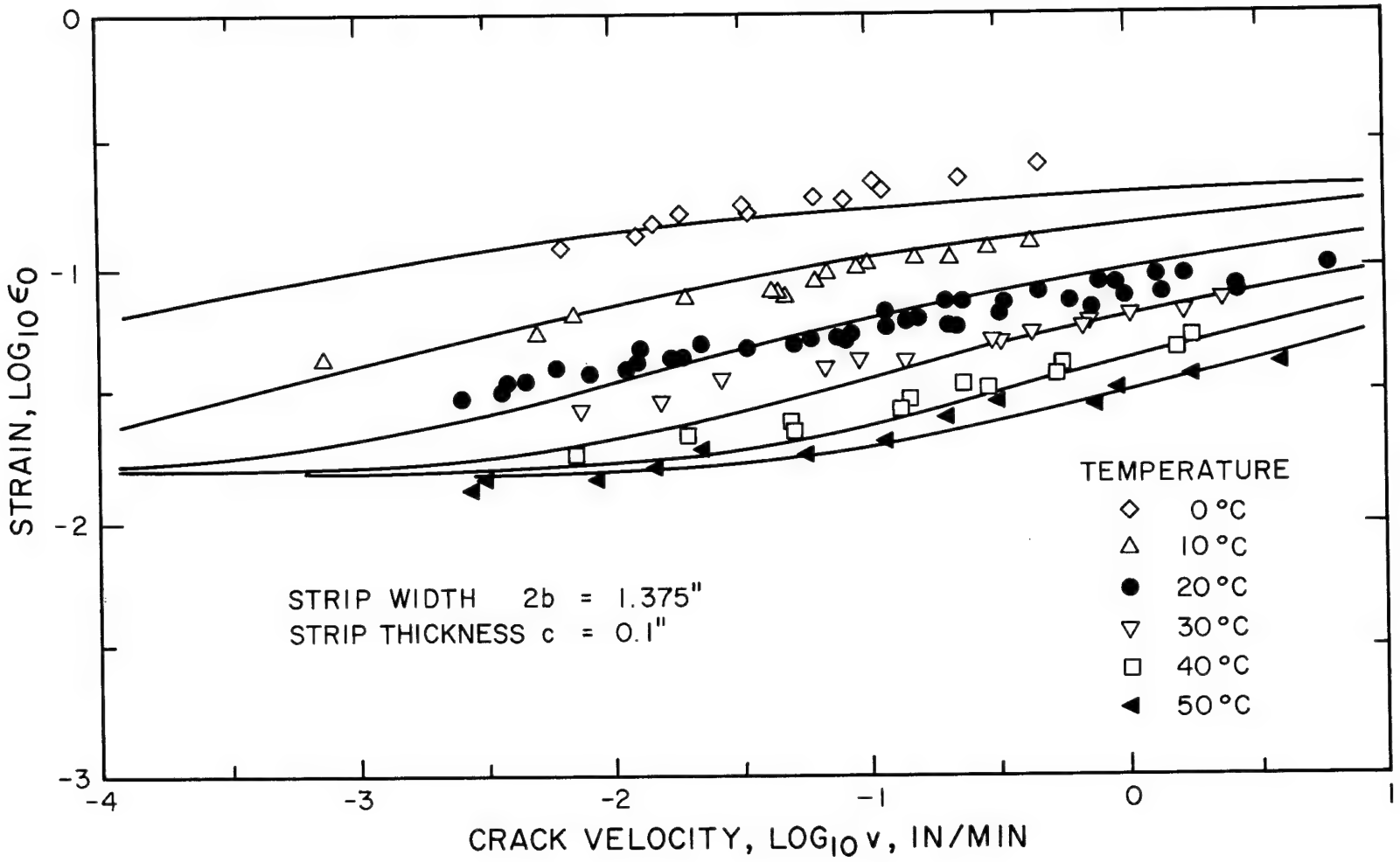

Fig. 37 THEORETICAL AND EXPERIMENTAL RELATIONSHIP BETWEEN CRACK VELOCITY, STRAIN AND TEMPERATURE FOR SOLITHANE 50/50.

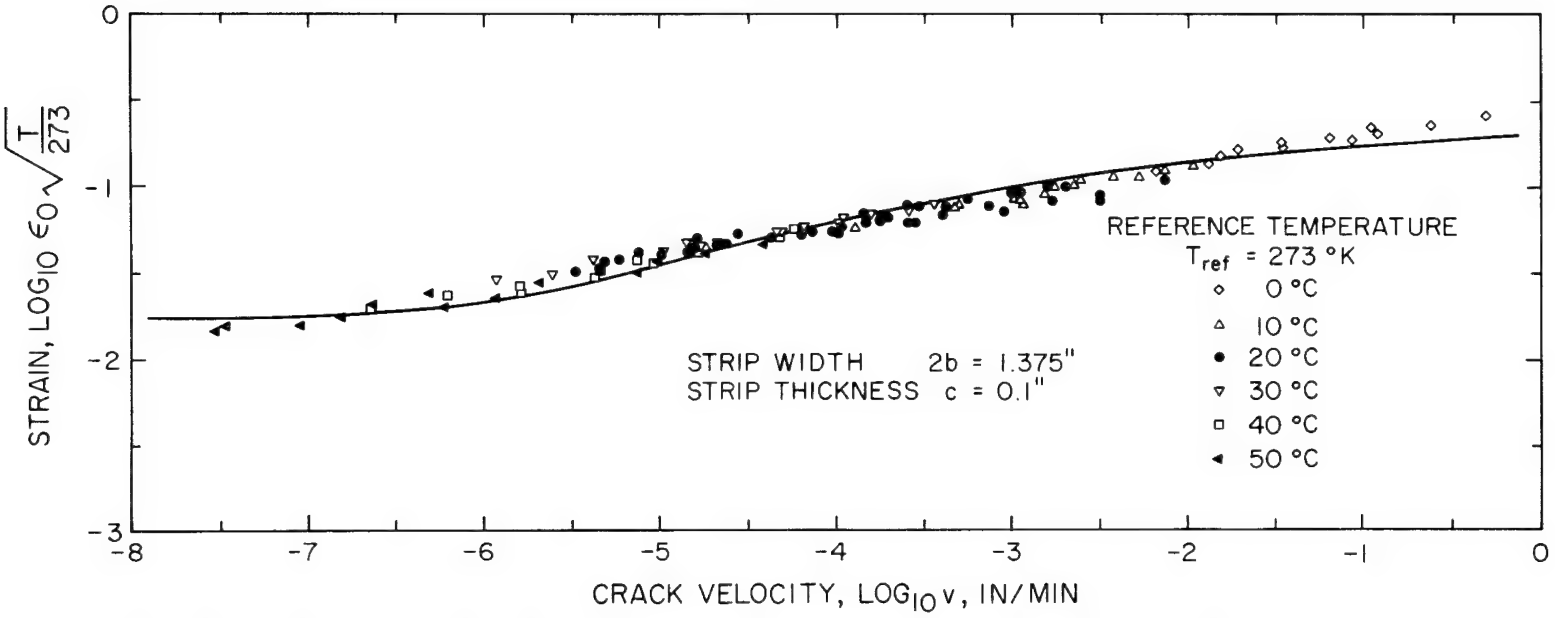

Fig. 38 THEORETICAL AND EXPERIMENTAL MASTER CURVE OF THE CRACK VELOCITY AS A FUNCTION OF STRAIN FOR SOLITHANE 50/50.

Table I

Z(1) as a function of a/b.

a/b	Numerical Solution	Asymptotic Solution Eq. (2.3-21)	$\sqrt{\frac{b}{2a}}$
0.0	1.2533	1.2533	
0.1	1.2381	1.2381	
0.2	1.1957	1.196	1.5811
0.3	1.1341	1.1364	1.291
0.4	1.0627	1.0752	1.1180
0.5	0.9896	1.0256	1.0
0.6	0.9204	0.9838	0.9126
0.7	0.8579		0.8452
0.8	0.8030		0.7906
0.9	0.7555		0.7454
1.0	0.7146		0.7071
1.1	0.6794		0.6742
1.2	0.6489		0.6455
1.3	0.6223		0.6202
1.4	0.5989		0.5976
1.5	0.5781		0.5774
2.0	0.5		0.5
3.0	0.4082		0.4082

Table II

Swelling Agents

Name	Solubility parameter Ref. (63) $\sqrt{cal/cm^3}$
n-pentane	7.0
n-hexane	7.3
n-heptane	7.4
Methylcyclohexane	7.8
Cyclohexane	8.2
Carbontetrachloride	8.6
Toluene	8.9
Benzene	9.2
Chlorobenzene	9.5
o-dichlorobenzene	10.0
1-bromonaphtaline	10.6
Methylcellosolve	10.8
Acetronitrile	11.8
Nitromethane	12.7

REFERENCES

1. "Fracture Processes in Polymeric Solids", edited by B. Rosen, Interscience Publishers, New York (1964).

2. Williams, M. L. in "Fracture of Solids", edited by D. C. Drucker and J. J. Gilman, Interscience Publishers, New York (1963).

3. Halpin, J. C.: "Molecular View of Fracture in Amorphous Elastomers", Rubber Chem. and Tech., Vol. 38, No. 5, pp. 1007-1038 (1965).

4. Halpin, J. C., Bueche, F.: "Fracture of Amorphous Polymeric Solids: Time to Break, Reinforcement", Rubber Chem. and Tech., Vol. 38, No. 2, pp. 263-277 and pp. 278-291 (1965).

5. Smith, T. L.: "Ultimate Tensile Properties of Elastomers",
   I. "Characterization by a Time and Temperature Independent Failure Envelope", J. Polymer Sc., Vol. 1, pp. 3597-3615 (1963).
   II. "Comparison of Failure Envelopes for Unfilled Vulcanizates", J. Appl. Physics, Vol. 35, pp. 27-36 (1964).
   III. "Dependence of the Failure Envelope on Crosslink Density", Proceedings of the Fourth Int. Conf. on Rheology, Brown Univ., Providence, Rhode Island (1963).

6. Griffith, A. A.: "The Phenomena of Rupture and Flow in Solids", Phil. Trans. Roy. Soc., London, Ser. A, Vol. 221, pp. 163-198 (1921).

7. Mott, N. F.: "Brittle Fracture in Mild Steel Plates - II", Engineering, Vol. 165, pp. 16-18 (1948).

8. Berry, J. P.: "Some Kinetic Considerations of the Griffith Criterion for Fracture, I and II", J. Mech. and Phys. of Solids, Vol. 8, pp. 194-216 (1960).

9. Craggs, J. W. in "Fracture of Solids", edited by D. C. Drucker and J. J. Gilman, Interscience Publishers, New York (1963).

10. Erdogan, F.: "Crack Propagation Theories", NASA contractor report, NASA CR-901, Washington (1967).

11. Broberg, K. B.: "The Propagation of a Brittle Crack", Archiv för Fysik, Vol. 18, No. 10, pp. 159-192 (1960).

12. Schardin, H.: "Velocity Effects in Fracture", Conference on Fracture, Swampscott, Massachusetts (1959).

13. Irwin, G. R.: "Analysis of Stresses and Strains Near the End of a Crack Traversing a Plate", J. Appl. Mech., Vol. 24, Trans. ASME, Ser. E, pp. 361-364 (1957).

14. Sanders, J. L.: "On the Griffith-Irwin Theory", J. of Appl. Mech., Vol. 27, Trans. ASME, Ser. E, pp. 352-353 (1960).

15. Rivlin, R. S., Thomas, A. G.: "Rupture of Rubber, I. Characteristic Energy for Tearing", J. of Polymer Sc., Vol. 10, No. 3, pp. 291-318 (1953).

16. Greensmith, H. W., Thomas, A. G.: "Rupture of Rubber; III Determination of Tear Properties", J. of Polymer Sc., Vol. 18, pp. 177-188 (1955).

17. Schapery, R. A., Williams, M. L.: "On the Acceleration of Cracks in Viscoelastic Media", GALCIT SM 62-39, California Institute of Technology (1962).

18. Williams, M. L.: "Fracture in Viscoelastic Media", Proceedings of the Int. Conf. on Fracture, Sendai, Japan (1965).

19. Knauss, W. G.: "Rupture Phenomena in Viscoelastic Materials", Ph.D. Dissertation, California Institute of Technology (1963).

20. Bueche, F., Halpin, J. C.: "Molecular Theory for the Tensile Strength of Gum Elastomers", J. of Appl. Phys., Vol. 35, pp. 36-41 (1964).

21. Willis, J. R.: "Crack Propagation in Viscoelastic Media", J. Mech. and Phys. of Solids, Vol. 15, pp. 229-240 (1967).

22. Knauss, W. G.: "Failure Criteria for Viscoelastic Materials", GALCIT SM 66-2, California Institute of Technology (1966).

23. Sneddon, I. N.: "The Use of Transform Methods in Elasticity", Technical Report AFOSR 64-1784, Department of Mathematics, North Carolina State College, Raleigh (1964).

24. Graham, G. A. C.: "The Correspondence Principle of Linear Viscoelasticity Theory for Mixed Boundary Value Problems Involving Time Dependent Boundary Regions", File No. PSR-47/2,
"Two Extending Crack Problems in Linear Viscoelasticity Theory", File No. PSR-47/3, Appl. Math. Research Group, North Carolina State University, Raleigh (1966).

25. Knauss, W. G., Mueller, H. K.: "The Mechanical Characterization of Solithane 113 in the Swollen and Unswollen State", GALCIT SM 67-8, California Institute of Technology (1967).

26. Ferry, J. D.: "Viscoelastic Properties of Polymers", J. Wiley and Sons, New York (1961).

27. Gross, B.: "Mathematical Structure of the Theories of Viscoelasticity", Herman and Cie., Paris, France (1953).

28. Leaderman, H.: "Viscoelasticity Phenomena in Amorphous High Polymeric Systems", in "Rheology", Vol. 2, edited by F. R. Eirich, Academic Press, New York (1958).

29. Staverman, A. J., Schwarzl, F. in "Die Physik der Hochpolymeren", Vol. 4, edited by H. Stuart, Springer Verlag, Berlin, Germany (1956).

30. Beebe, W. M.: "An Experimental Investigation of Dynamic Crack Propagation in Plastic and Metals", Ph.D. Dissertation, California Institute of Technology (1966).

31. Knauss, W. G.: "Stresses in an Infinite Strip Containing a Semi-Infinite Crack", J. of Appl. Mech., Vol. 33, Trans. ASME, Ser. E, pp. 356-362 (1966).

32. Inglis, C. E.: "Stresses in a Plate due to the Presence of Cracks and Sharp Corners", Trans. of the Inst. of Naval Architects, London, Vol. 60, pp. 219-230 (1913).

33. Williams, M. L.: "On the Stress Distribution at the Base of a Stationary Crack", J. of Appl. Mech., Vol. 24, Trans. ASME, Ser. E, pp. 109-114 (1957).

34. Fung, Y. C.: "Foundations of Solid Mechanics", Prentice Hall, Englewood Cliffs (1965).

35. Lee, E. H.: "Stress Analysis in Visco-Elastic Bodies", Quarterly of Appl. Math., Vol. 13, pp. 183-190 (1955).

36. Lee, E. H., Radok, J. R. M., Woodward, W. B.: "Stress Analysis for Linear Viscoelastic Materials", Trans. Soc. of Rheology, Vol. 3, pp. 41-59 (1959).

37. Courant, R., Hilbert, D.: "Methods of Mathematical Physics", Vol. 1, Interscience Publishers, New York (1953).

38. Muki, R., Sternberg, E.: "The Influence of Couple-Stresses on Singular Stress Concentrations", Zeitschrift für Angewandte Mathematik und Physik, Vol. 16, pp. 611-648 (1965).

39. Lovitt, W. V.: "Linear Integral Equations", Dover Publications, New York (1950).

40. Lowengrub, M.: "A Two-Dimensional Crack Problem", Int. J. Eng. Sc., Vol. 4, Pergamon Press, pp. 284-299 (1966).

41. Buckingham, R. A.: "Numerical Methods", Ritman and Sons, London (1962).

42. Tranter, C. J.: "Integral Transforms", Methuen Monographs on Physical Subjects, Methuen and Co., London (1962).

43. Rice, J.C.: "Discussion", J. of Appl. Mech., Vol. 34, Trans. ASME, Ser. E, pp. 248-249 (1967).

44. Swedlow, J.: "On Griffith's Theory of Fracture", GALCIT SM 63-8, California Institute of Technology (1963).

45. Williams, M. L., Landel, R. F., Ferry, J. D.: "The Temperature Dependence of Relaxation Mechanisms in Amorphous Polymers and Other Glass-Forming Liquids", J. Am. Chem. Soc., Vol. 77, pp. 3701-3707 (1955).

46. Treloar, L. R. G.: "The Physics of Rubber Elasticity", Clarendon Press, Oxford (1958).

47. Lindsay, G.: "Hydrostatic Tensile Fracture of a Polyurethane Elastomer", Ph.D. Dissertation, California Institute of Technology (1966).

48. Zak, A. R.: "Multiaxial Failure of Viscoelastic Materials", Aerospace Research Laboratories, ARL 64-144, Wright Patterson AFB, Ohio (1964).

49. Knauss, W. G.: "A Cross-Linked Polymer Standard Report on Polymer Selection", Matscit PS 65-3, California Institute of Technology (1965).

50. Knauss, W. G., Clauser, J. F., Landel, R. F.: "Second Report on the Selection of a Cross-Linked Polymer Standard", Matscit PS 66-1, California Institute of Technology (1966).

51. Mooney, M. J.: "A Theory of Large Deformation", J. of Appl. Phys., Vol. 11, pp. 582-592 (1940).

52. Rivlin, R. S.: "Large Elastic Deformations of Isotropic Materials", Phil. Trans. Roy. Soc., London, Ser. A, Vol. 240, pp. 459-525 (1946-48), and Vol. 241, pp. 379-397 (1948-49).

53. Smith, T. L.: "Dependence of the Ultimate Properties of a GR-S Rubber on Strain Rate and Temperature", J. of Polymer Sc., Vol. 32, pp. 99-113 (1958).

54. Bueche, A. M., Berry, J. P.: "The Mechanics of Polymer Failure", Conference on Fracture, Swampscott, Massachusetts (1959).

55. Knauss, W. G.: "The Time Dependent Fracture of Viscoelastic Materials", Proceedings of the First Int. Conference on Fracture, Sendai, Japan (1965).

56. Meares, P.: "Polymers, Structure and Bulk Properties", Van Nostrand Company, London (1965).

57. Hopkins, I. L., Hamming, R. W.: "On Creep and Relaxation", J. of Appl. Phys., Vol. 28, pp. 906-909 (1957).

58. Tobolsky, A. V.: "Stress Relaxation Studies of the Viscoelastic Properties of Polymers", J. of Appl. Phys., Vol. 27, pp. 673-685 (1956).

59. Leaderman, H.: "Elastic and Creep Properties of Filamentous Materials and other High Polymers", The Textile Foundation, Washington (1943).

60. Ferry, J. D. J.: "Mechanical Properties of Substances of High Molecular Weight", J. Am. Chem. Soc., Vol. 72, pp. 3746-3752 (1950).

61. Landel, R. F., California Institute of Technology, personal communication.

62. Bueche, F.: "Physical Properties of Polymers", Interscience Publishers, New York (1962).

63. "Polymer Handbook", edited by J. Brandrup and E. H. Immergut, Interscience Publishers, New York (1966).

64. Sax, J. N.: "Handbook of Dangerous Materials", Reinhold Publishing Corporation, New York (1951).

65. Flory, P. J.: "Principles of Polymer Chemistry", Cornell University Press, Ithaca, New York (1953).

66. Dudek, T. J., Bueche, F.: "Polymer-Solvent Interaction Parameter and Creep of Ethylene-Propylene Rubber", Rubber Chem. and Tech., Vol. 37, No. 4, pp. 894-903 (1964).

67. Knauss, W. G.: "Stable and Unstable Crack Growth in Viscoelastic Media", GALCIT SM 68-10, California Institute of Technology (1968).

68. Williams, M. L., Blatz, P. J., Schapery, R. A.: "Fundamental Studies Relating to Systems Analysis of Solid Propellants", GALCIT SM 61-5, California Institute of Technology (1961).

"The aeronautical and space activities of the United States shall be conducted so as to contribute . . . to the expansion of human knowledge of phenomena in the atmosphere and space. The Administration shall provide for the widest practicable and appropriate dissemination of information concerning its activities and the results thereof."

—NATIONAL AERONAUTICS AND SPACE ACT OF 1958

NASA SCIENTIFIC AND TECHNICAL PUBLICATIONS

TECHNICAL REPORTS: Scientific and technical information considered important, complete, and a lasting contribution to existing knowledge.

TECHNICAL NOTES: Information less broad in scope but nevertheless of importance as a contribution to existing knowledge.

TECHNICAL MEMORANDUMS: Information receiving limited distribution because of preliminary data, security classification, or other reasons.

CONTRACTOR REPORTS: Scientific and technical information generated under a NASA contract or grant and considered an important contribution to existing knowledge.

TECHNICAL TRANSLATIONS: Information published in a foreign language considered to merit NASA distribution in English.

SPECIAL PUBLICATIONS: Information derived from or of value to NASA activities. Publications include conference proceedings, monographs, data compilations, handbooks, sourcebooks, and special bibliographies.

TECHNOLOGY UTILIZATION PUBLICATIONS: Information on technology used by NASA that may be of particular interest in commercial and other non-aerospace applications. Publications include Tech Briefs, Technology Utilization Reports and Notes, and Technology Surveys.

Details on the availability of these publications may be obtained from:

SCIENTIFIC AND TECHNICAL INFORMATION DIVISION

NATIONAL AERONAUTICS AND SPACE ADMINISTRATION

Washington, D.C. 20546